Necessary Conditions for Geo-Acoustic Parameter Inversions to Become Asymptotically Unbiased and Attain the Cramer-Rao Lower Bound

by

Ian Lionel Henry Ingram

Submitted to the Department of Ocean Engineering
in partial fulfillment of the requirements for the degree of

Masters of Science in Ocean Engineering

at the

MASSACHUSETTS INSTITUTE OF TECHNOLOGY

February 2002

Author .....
Department of Ocean Engineering
February 12, 2002

Certified by .....
Nicholas C. Makris
Associate Professor
Thesis Supervisor

Accepted by .....
Henrik Schmidt
Chairman, Department Committee on Graduate Students

Necessary Conditions for Geo-Acoustic Parameter Inversions to Become Asymptotically Unbiased and Attain the Cramer-Rao Lower Bound

by

Ian Lionel Henry Ingram

Submitted to the Department of Ocean Engineering
on February 12, 2002, in partial fulfillment of the
requirements for the degree of
Masters of Science in Ocean Engineering

Abstract

Analytic expressions for the first-order bias and second order covariance of a maximum likelihood estimator (MLE) are applied to the problem of estimating geo-acoustic parameters of the sediment layers beneath a shallow ocean using a vertical hydrophone array. These expressions are used to determine *necessary* conditions on sample size for the geo-acoustic MLE to become asymptotically unbiased and attain the minimum variance as expressed by the Cramer-Rao Lower Bound. These conditions are then used to evaluate the performance of estimates for various combinations of unknown parameters in two canonical waveguide models. Since acoustical oceanographers typically use deterministic sources for their inversions, signals are modeled as deterministic. As the energy ratio of the received signal to noise (SNR) is decreased and the source-to-receiver range is increased, seafloor geo-acoustic parameter estimates made using few samples exhibit variances that exceed the Cramer-Rao Lower Bound by orders of magnitude. These variances worsen, and biases become non-negligible, as the number of inversion parameters is increased. This behavior is probably due to a combination of factors including physical coupling between parameters and loss of modes due to attenuation. Samples sizes necessary for estimates of geoacoustic parameters to attain the Cramer-Rao Lower Bound and become asymptotically unbiased are shown to often be in the thousands of samples and, in particular cases, in the hundreds of thousands. The efficacy of the Cramer-Rao Lower Bound as a measure of feasibility of geo-acoustic parameter inversions and the notion that these inversions can be assumed to be unbiased for low sample size are therefore put into question. Researchers can use the method described in this thesis as a tool to design future experiments and ensure that estimates are asymptotically unbiased and do attain minimum variance.

Thesis Supervisor: Nicholas C. Makris
Title: Associate Professor

Acknowledgments

I would like to thank my patient advisor, Nicholas Makris, for giving me the chance to work with him and others on this problem. I have benefited in a great number of ways, academic and otherwise, from my time spent as a graduate student at MIT. The guidance and friendship of Nick, of Aaron Thode, and of Michele Zanolin has been of great importance during that time.

My parents, Lionel and Trina Ingram, and sisters, Sarah Morgan and Katharine Ingram, have been a continual source of support, encouragement and advice. I, as from my beginning, am continually in their debt.

I would like to thank my buddies.

Thanks go to my buddies in the Acoustics Group: the Upstairs Crew, the Downstairs Crew, and the Downstairs-to-Upstairs-Defector Crew. I especially want to thank fellow King of the Basement, Jeremie Eskanazi, for the good times when we ruled the Basement uncontested by Hurricane Tanks, Slam Chairs and the like.

Thanks go to the other favaNaUts: Beta (The Big O), Gamma (Doctor No), Beta Deuteron and He-Who-Would-Not-Be-A-favaNaUt.

Thanks go to all of my buddies who housed me during my time of homelessness, particularily Orion Smith, Erin Palacios, and Brian Bingham.

Thanks go to Megan Galbraith, just because.

Finally I would like to dedicate this thesis to Bitty Kitty and Georges. Georges' aid was pivotal to my academic "success" from Kindergarden til the day he died and probably beyond it. Without his mushy lackadaisical attitude as a model, I would never have forgotten how to read after first grade and learned my true calling as a slacker and a fool. It was Georges' guidance that led me to choose to go to MIT and pursue Ocean Engineering. Bitty Kitty provided a shrewd foil to Georges' dilatoriety. Her input on my research is heavily reflected throughout this thesis which she did not live to see me begin.

Parameter definitions and waveguide models

Parameters for both the Case A and the Case B waveguides

c_w: the compressional wave speed in the water column, in meters per second

ρ_w: the density in the water column, in grams per cubic centimeter

α_w: the coefficient of attenuation in the water column, in dB per lambda

c_s: the compressional wave speed in the sediment layer, in meters per second

ρ_s: the density in the sediment layer, in grams per cubic centimeter

α_s: the coefficient of attenuation in the sediment layer, in dB per lambda

Additional parameters for the Case B waveguide

g_s: the gradient of the compressional wave speed with respect to depth in the sediment layer, in meters per second per meter.

h_s: the thickness of the sediment layer, in meters.

c_b: the compressional wave speed in the basement, in meters per second

ρ_b: the density of the basement, in grams per cubic centimeter

α_b: the coefficient of attenuation in the basement, expressed in dB per lambda

ATMOSPHERE

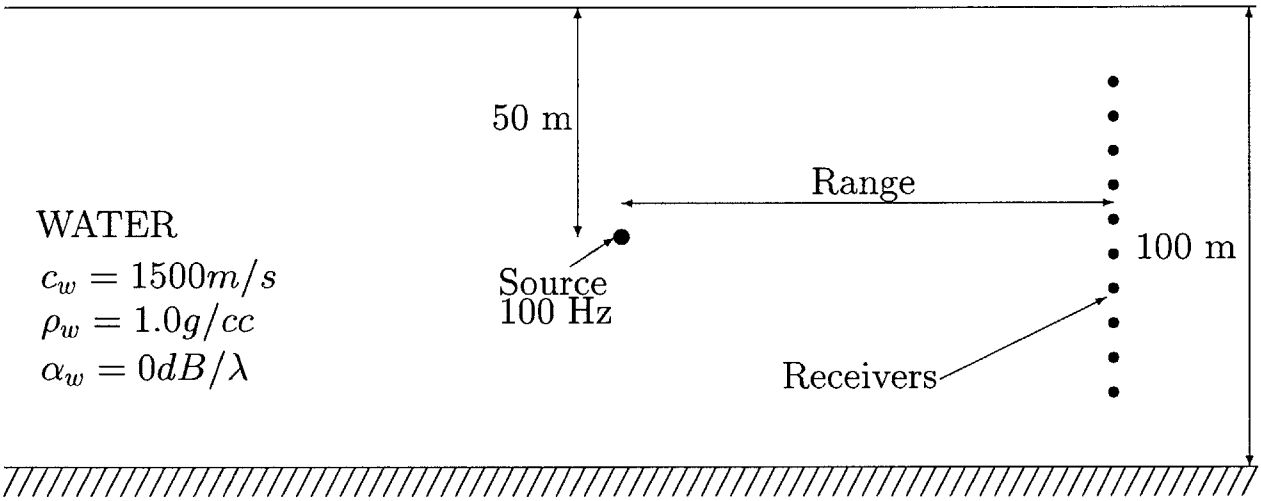

WATER

$c_w = 1500m/s$

$\rho_w = 1.0g/cc$

$\alpha_w = 0dB/\lambda$

SEDIMENT

$c_s = 1700m/s$

$\rho_s = 1.9g/cc$

$\alpha_s = 0dB/\lambda$

Figure 0-1: Case A: Pekeris environmental model.

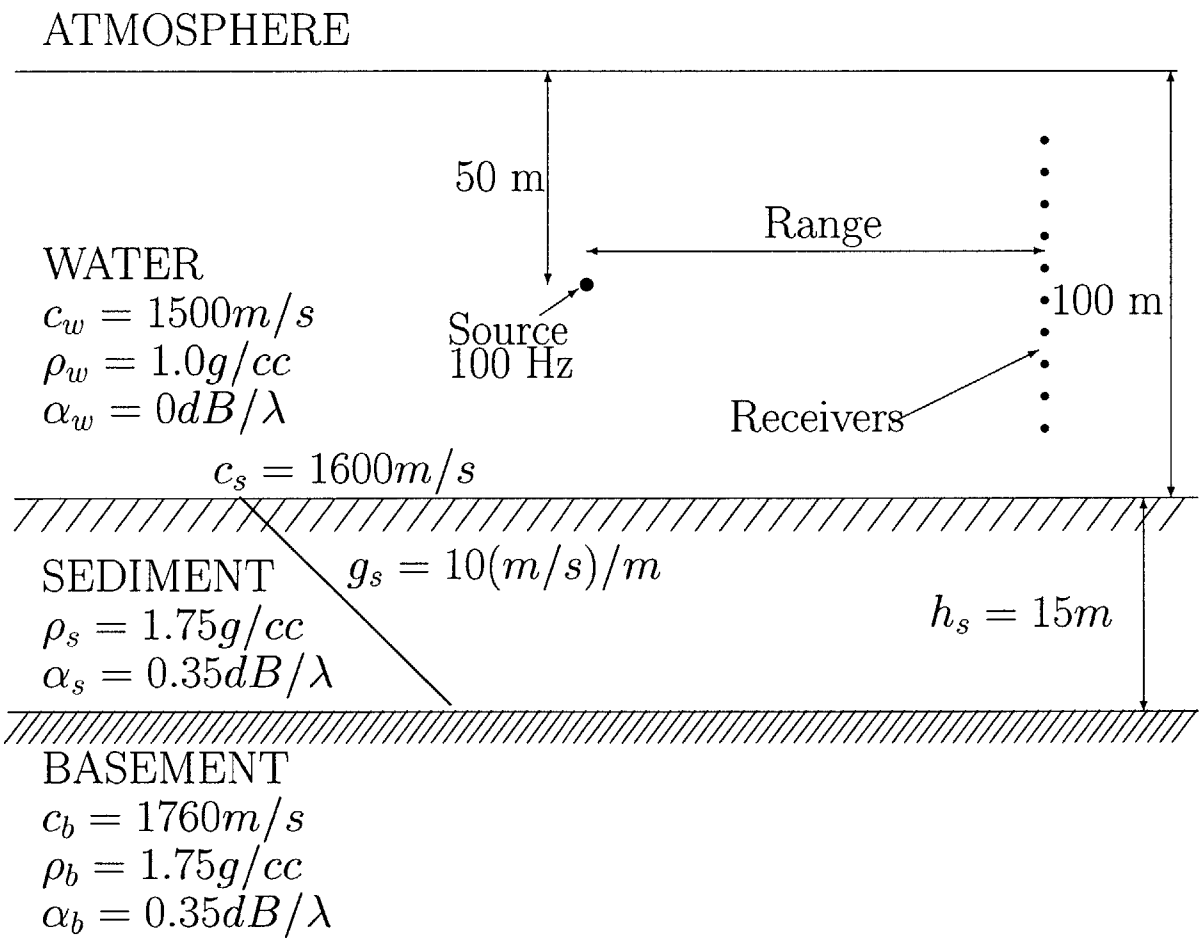

Figure 0-2: Case B: Three layer environmental model with gradient sound speed in sediment layer.

Contents

List of Figures

Chapter 1

Introduction

1.1 Geoacoustical Inversions

The acoustical parameters of the ocean seafloor have a large effect on the propagation of sound in the ocean. Therefore, knowledge of these parameters is important for the effective implementation of many underwater acoustical systems, especially in shallow water where extensive bottom interaction typically occurs during acoustic propagation [1, 2, 3]. Additionally, acoustical oceanographers interested in identifying and mapping sedimentary layers can infer sediment types from such parameters [4]. For both reasons, significant work has been done in recent years to create and improve methods for determining geoacoustical parameters.

The primary acoustical seafloor parameters are the compressional wave speed, the compressional wave attenuation, the shear wave speed, the shear attenuation and the density. In most scenarios the waveguide is assumed to be horizontally stratified and therefore these properties are modeled as being functions of ocean depth only. If the parameters were further constrained to be constant in depth and nothing else was known, the inversion would require the simultaneous estimation of all five parameters. If the relationship of a parameter with depth is more complicated, that relationship must be parameterized and the number of parameters would then be more than five e.g. were sound speed known to be linearly related to depth in a given layer of sediment that relation could be parameterized as a initial sound speed

and a gradient yielding a total of six parameters. The more complicated the model of the waveguide used, the more parameters are needed to describe it. Anything known about the environment beforehand reduces the number of parameters of the inversion. Sometimes the bottom is assumed to be made up of an unknown number of layers each with its own set of geo-acoustic parameters. This introduces the layer thicknesses as possible parameters and, depending on the limit on number of layers, the total number of inversion parameters can be very large. In some field and modeling research the number of parameters ostensibly being estimated simultaneously is in the tens, sometimes hundreds [5].

A variety of acoustical methods have been used to determine seafloor parameters. Most involve the non-linear inversion of the parameters from measurements of the acoustic field in the water-column. A typical scheme involves the comparison of this field to synthetic fields generated using some forward propagation model and a parametric model of the environment. The parameters of the model are varied iteratively until a match is achieved. This method is called matched field inversion. Methods where the modal components of the full-field are inverted for individually are also employed [1]. Most schemes involve the following elements [6]:

- a source of low enough frequency (or frequency range) to allow bottom penetration coupled with a receiving array with a large enough aperture to measure spatial diversity in the field; a method for localizing both.

- a parametric model that accurately and succinctly describes the ocean waveguide and seafloor acoustical structure.

- a model for synthetically generating the acoustic field due to a simulated source from the parametric environmental model.

- a model for comparing the measured field to the synthetic field, called the objective function or cost function. A criterion for what constitutes a good match typically comes from a statistical theory.

- a search algorithm that locates in the output of the cost function the globally

extreme stationary point that corresponds to the set of parameters that create the best match between the real and synthetic field.

All five elements of this process are active areas of research. Hence a number of methods exist to fill each role. Receiving array geometries vary due to differing project goals or availability. Moored vertical arrays are sometimes employed, as are horizontal, towed arrays, as are more complicated configurations. The energy ratio of the received signal to noise (SNR) used can vary between 20 dB to lower than 0 dB. A number of different forward propagation models are used to generate the synthetic pressure fields: normal mode summation [7, 8], wave number integration [9], parabolic equation based methods [2] and so on. For the correlation of the synthetic field with the true field, different types of cost function are used; most are based on the linear least squares function. Search algorithms that have been employed for geoacoustic inversion include basic grid search methods, stochastic optimization methods like simulated annealing [2], genetic algorithms [10], and neural nets [11].

Parameterization of the seafloor varies as well. Some methods rely on estimating the reflection coefficient of the ocean/sediment interface only, rather than the layer structure. Some break the field into its modal components and use those as the data for the inversion, rather than the full-field [12]. For those who attempt to invert for more than one parameter in multi-parameter models of the seafloor, the number of simultaneously estimated parameters is typically in the teens [5] and often can be even higher. Source position and frequency influence geoacoustic inversions as well [13]. Generally, lower-frequency broad-band and narrow-band signals are used. If only a few frequencies are used these are usually chosen to optimize estimation for whichever geo-acoustic parameters are of interest. Some researchers have broken up broad-band data for multi-parameter problems so that different bands are used to estimate different parameters separately, depending on parameter sensitivities [14].

Given the many different methods for performing geoacoustic inversions, it is difficult to determine which is the most effective, or, as different methods have different strengths, which is more effective in which circumstances. In recent years, efforts have been made to bring together researchers doing geo-acoustic inversions [6] and to

benchmark methods against standardized data [5]. In Ref. [5], a synthetic set of data for a variety of ocean waveguides were created, the data were made available along with waveguide descriptions from which the values for the inversion parameters had been removed to groups of researchers in the geoacoustic inversion community. Each group then made its best effort to estimate the original parameters. Many methods yielded moderately accurate results. However, it is very important to point out that the provided data were noiseless and hence very little discussion is applied to the statistical properties of real-world data. Only one group added a marginal amount of noise to their data before performing their inversion scheme [11].

This lack of consideration for the statistical characteristics of the ocean waveguide is a general trend in the geoacoustic inversion community [15]. Most researchers *assume* that the biases and variances of their estimates are negligible. However, this assumption should be made more carefully. Field geoacoustic estimates are nonlinear inversions performed on data randomized by the ocean waveguide, making the behavior of the bias and variance of estimates difficult to predict and their values difficult to determine directly.

Sometimes marginal effort is made, using either a Bayesian or classical statistical approach, to determine bounds on the bias and the variance, and on other statistics, instead of attempting to compute them directly. The Ziv-Zakai Bound and the Weiss-Weinstein Bound [16, 17] are examples of bounds that are based on the Bayesian approach. One particularly popular classical estimation bound is the Cramer-Rao Lower Bound, which gives the minimum variance possible for an unbiased estimator [18]. Relatively simple to compute, this bound is applied to estimation problems that run the gamut of science and engineering fields. Schmidt and Baggeroer [19, 20] applied the Cramer-Rao Lower Bound to seafloor parameter inversions and suggested its general use for calculating parameter resolutions for such problems. Since then it has been assumed to be a reliable tool for gauging the feasibility of geoacoustic estimates. However, the CRLB is only applicable to unbiased estimators. It gives the *lowest possible* variance for such estimators. That variance is unlikely to be attained for instances where the sample size or the SNR is low, regimes typically encountered

in ocean acoustical experiments.

In this thesis I use higher order approximations of the bias and variance with models that do have noise to show that geoacoustic inversions often *will* be unbiased and *can* very easily have non-minimum variances. I then use these same tools to develop necessary conditions on sample size for estimates to be unbiased and attain the Cramer Rao Lower Bound, exploring in the process correlation between parameters.

1.2 The Maximum Likelihood Estimate and the CRLB

Consider a set of n independent and identically distributed experimental data vectors $\mathbf{X}_i = X_{i1}, \ldots, X_{iN}$, where N is the dimension of every vector. We assume that these data are described by a probability density $P(\mathbf{X}, \boldsymbol{\Theta}) = \prod_{i=1}^{n} p(\mathbf{X}_i, \boldsymbol{\Theta})$ that depends on a m-dimensional parameter vector $\boldsymbol{\Theta} = \Theta_1, \ldots, \Theta_m$, where $m \leq N$. According to Lawley's formulation [21], we suppose that the Maximum Likelihood Estimate (MLE) $\hat{\boldsymbol{\Theta}} = \hat{\Theta}_1, \ldots, \hat{\Theta}_m$ of $\boldsymbol{\Theta}$ is given by a stationary point of the likelihood function $\ell(\mathbf{X}, \boldsymbol{\Theta}) = \ln(P(\mathbf{X}, \boldsymbol{\Theta})) = \sum_{i=1}^{n} \ln(p(\mathbf{X}_i, \boldsymbol{\Theta}))$ with respect to the components of Θ

$$\ell_r(\mathbf{X}, \hat{\boldsymbol{\Theta}}) = \left. \frac{\partial \ell(\mathbf{X}, \boldsymbol{\Theta})}{\partial \Theta_r} \right|_{\boldsymbol{\Theta}=\hat{\boldsymbol{\Theta}}} = 0 \qquad r = 1, \ldots, m. \tag{1.1}$$

For a given estimation problem, a minimum variance unbiased estimator, one that attains the Cramer-Rao Lower Bound, does not necessarily exist. However, if an estimate becomes asymptotically unbiased and attains minimum variance at large sample sizes, it is guaranteed to be the MLE [22]. Studying the performance of the MLE then gives an upper limit on the asymptotic performance of all estimators. Therefore, in this thesis we investigate the asymptotic behavior of the MLE to construct *necessary* conditions for any estimator to become asymptotically unbiased and attain the CRLB in the context of geoacoustic inversions.

Assuming the existence of the likelihood function and of its derivatives with respect

to Θ and assuming that

$$E\left[\frac{\partial \ln p(\mathbf{X}_i;\Theta)}{\partial\Theta}\right] = 0 \tag{1.2}$$

we can prove that the MLE of Θ is consistent and the variance of the MLE is a function of $\frac{1}{n}$ that satisfies

$$V\left(\hat{\Theta}, \frac{1}{n}\right) \to \frac{V_1}{n} \tag{1.3}$$

or

$$nV\left(\hat{\Theta}, \frac{1}{n}\right) \to V_1 \tag{1.4}$$

for $n \to \infty$ [22]. We can also prove [23] that

$$V\left(\hat{\Theta}, \frac{1}{n}\right) = \frac{V_1}{n} + \frac{V_2}{n^2} + E_3; \tag{1.5}$$

where V_1 and V_2 are the first and second order terms of the variance expansion for a given parameter and a single sample and where E_3 is a polynomial in $\frac{1}{n}$ containing powers higher than $\frac{1}{n^2}$. Equation 1.3 indicates that we can always find an n_0 such that for any n larger than n_0

$$\frac{\left|\frac{V_2}{n^2} + E_3\right|}{\frac{V_1}{n}} < \epsilon \tag{1.6}$$

for an ϵ chosen for the accuracy needed. From Equation 1.3 we know $\frac{V_2}{n^2} + E_3 \to 0$ as $n \to \infty$ and $\left[\frac{V_2}{n} + nE_3\right] \to 0$ as $n \to \infty$. Therefore $\frac{V_2}{n^2} \to 0$ as $n \to \infty$ and $E_3 \to 0$ as $n \to \infty$ independently in the asymptotic regime. In this asymptotic regime, it is then necessary that

$$\frac{\left|\frac{V_2}{n^2}\right|}{\frac{V_1}{n}} < \epsilon \tag{1.7}$$

in order to satisfy Equation 1.6 for $n > n_0$. From Equation 1.7 an approximate number of samples necessary for Equation 1.6 to hold in the asymptotic regime is then

$$n_{\text{nec}} \approx \frac{|V_2|}{V_1\epsilon} \tag{1.8}$$

It can also be proven that the bias can be represented as a series expansion similar to Equation 1.5 for the variance where B_1 would be the first order term. Again, as the

sample size is increased, the terms in this expansion will become smaller, this time asymptotically approaching zero as sample size is increased. At some sample size the bias will be small enough when compared to the true value of the parameter to assume that the estimate is unbiased. Therefore, by a similar argument of independent minimization of terms in the asymptotic regime a sample size can always be found where

$$\frac{|\frac{B_1}{n}|}{\Theta} < \epsilon_2 \tag{1.9}$$

where ϵ_2 is chosen for the accuracy needed. An approximate number of samples for an estimate to be considered unbiased is then

$$n_{\text{nec2}} \approx \frac{|B_1|}{\Theta \epsilon_2} \tag{1.10}$$

If the sample size is greater than n_{nec2} and n_{nec} the estimate can be considered to be unbiased and have attained the Cramer-Rao Lower Bound. In this case, the probability density function of the estimator would look very much like the one on the left of Figure 1-1 and the variance, by definition, would be equal to the Cramer-Rao Lower Bound.

Analytical formulas exist for the first order term of the bias expansion and the first and second order terms of the variance expansion for an inversion for multiple parameters performed using a deterministic signal [24][1]. These three terms can therefore be calculated for a given estimation problem that fits these criteria and then used in Equations 1.8 and 1.10 to determine the minimum sample sizes to meet goals on resolution of the estimate as represented by the bias and the variance.

In this thesis, we use an ϵ of $\frac{1}{10}^{\text{th}}$ for estimates of all parameters. How small the bias ought to be relative to the true value of the parameter to make Equation 1.9 true depends more on the particular parameter than it does for the variance condition. In this thesis, $\epsilon_2 = \frac{1}{10}^{\text{th}}$is considered reasonable for most parameters but for sound speeds $\epsilon_2 = \frac{1}{200}^{\text{th}}$ is used. Sound propagation is more sensitive to sound speeds and

[1]They also exist for the case where the signal is completely randomized and has zero mean but this scenario is far less typical for geo-acoustic inversions and therefore these formulas are not used

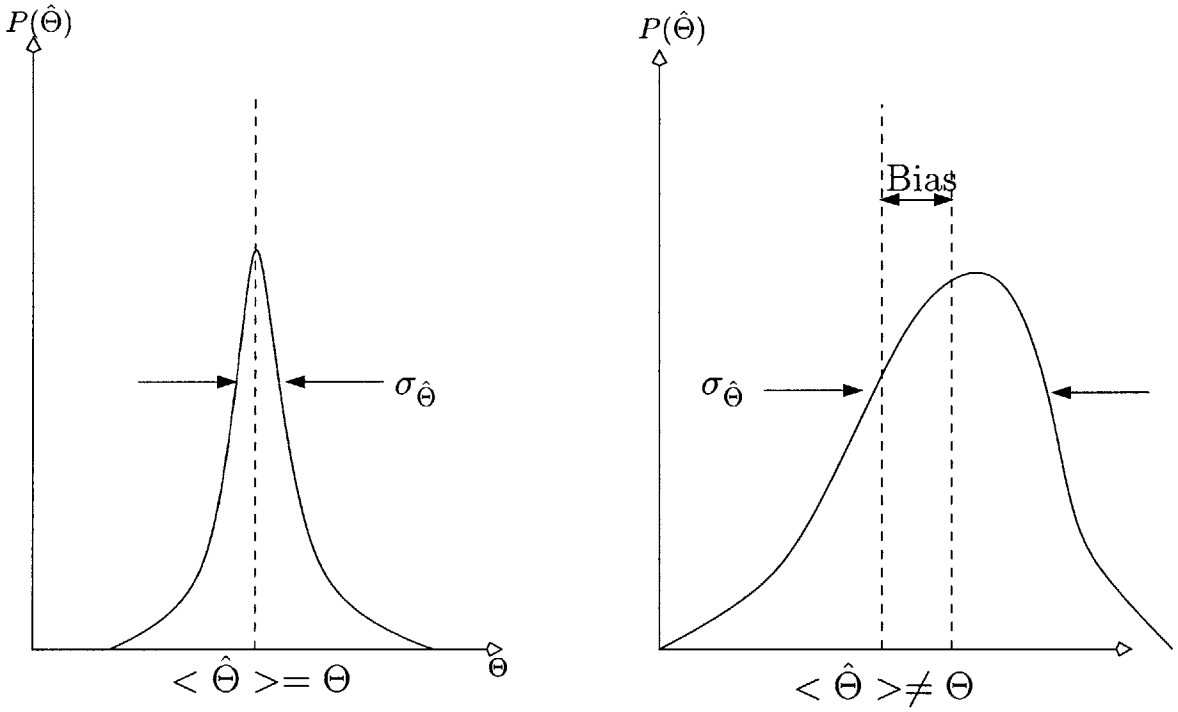

Figure 1-1: Schematic probability density functions for a scalar estimate. Left hand side representive of the probability density function for an estimate made with a large number of samples. Right-hand-side, for an estimate made with a small number of samples.

therefore smaller biases can have a more detrimental effect, drastically changing the accuracy of a model that makes use of the biased parameters.

1.3 Application to canonical problems

In this thesis, the conditions on sample size in Equations 1.10 and 1.8 are used to evaluate the performance of geoacoustic parameter set estimates in two canonical shallow water ocean waveguide models chosen to represent environments in which geoacoustic inversions are often performed. Figures 0-1 and 0-2 display the two models, their sound speed profiles and bottom compositions.

The first model, referred to as Case A, is a Pekeris waveguide (Figure 0-1). A constant velocity water-column of 100 m depth overlays a halfspace of constant-velocity sediment. The sediment is modeled as sand but with zero attenuation. The second waveguide model (Figure 0-2) is similar to the first in water column properties but beneath the water is a sediment layer overlying an infinite halfspace basement. The sound speed in the sediment varies proportionally with depth, starting at 1600 m/s at the water/sediment interface and increasing with a slope of 1.5 m/s per meter until the sediment/basement interface where it is $1750m/s$. This waveguide model, referred to as Case B, is meant to represent a typical continental shelf environment.

Both simulations employ a 100 Hz deterministic monopole source at 50 m depth, and a ten-element vertical array at a range, r, from the source. The array is centered in the water column with 7.5 m spacing between each element so that the shallowest element is at 16.25 m depth, as depicted in the figures. Noise is modeled as Gaussian. The configuration is chosen to represent a common experimental set-up. For both waveguides there are relatively few propagating modes[2] at 100 Hz, six for Case A and seven for Case B.

To gain insight into how the bias and the variance terms behave at varying SNRs, the SNR is set to a particular value when the source is 1 km distant from the receiver

[2]As calculated by KRAKEN. As will be discussed in Section 3.3.6, such a small number of modes allows mode stripping due to attenuation to greatly affect estimation performance at long range.

array, for most examples this is 15 dB. Then, while holding the noise and source levels constant, the first order bias and variance and second order variance are computed as this range is increased. Due to attenuation and spreading, the SNR decreases as range increases.

The statistical moment terms and the minimum sample sizes for estimates to attain the CRLB and become asymptotically unbiased are calculated for a number of different parameter sets in the two waveguides. The parameters sets to be estimated include fundamental physical ones such as sound speed, density, and attenuation, and some morphological ones such as the sound speed gradient and the sediment layer thickness. Various combinations of parameters are chosen to explore how parameter coupling and the number of parameters to be simultaneously estimated affects the statistical performance of the estimates.

Chapter 2

Statistical Theory

2.1 Bias and variance of nonlinear inversions

The bias of an estimator is defined as,

$$b(\hat{\Theta}) = E[\hat{\Theta}(\mathbf{X}) - \Theta] \tag{2.1}$$

and the covariance matrix of an estimator is given by,

$$\mathbf{C}(\hat{\Theta}) = E[(\hat{\Theta}(\mathbf{X}) - E[\hat{\Theta}])(\hat{\Theta}(\mathbf{X}) - E[\hat{\Theta}])^T] \tag{2.2}$$

For estimation problems where the data is related to the parameter or parameters to be estimated in a nonlinear way, the estimates can be biased and have non-minimum variances. These biases and variances can often be reduced by increased sampling. A simple classical estimation example that illustrates these ideas (shown graphically in Figure 2-1) is the scalar MLE for the square of a deterministic signal embedded in Gaussian noise. The data is given by $x = \mu + g$ where $g = \mathcal{N}(0, \sigma^2)$ which means that $E[g^2] = \sigma^2$. The MLE for μ is $\hat{\mu} = x$ so the MLE for μ^2 is $\hat{\mu}^2 = x^2$. However, this yields $E[\hat{\mu}^2] = \mu^2 + \sigma^2$. The estimate is biased by σ^2. If n independent samples are taken of a signal embedded in identically distributed noise, $\hat{\mu}^2 = \frac{1}{n}\sum x^2$ and $E[\hat{\mu}^2] = \mu^2 + \frac{\sigma^2}{n}$. So the bias is now $\frac{\sigma^2}{n}$ and it is apparent that at least the bias

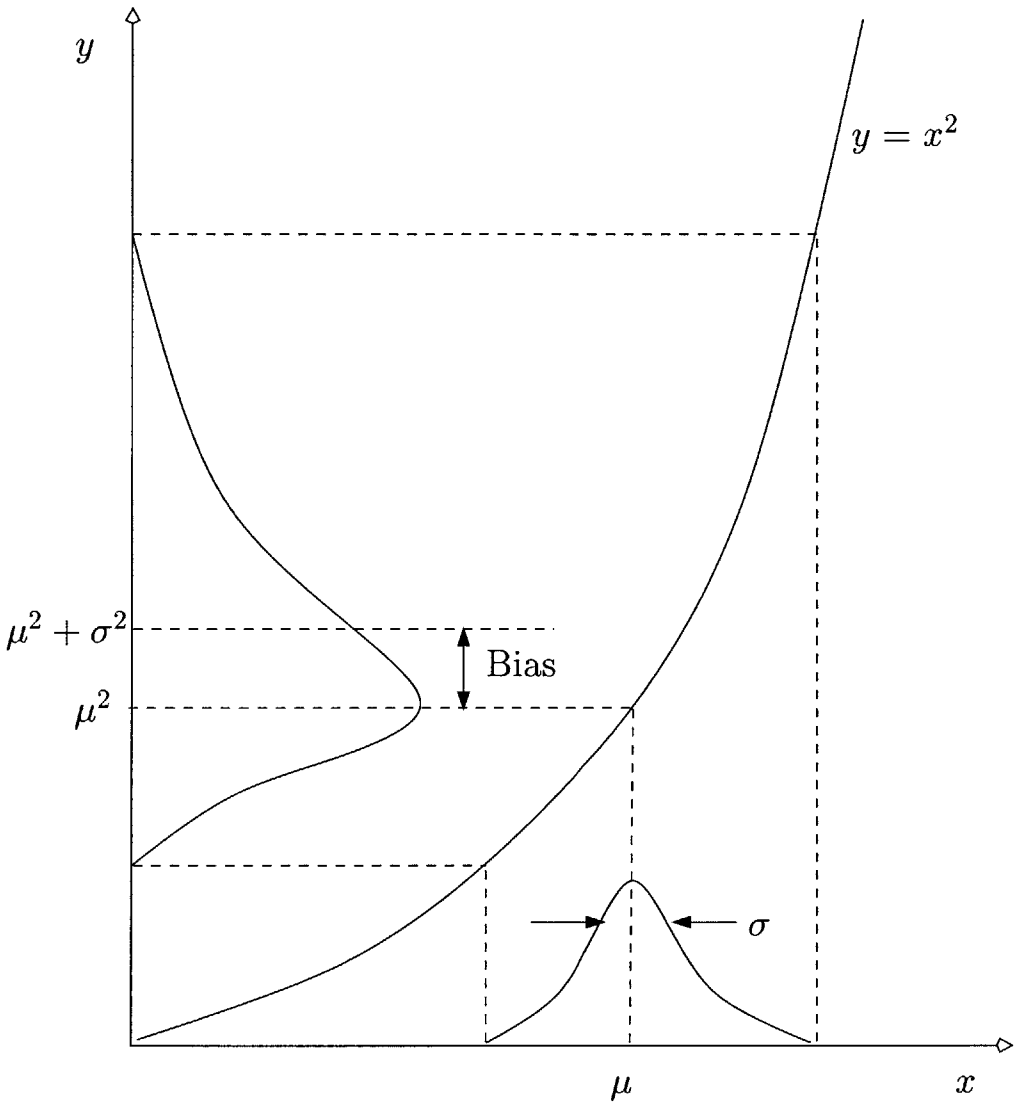

Figure 2-1: Demonstration of how a nonlinear relationship between data and estimation parameter can lead to biases.

will be reduced for larger sample sizes. Figure 1-1 illustrates intuitively the maximum likelihood estimator's performance at high and low sample sizes for a scalar estimate for an estimation problem where an efficient estimator exists. On the left is the probability density function for an estimate made at high sample sizes. It is symmetric around the true value of the parameter, meaning that the expected value of the probability density function equals the true value and the estimate is unbiased. The probability density function also has a relatively small variance and is asymptotically Gaussian. On the right is an example of a probability density function for an estimate made with a relatively small number of samples. Its expected value might not be the true value and the estimate is therefore biased. Additionally the variance of this probability density function might be greater than that of the example on the left.

2.2 Asymptotic expressions for the first order bias and first and second order variance

Let the random data vector $\mathbf{X}$, given m-dimensional parameter vector $\mathbf{\Theta}$, defined in Section 1.2, obey the conditional probability density function (PDF) $p(\mathbf{X};\mathbf{\Theta})$. The first-order derivative of the log-likelihood function with respect to a given parameter is then defined as $\ell_r = \partial\ell(\mathbf{\Theta})/\partial\Theta^r$, where Θ^r is the r-th component $\mathbf{\Theta}$. The higher log-likelihood derivatives are written in the following notation,

$$\ell_{a_1 a_2 \ldots a_s} = \ell_{a_1 a_2 \ldots a_s}(\mathbf{X}, \mathbf{\Theta}) = \frac{\partial^s \ell(\mathbf{X}, \mathbf{\Theta})}{\partial\Theta_{a_1}\partial\Theta_{a_2}\ldots\partial\Theta_{a_s}} \tag{2.3}$$

Moments of the log-likelihood derivatives are written

$$\nu_{a_1 a_2 \ldots a_s, b_1 b_2 \ldots b_s, \ldots, z_1 z_2 \ldots z_s} = E[\ell_{a_1 a_2 \ldots a_s}\ell_{b_1 b_2 \ldots b_s}\ldots\ell_{z_1 z_2 \ldots z_s}] \tag{2.4}$$

so for example $\nu_{s,tu} = E[l_s l_{tu}]$ and $\nu_{a,b,c,de} = E[l_a l_b l_c l_{de}]$.

The expected Fisher information matrix is defined as $i_{rs} = E[l_r l_s]$, for arbitrary

indices r, s [18]. We use the lifted notation to denote inverse matrices and the Einstein summation convention is used, in that whenever an index appears as both a superscript and a subscript in a term, summation over that index is implied. For instance the Fisher Information matrix (one of the moments of the log-likelihood function derivatives), $i_{rs} = E[\ell_r \ell_s]$, has the inverse, i^{rs}, which is the Cramer-Rao Lower Bound (CRLB) [18, 22, 27], the lower bound on the variance of unbiased estimators.

According to [24, 28] the first-order bias of the MLE [1] can be written as:

$$B_1[n]^r = \frac{1}{2} i^{ra} i^{bc} (\nu_{abc} + 2\nu_{a,bc}) \tag{2.5}$$

and the first order covariance of the MLE as [18, 28]:

$$V_1[n]^r = i^{ra} \tag{2.6}$$

The second order covariance of the MLE as [24, 28]:

$$\begin{aligned} V_2[n]^r \;=\; & 2i^{mb} i^{nc} \nu_{lmn} (i^{rs} i^{la} + i^{as} i^{lr}) \nu_{s,b,c}(n^1) + \frac{1}{2} i^{cd} i^{ef} (i^{rs} i^{ab} + i^{as} i^{rb}) \nu_{bce,d,f,s}(n^2) \\ & + i^{tu} (i^{rs} i^{ab} i^{cd} + i^{rd} i^{ab} i^{cs} + i^{ad} i^{rb} i^{cs}) \nu_{st,u,bc,d}(n^2) \\ & + i^{bm} i^{cq} i^{tp} \nu_{lmn} \nu_{opq} (\frac{1}{4} i^{rl} i^{ao} i^{sn} + \frac{1}{2} i^{rs} i^{al} i^{on} + \frac{1}{2} i^{as} i^{rl} i^{on}) \nu_{s,t,b,c}(n^2) \\ & + \frac{1}{2} i^{sm} \nu_{lmn} (i^{tn} i^{cd} (i^{rl} i^{ab} + i^{al} i^{rb}) + 2 i^{bn} i^{cd} (i^{rl} i^{at} + i^{al} i^{rt}) \\ & + i^{cl} i^{tn} (i^{rd} i^{ab} + i^{ad} i^{rb})) \nu_{s,t,bc,d}(n^2) + \frac{1}{6} i^{mb} i^{nc} i^{od} \nu_{lmno} (i^{rs} i^{la} + i^{as} i^{rl}) \nu_{s,b,c,d}(n^2) \\ & + 4 i^{bm} (i^{rs} i^{al} + i^{as} i^{rl}) \nu_{s,m,lb}(n^1) - \frac{1}{4} i^{rs} i^{tu} i^{aw} i^{yz} \nu_{stu} \nu_{wyz} \\ & - i^{rs} i^{tu} i^{aw} i^{yz} \nu_{stu} \nu_{wy,z}(n^1) - i^{rs} i^{tu} i^{aw} i^{yz} \nu_{st,u}(n^1) \nu_{wy,z}(n^1) \end{aligned} \tag{2.7}$$

The notation $\nu_{bce,d,f,s}(n^2)$ indicates that in the joint moment $\nu_{bce,d,f,s}$ only terms proportional to n^2 are retained. The first-order covariance term is simply the CRLB.

The general bias and variance expressions of Equation. 2.5- 2.7 are now applied to

[1] Analytical expressions for the second order bias and a method for generating higher order terms of both the bias and variance expansions can be found in [23]

the specific case of data that obey the conditional Gaussian probability density [22]. If $\mathbf{x}_i = \boldsymbol{\mu} + \mathbf{g}_i$ and $\mathbf{g}_i = \mathcal{N}(0, C)$

$$p(\mathbf{X};\boldsymbol{\Theta}) = \frac{1}{(2\pi)^{nN/2}|\mathbf{C}(\theta)|^{n/2}} e^{-\frac{1}{2}\sum_{i=1}^{n}(\mathbf{X}_i - \boldsymbol{\mu}(\theta))^T \mathbf{C}(\theta)^{-1}(\mathbf{X}_i - \boldsymbol{\mu}(\theta))} \tag{2.8}$$

Here $\mathbf{X}_i$ is one of the n independent and identically distributed N-dimensional real-valued data vectors, $\mathbf{C}$ is the real-valued covariance matrix, and μ is the real-valued mean of the random data. For the present study of geo-acoustic inversion, $\mathbf{X}_i$ represents the narrow-band acoustic data collected around a given frequency across an array of N sensor. The parameter set $\boldsymbol{\Theta}$ represents a vector of whichever geo-acoustic parameters are chosen for a particular inversion, i.e. sediment density, attenuation or sediment sound speed.

Since additive noise typically arises from a large number of independent noise sources distributed over the sea surface [29], like wind action, wave interactions, or ocean-going vessels, the total noise field can generally be modeled as the sum of large numbers of statistically independent contributions. Therefore, if none of the noise contributions dominates the others, the central limit theorem is applicable and the noise distribution is considered to be Gaussian [30]. The Gaussian probability density of Equation. 2.8 is then a valid representation of a deterministic signal embedded in additive noise [30].

In general, both the data mean and the covariance in Equation 2.8 are functions of the desired parameter set $\boldsymbol{\Theta}$. The evaluation of the joint moments in Equation 2.5- 2.7 has recently been performed in [24] . However the analysis of this paper is focused on a deterministic signal in additive noise, where the covariance $\mathbf{C}$ is independent of the parameter vector matrix $\boldsymbol{\Theta}$, while the mean μ depends on $\boldsymbol{\Theta}$. In this case the terms referred to in Equations 2.5- 2.7 are those given in Appendix B of Reference [24].

2.3 Preparing the covariance matrix and the mean vector

The covariance matrix for a deterministic signal embedded in zero-mean Gaussian noise measured on a vertical array is an $N \times N$ identity matrix, where N is the number of elements in the array, in this case 10. We define the SNR as,

$$\mathrm{SNR} = \frac{E_s}{E_n} \tag{2.9}$$

where E_s is the energy of the field at the range of the array and E_n is the energy of the spatially uncorrelated background noise. For a given source to receiver array range, the value of E_s can be obtained by summing the energy of each of the elements of the vertical array, as calculated from the complex pressure field value. Re-arrangement of Equation 2.9 allows the computation of E_n and the subsequent scaling of the covariance matrix. In essence, the covariance matrix, $\mathbf{C}$, is calculated by,

$$\tilde{\mathbf{C}} = \frac{\sum_{m=1}^{N} |P_m|^2}{\mathrm{SNR} \cdot N} \cdot \begin{bmatrix} 1 & 0 & 0 & \cdots \\ 0 & 1 & 0 & \cdots \\ 0 & 0 & 1 & \cdots \\ \vdots & \vdots & \vdots & \ddots \end{bmatrix} \tag{2.10}$$

where N is the number of elements in the hydrophone array, SNR is the signal-to-noise ratio in dB, P_m is the value of the N-th element of the N element vector of complex pressure values measured on the vertical array. In our simulations P_m is calculated by a summation of normal modes, using mode functions and wavenumbers generated by the KRAKEN software package

In our model, $x_i = \mu(\Theta) + g_i$, where $i = 1, 2, ...n$, $E_s = \mu^2(\theta)$ and the energy of the average noise is given by

$$E\left[\left(\frac{1}{n}\sum_{i=1}^{n} g_i\right)^2\right] = E[g_i g_j] = \delta_{ij}\sigma^2 \tag{2.11}$$

which gives

$$\frac{E_s}{E_n} = n \cdot \frac{\mu^2}{\sigma^2} \tag{2.12}$$

i.e. this SNR of n measurements is n times the SNR of a single measurement sample.

In realistic situations, it is unreasonable to assume the noise structure is incoherent when sampled at any time-rate. Even real-world noise that can be approximated as Gaussian will be coherent when sampled too quickly. For given noise there is a coherence time, τ_c, inside of which samples should be considered coherent. Therefore, if the time over which samples are taken, T, is much greater than τ_c, the sample size, n, is well approximated by $\frac{T}{\tau_c}$. If $T << \tau_c$, in effect, only one legitimate sample has been taken of the signal amplitude.

The computation of the signal mean, μ, and its derivatives is described in a later section. Once these quantities have been obtained, the joint moments are evaluated and inserted into Equation. 2.5- 2.7 to compute the first order bias and the first and second order variance of the bias and covariance expansions. These can then be used to ascertain the number of samples that are required to attain the Cramer-Rao Lower Bound and assure unbiasedness, using the conditions in Equations 1.9 and 1.9.

It is important to note that $\tilde{\mu}$ and its derivatives, and for the parameter-dependent covariance case $\tilde{\mathbf{C}}$ and its derivatives, are complex quantities, while the joint moments required to evaluate the asymptotic expansions in Appendix B presume a real mean vector, $\boldsymbol{\mu}$, and a real covariance matrix, $\mathbf{C}$.

If $\tilde{\mathbf{x}} = \mathbf{u} + j\mathbf{v}$ (the tilde denotes a complex quantity) obeys the complex Gaussian probability function,

$$\bar{p}(\tilde{\mathbf{x}}) = \frac{1}{\pi^n \det(\mathbf{C}_{\tilde{\mathbf{x}}})} \exp\left[-(\tilde{\mathbf{x}} - \tilde{\boldsymbol{\mu}})^H \mathbf{C}_{\tilde{\mathbf{x}}}^{-1} (\tilde{\mathbf{x}} - \tilde{\boldsymbol{\mu}})\right] \tag{2.13}$$

where $\mathbf{C}_{\tilde{\mathbf{x}}} = \mathbf{A} + j\mathbf{B}$ and $\tilde{\boldsymbol{\mu}} = \boldsymbol{\mu}_u + j\,\boldsymbol{\mu}_v$ then $\bar{p}(\tilde{\mathbf{X}}) = p(\mathbf{X})$ where $p(\mathbf{X})$ is the real Gaussian probability density function,

$$p(\mathbf{x}) = \frac{1}{(2\pi)^{\frac{2n}{2}} \det^{\frac{1}{2}}(\mathbf{C}_{\mathbf{x}})} \exp\left[-\frac{1}{2}(\mathbf{x} - \boldsymbol{\mu})^T \mathbf{C}_{\mathbf{x}}^{-1} (\mathbf{x} - \boldsymbol{\mu})\right] \tag{2.14}$$

with $\mathbf{x} = (u_1\ u_2 \ldots u_N\ v_1\ v_2 \ldots v_N)$, $\boldsymbol{\mu} = (\mu_{u,1}\ \mu_{u,2} \ldots \mu_{u,N}\ \mu_{v,1}\ \mu_{v,2} \ldots \mu_{v,N})$, and

$$\mathbf{C_x} = \frac{1}{2}\begin{bmatrix} \mathbf{A} & -\mathbf{B} \\ \mathbf{B} & \mathbf{A} \end{bmatrix} \tag{2.15}$$

while $\tilde{\mathbf{x}}$ and $\tilde{\boldsymbol{\mu}}$ are vectors of length N, $\mathbf{x}$ and $\boldsymbol{\mu}$ are vectors of length $2N$, while $\mathbf{C}_{\tilde{\mathbf{x}}}$, $\mathbf{A}$, and $\mathbf{B}$ are $N \times N$ matrices, $\mathbf{C_x}$ is a $2N \times 2N$ matrix.

Chapter 3

Geoacoustic inversion examples

3.1 Waveguide environment and array geometry

Two shallow water ocean waveguide environments are modeled to examine the effects of waveguide properties on geo-acoustic inversions. Figures 0-1 and 0-2 display the two models, their sound speed profiles and bottom compositions. All simulations employ a 100 Hz deterministic monopole source at 50 m depth, and a ten-element vertical array at a range, r, from the source. The array is centered in the water column with 7.5 m spacing between each element so that the shallowest element is at 16.25 m depth, as depicted in the figures.

The first model, hereafter referred to as Case A, is a Pekeris waveguide (Figure 0-1) where a constant velocity water-column of 100 m depth overlays a halfspace of constant-velocity sediment. The sound speed, density and sound speed attenuation in the water column are, respectively, 1500 m/s, 1.0 g/cc and 0 dB/λ. The sediment is modeled as sand but with zero attenuation. As is explained in more detail later, this case is useful for testing the numerical derivative implementation used to calculate derivatives of the log-likelihood function which are required to solve Equations 2.5-2.7. Derivatives for certain inversion parameter sets could be determined analytically for this non-attenuation case. However, zero attenuation is highly unphysical and results from this case should therefore be recognized as likely to also be unphysical.

The second waveguide model (Figure 0-2) is similar to the first in water column

properties: sound speed is 1500 m/s; density is 1.0 g/cc; and attenuation is 0 dB/λ. Beneath the water is a sediment layer overlying an infinite halfspace basement. The basement has a sound speed of 1700 m/s, a density of 1.75 g/cc, and an attenuation of 0.35 dB/λ. The sediment layer has a density and attenuation of 1.75 g/cc and 0.35 dB/λ respectively and is 100m deep. The sound speed in the sediment varies proportionally with depth, starting at 1600 m/s at the water/sediment interface and increasing with a slope of 1.5 m/s per meter until the sediment/basement interface where it is 1750m/s. This waveguide model, hereafter referred to as Case B, is chosen as it represents well the sediment structure in many typical continental shelf environments.

For both waveguides there are relatively few propagating modes[1] at 100 Hz, six for Case A and seven for Case B. As is discussed in Section 3.3.6, such a small number of modes allows attenuation to greatly affect estimation performance at long range.

To gain insight into how the bias and the variance terms behave at varying SNRs, the SNR is set to a particular value when the source is 1 km distant from the receiver array, for most examples this is 15 dB. Then, while holding the noise and source levels constant, the first order bias and variance and second order variance are computed as this range is increased. Due to attenuation and spreading, the SNR decreases as range increases.

3.2 Estimates in the Case A waveguide

As a benchmark of the numerical derivative method that is used, analytical derivatives are calculated for Case A, for a parameter set, $\boldsymbol{\Theta}$ that included only the water sound speed, c_w, and the sediment sound speed, c_s. For this case, it is possible to determine the derivatives of the Green function with respect to the inversion parameters via a decomposition of the modes into downward and upward propagating waves (see Appendix B). These are compared to derivatives calculated numerically to show that, for the intents and purposes of this work, the numerical method is valid.

[1] As calculated by KRAKEN

3.2.1 Estimate of c_w and c_s

Figure 3-1 illustrates the results generated in the Case A waveguide for an inversion for the sound speed in the water column, c_w, and the sound speed in the sediment bottom, c_s. For this example, 10 log SNR at 1 km is set to 0 dB. The example is performed using both numerically (see Appendix A) and analytically (see Appendix B) generated derivatives. The results via the two methods are visually identical when displayed, so Figure 3-1 represents the results of both methods. The dashed, lighter curve shows the first order bias and the black and gray solid curves show, respectively, the square roots of the absolute values of the first and second order variance terms as a function of source to receiver array range. All the values are for a single sample.

Figure 3-1a shows the three statistical moment terms for the sound speed of the sediment layer. At a range of 500 m, the first order bias is about 40 m/s. As range is increased (SNR decreased), this bias drops and becomes more oscillatory. By 2 km, the bias is around 0.1-3 m/s. The square root of the first and second order variance are both about 100 m/s ($\approx \frac{1}{17}$ the true value of the parameter) at the closest ranges but also drop as range is increased. The second order variance, however, drops less than the first order term so that, by 2 km range, 10 log SNR is -13 dB, the second order variance is 30 m/s, while the first order variance is closer to 15 m/s. The general pattern of decrease in all three statistical moment terms is probably due to increased sampling of the bottom at greater source-to-receiver range, an effect that would be countered by attenuation in the bottom were it non-zero as is shown in later examples. However, it is not unreasonable to believe that the ratio of the second- to first-order variance terms eventually grows with range, as, per our method, higher range is coupled to lower SNR due to cylindrical spreading.

Similar behavior is observed for the moments of the water column sound speed MLE in Figure 3-1b. The biases for the water column sound speed is relatively low with respect to its true value indicating that the estimates for this example could possibly be treated as unbiased for all the tested ranges and SNRs as all the higher order terms are likely to be smaller. This is not true for the bottom sound speed bias

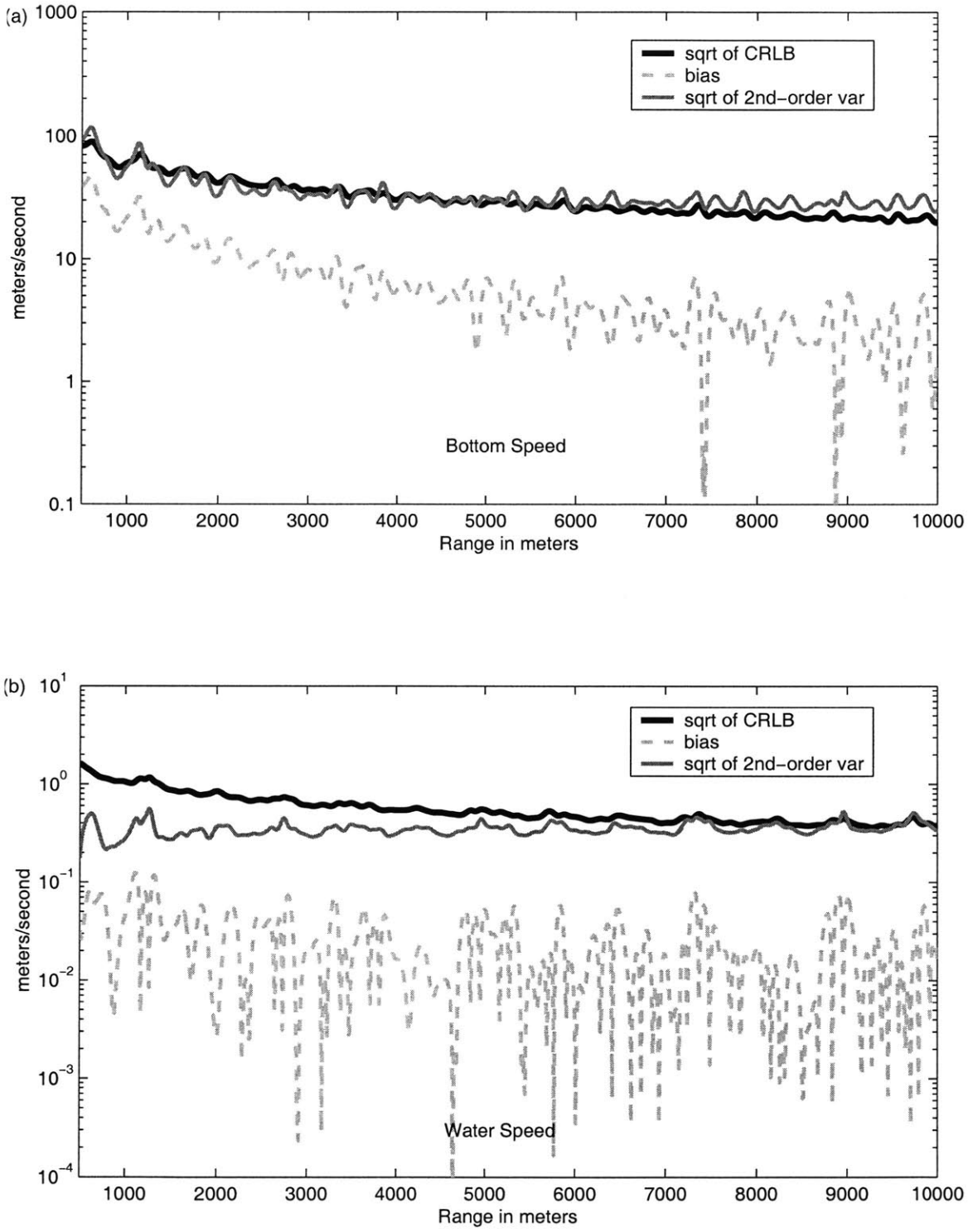

Figure 3-1: Bias and variance terms for an inversion for parameters c_s and c_w in the Case A waveguide for a lower range of SNRs. (See next figure for SNR vs. range.)

bias. The first order and second order variance are also relatively low for the water speed estimate. The bottom sound speed estimate has significant error. However, of more import than the value of the second order variance is the ratio of that value to the first order variance. The larger this ratio, the more likely it is that higher order terms in the variance expansion could also have higher values which, when all summed, might result in a non-negligible total variance. Additionally, it is important to compare the bias to the true value of the parameter to get a sense of how significant it is. The same goes for the first order variance. Even if the CRLB is attained, if it is too large the estimate will not be useful.

The information displayed in Figure 3-1 is represented differently in Figures 3-2 and 3-3. In Figure 3-2, the minimum sample size for the estimates to be considered unbiased, as calculated per Equation 1.10, is shown for all ranges for the inversion of parameters, c_s and c_w, in the Case A waveguide. Shown in the Figure 3-2a is the input signal-to-noise ratio at all tested ranges. As discussed before, due to the method of holding source level fixed while moving the source away from the receiver, the SNR decreases as range is increased. Therefore, at higher ranges, and hence lower SNRs, the number of samples required for any inversion is expected to be higher. Certainly, a fractional number of samples is not possible, so very low values serve to say that a single sample meets our condition for this particular estimate to meet our bias minimization condition.

It is worthwhile to note that the curves for the bias of the bottom sound speed estimate in Figure 3-2b follow the same inverse exponential dependence as the signal-to-noise ratio curve in Figure 3-2a. Minimalization of the bias for the the bottom speed only requires more than a single sample at ranges less than two kilometers. For the water speed, the minimum sample size is less than one at all ranges.

Figure 3-3 shows the minimum sample size for the two estimates to attain the Cramer-Rao Lower Bound, as calculated per Equation 1.8, for ranges from 500m to 10 km. Despite the lack of attenuation and the behavior of the minimum sample size for bias, the two curves for the minimum sample size for attainment of the CRLB increase with decreasing SNR. This indicates, as makes intuitive sense, that the second

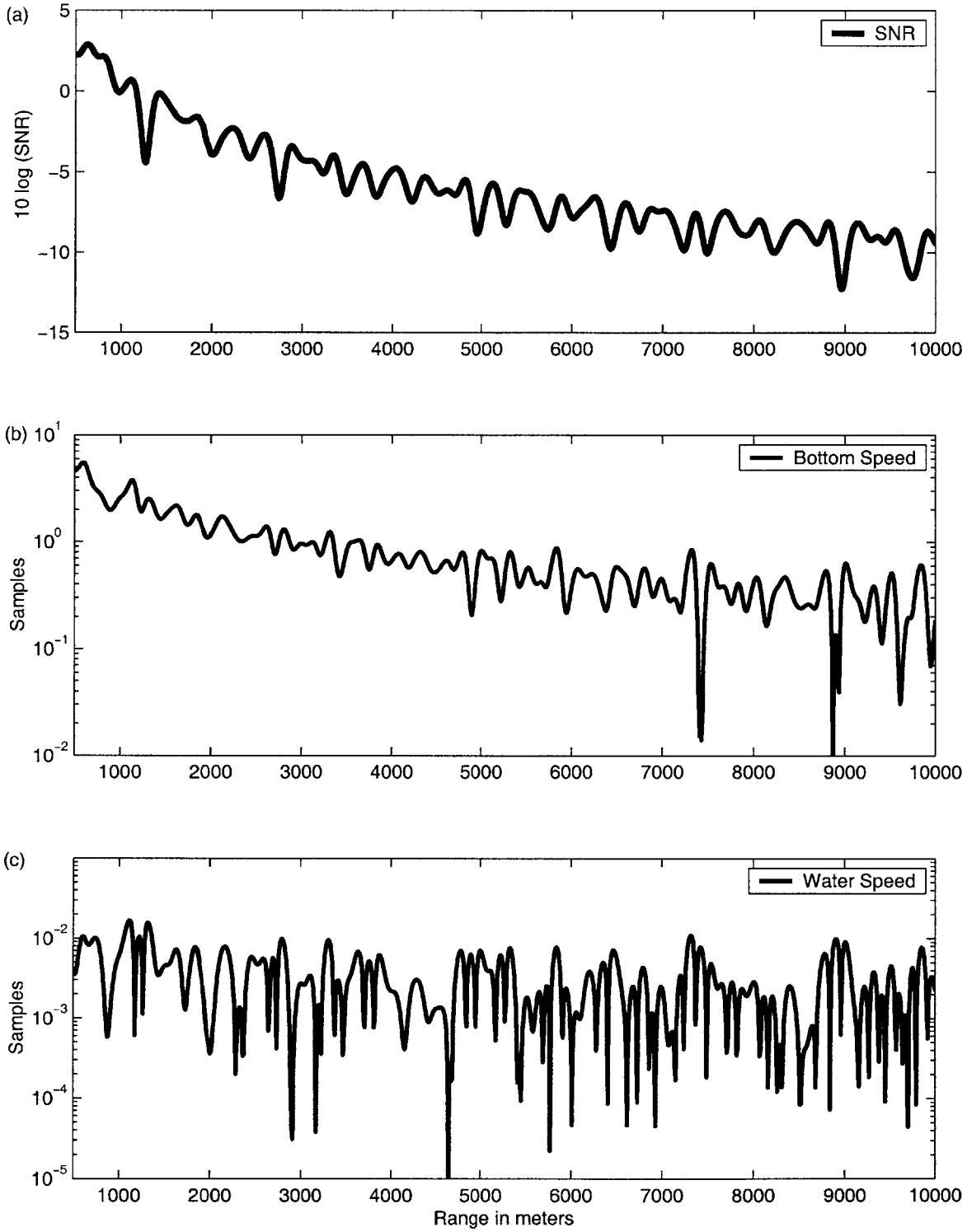

Figure 3-2: SNR versus range and necessary sample sizes for estimates of parameters c_s and c_w in the Case A waveguide for a lower range of SNRs to be asymptotically unbiased.

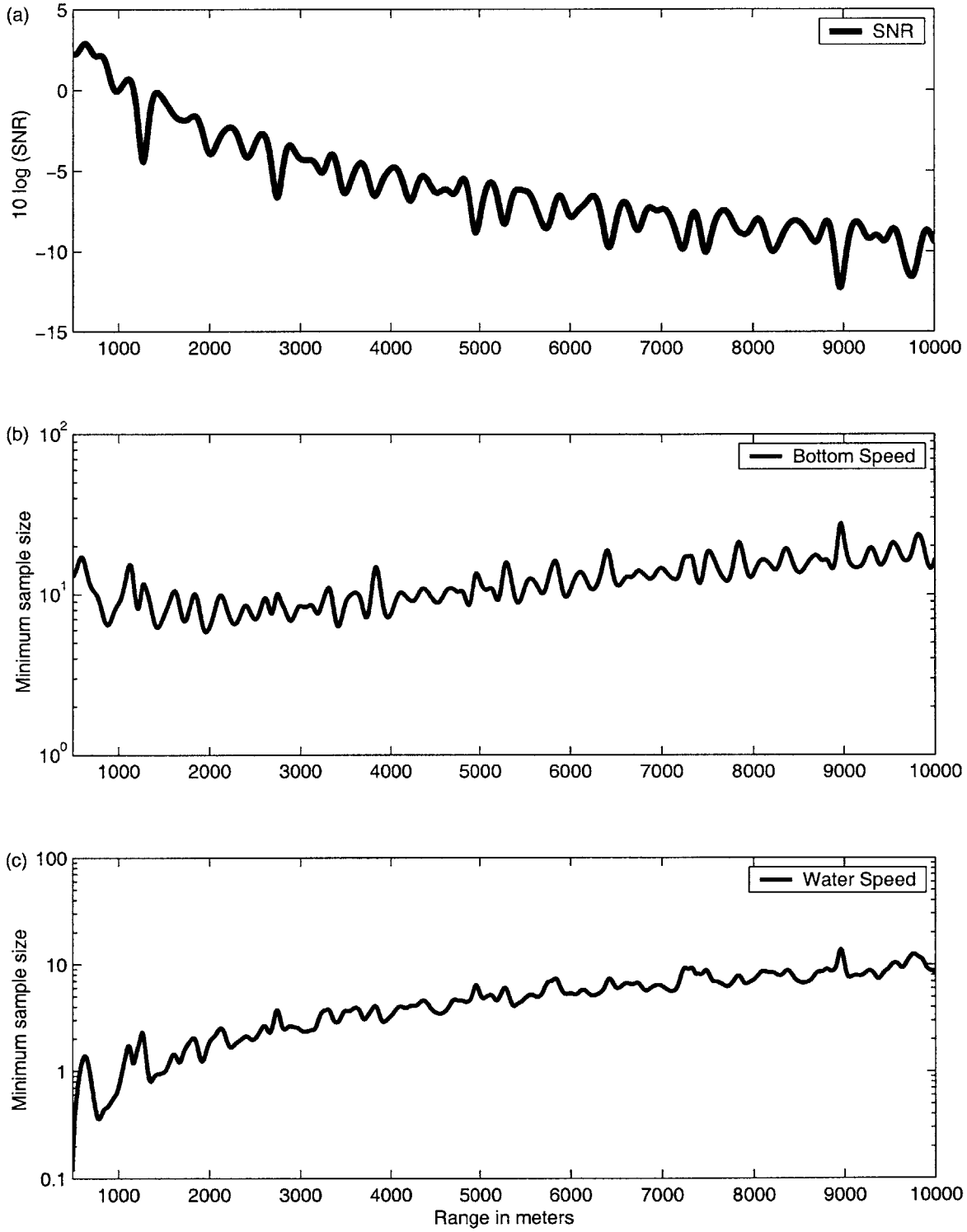

Figure 3-3: SNR versus range and necessary sample sizes for an inversion for parameters c_s and c_w in the Case A waveguide for a lower range of SNRs to attain the Cramer Rao Lower Bound.

order variance term increases more quickly with decreased SNR than the first order term. Again unlike the result for bias, the minimum sample size for both the c_s and the c_w estimates to attain the CRLB are well above unity for this range of SNRs. For the water speed estimate, the minimum sample size is very low at the highest value of 10 log SNR of about 3dB but grows in a pattern that definitely appears to be linked quite strongly to the SNR curve to a value of 10 samples. The bottom sound speed estimate requires 10-20 samples for this range of SNRs.

3.2.2 Estimate of c_w and c_s with higher SNRs

The previous example is performed using a range of SNRs that are relatively low compared to those generally used for geoacoustical inversions. The example gives a good impression of the possibility of non-negligible values for estimator bias and non-minimum variance in such regimes. To illustrate how the three statistical moment terms behave in regimes with higher SNR, the previous example is repeated for the exact same scenario but where 10 log the SNR at 1 km is set to 15 dB instead of 0 dB. The results are shown in Figure 3-4 through 3-6. In Figure 3-4, the values of the square root of first and second order variance and the first order bias of the two parameter estimates are shown; c_s in Figure 3-4a and c_s in the Figure 3-4b. The curves in the two graphs appear to be *exactly* the same shape, when drawn on a logarithmic scale, as those generated for the lower SNRs in Figure 3-1. The curves have merely shifted down the y-axis to lower values due to the reduction in SNR. However, the three curves shift by differing amounts. The square root of the CRLB shifts by a factor proportional to $\mathrm{SNR}^{-\frac{1}{2}}$ while the square root of the second order variance and the first order bias shift by a factor proportional to SNR^{-1}. As the curves in Figures 3-5 and 3-6 are generated from those in Figure 3-4 they too are the same shape as those for the lower SNRs but shifted down. This is an important result, that comes from a yet unpublished analytical relation between SNR and sample size. Essentially, the terms of the bias and variance expansions discussed in the Introduction are really proportional to inverse powers of SNR *and* sample size so once values are generated for a particular sample size and SNR they can be scaled in a predictable way for

another SNR or sample size. Therefore, for further examples in this thesis, I show the results generated for scenarios where 10 log the SNR at 1 km is fixed as 15 dB since generating results for different SNRs is only a matter of scaling.

The biases for the two estimates shown in Figure 3-4 are so low as to be definitely considered negligible and hence the minimum sample sizes shown in Figure 3-2 are also very low. The bias for the bottom speed estimate is roughly one thousandth of the true value of the parameter at the close ranges where the signal has not adequately penetrated the bottom. The minimum sample sizes for the two estimates to be considered to have attained the CRLB per our condition which are shown in Figure 3-3 are also less than one. However the CRLB itself for the bottom speed estimate is roughly 10 m/s for this set of SNRs which is on the verge of being significant error.

3.3 Estimates performed in the Case B waveguide

The Pekeris waveguide of Case A is not a good model of a typical shallow water environment because bottom attenuation is neglected. Also, most geoacoustic inversions are performed in waters where there are, or there are presumed to be, layers of sediment overlying a basement instead of sediment half-spaces. Many real-world shallow water environments can be successfully approximated with models similar to Case B.

3.3.1 Single parameter estimate

Figure 3-7 illustrates the results generated in the Case B waveguide of an inversion for the parameter c_s. Important to keep in mind is that, while in the Case A example the SNR at 1 km is 0 dB, in this example and in all successive examples involving Case B waveguide, the SNR at 1 km is 15 dB. Therefore, the range of values of SNR tested is from 2-18 dB, similar to those typically used in geoacoustic inversions.

Again, the dashed, lighter curve shows the first order bias and the black and gray solid curves show, respectively, the square roots of the absolute values of the first and second order variance terms, all as a function of source to receiver array range. All

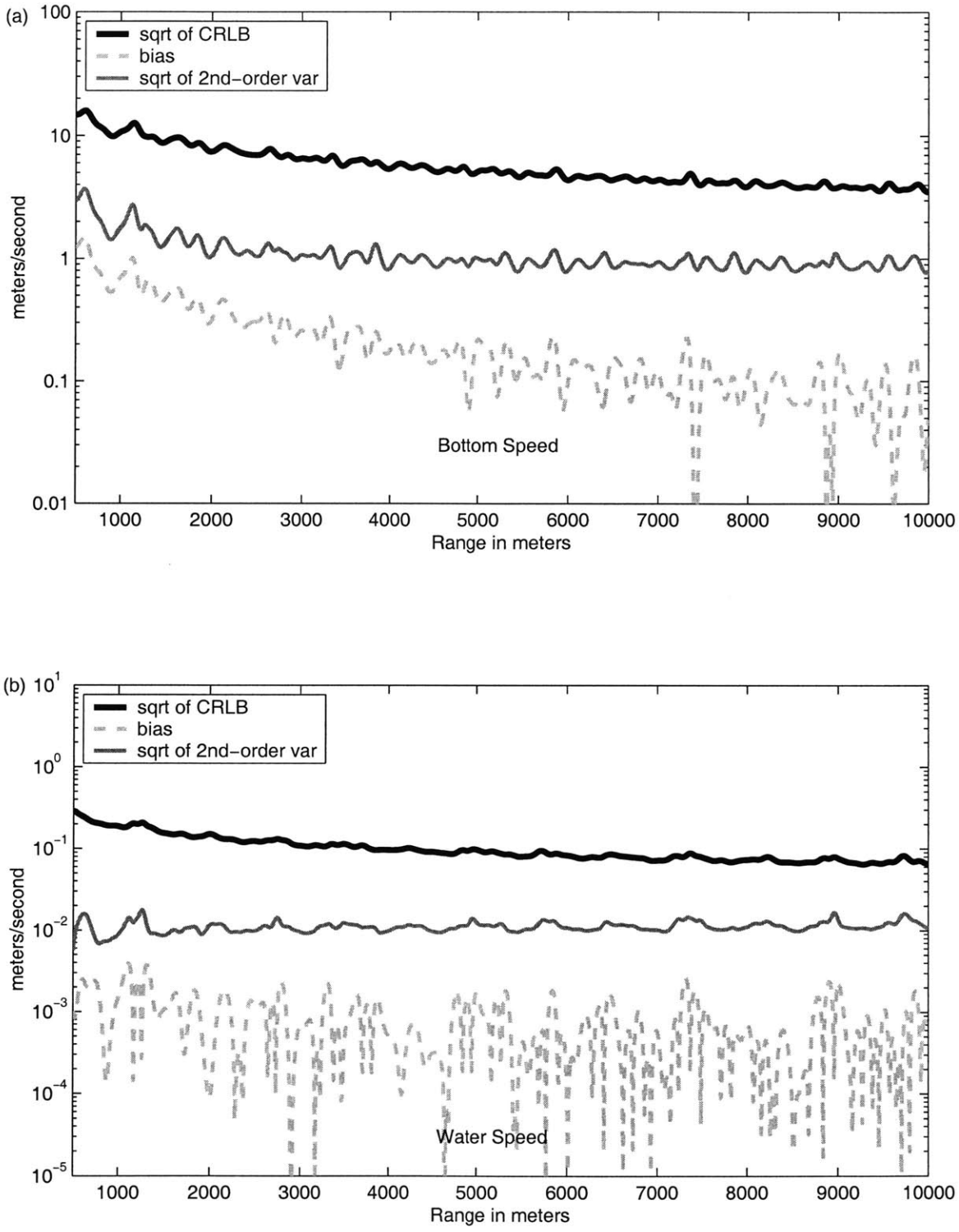

Figure 3-4: Bias and variance terms for an inversion for parameters c_s and c_w in the Case A waveguide for a higher range of SNRs.(See next figure for SNR vs. range.)

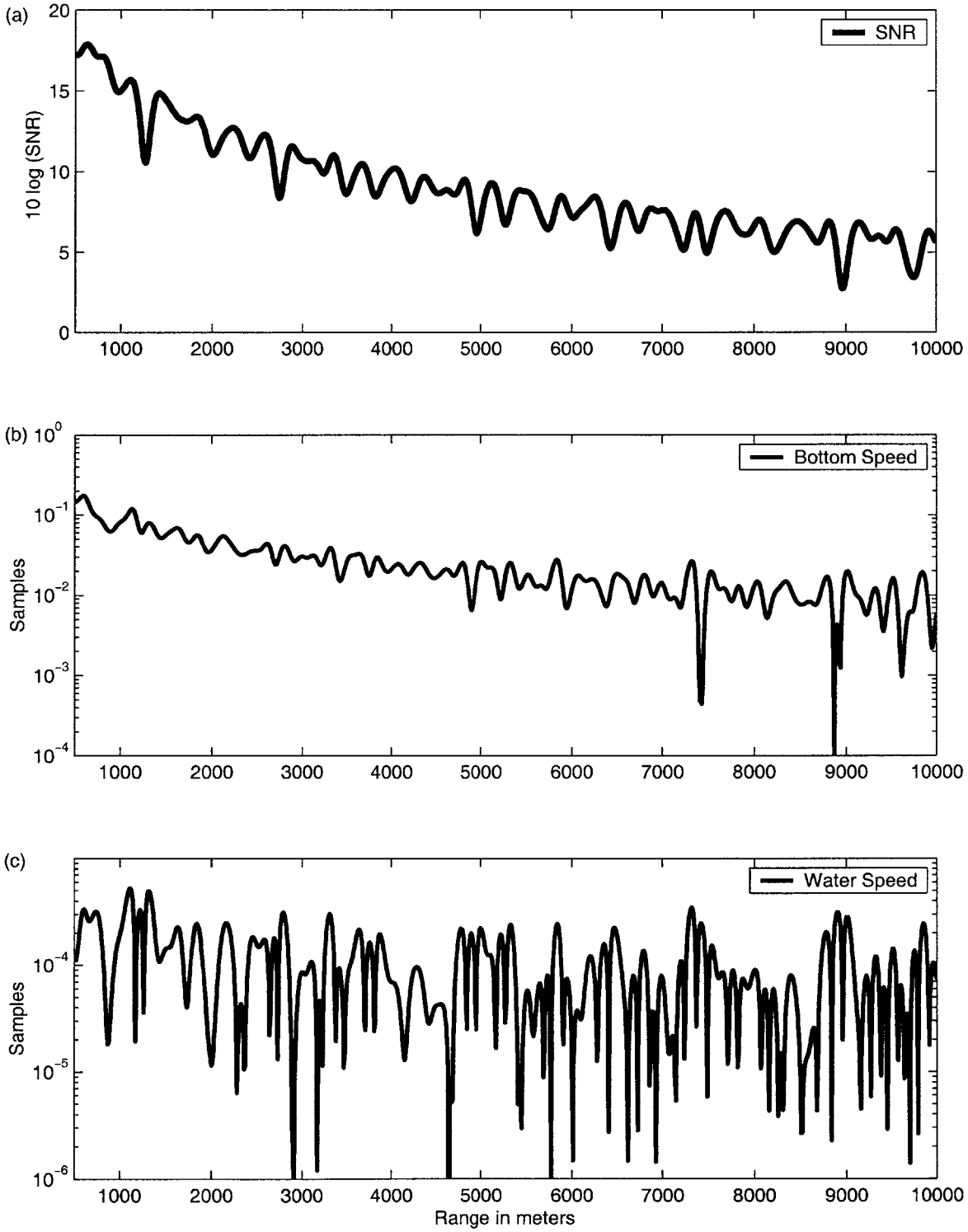

Figure 3-5: SNR versus range and necessary sample sizes for estimates of parameters c_s and c_w in the Case A waveguide for a higher range of SNRs to be asymptotically unbiased.

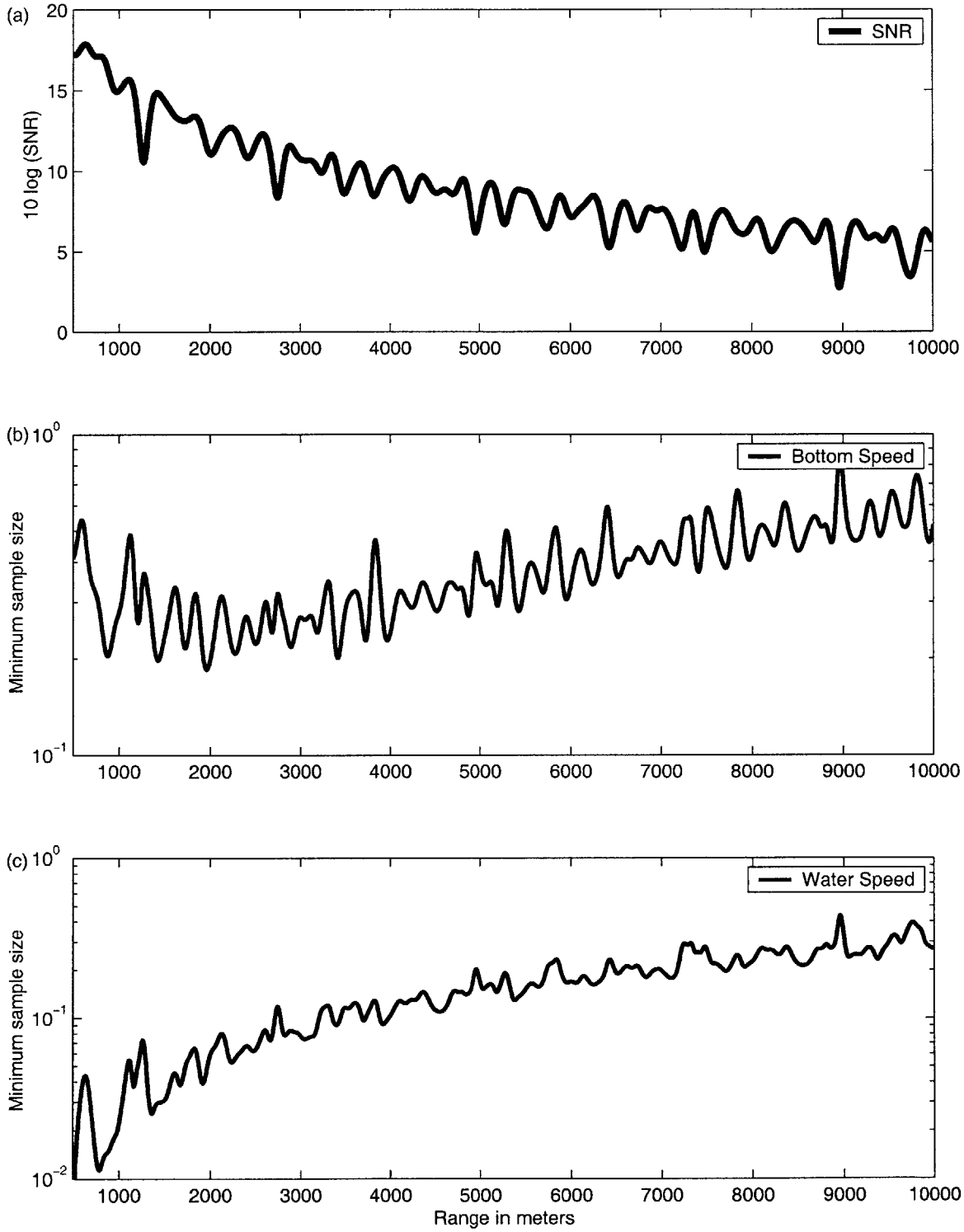

Figure 3-6: SNR versus range and necessary sample sizes for an inversion for parameters c_s and c_w in the Case A waveguide for a higher range of SNRs to attain the Cramer Rao Lower Bound.

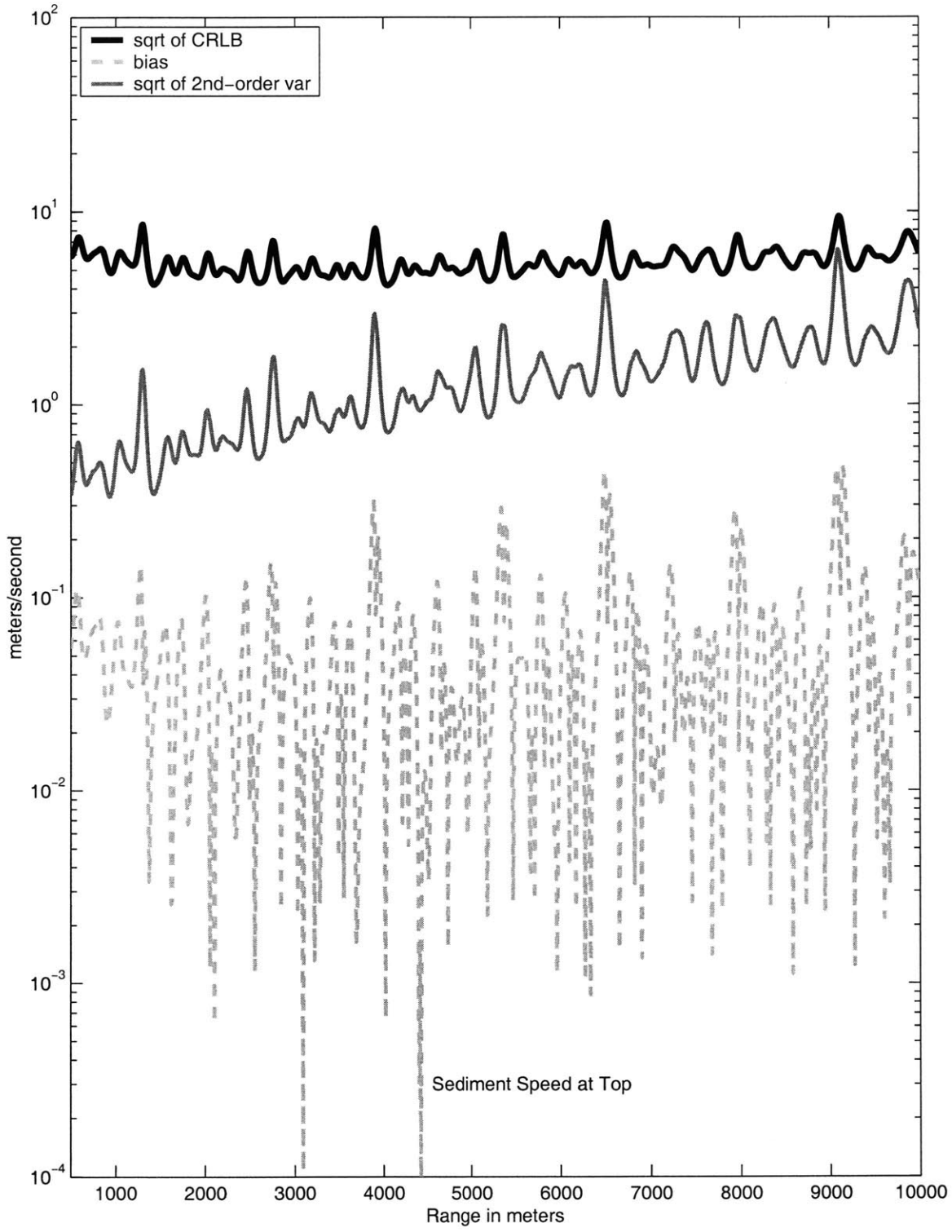

Figure 3-7: Bias and variance terms for an inversion for parameters c_s in the Case B waveguide.(See next figure for SNR vs. range.)

the values are for a single sample.

At a range of 500m the first order bias has a value of close to 10^{-1} m/s. As range is increased, the bias value oscillates from as low as 10^{-3} m/s to as high as 5×10^{-1} m/s. However, there is a general increase of this term as the range goes up, as SNR goes down. The peak value of the bias, $\approx 5 \times 10^{-1}$ m/s, is very small compared to the true value of the parameter, 1.6×10^{3} m/s.

The square-root of the first order variance is quite stable at a value between $5 - 10$ m/s, about $\frac{1}{100}$ of the value of the parameter, for all the ranges and SNRs. The square root of the second order variance, while at 500 m range has a value of about 3 m/s, gradually creeping up as range is increased until, at 10 km (2 dB for 10 log the SNR), it is about 4 m/s, peaking around 8 m/s at 9 km, just under the value of the square root of the first order variance at that range. The general pattern of increase in the three statistical quantities, which is more evident in later examples, is due to the decrease in SNR resulting from spreading as well as attenuation in the sediment. Bottom attenuation leads to stripping of higher order modes and hence loss of sensitivity to acoustical parameters in the received field

In essence, this graph shows that, for a single sample, the c_s estimate is essentially unbiased, that for higher SNRs, the second order variance, and ostensibly each of the additional higher order variance terms, is low in comparison to the first order variance and that for low SNRs the second order variance is large enough to warrant additional samples. The CRLB of roughly 6 m/s is on the verge of being negligible as an error for applications in shallow water acoustics.

Figures 3-8 and 3-9 show the minimum sample size for the c_s estimate to be considered unbiased and to attain the CRLB, respectively, as calculated per Equations 1.10 and 1.8. Shown in Figure 3-8a is the input signal-to-noise ratio at all tested ranges. As discussed before, due to the method of holding source level fixed while moving the source away from the receiver, the SNR decreases as range is increased. Therefore, at higher ranges, and hence lower SNRs, the number of samples required for any inversion is expected to be higher. For this single parameter inversion, the result suggested by the previous figure, that this estimate is essentially unbiased, is

reinforced in Figure 3-8b, as the required number of samples oscillates never grows beyond 8×10^{-2} m/s. One sample is all that is required to ensure that this particular estimate more than meets our bias minimization condition.

In Figure 3-9b, it is shown that at an initial range of 500 m (10 log SNR of 18dB) the samples required is about 3×10^{-2} and remains less than 1 until 4 km (8 dB), indicating for this range of SNRs that a single sample is all that is required to meet our criterion for attainment of the Cramer-Rao Lower Bound, beyond 4 km the minimum sample size continues to grow, peaking at about 9 km, at a value of 4 samples: the first indication that situations could arise where a single sample is not enough to meet our necessary condition on Cramer-Rao Lower Bound attainment for estimates in the Case B waveguide.

In summary of this example, the sound speed at the top of the sediment layer does not seem to be a difficult parameter to estimate when it is the only unknown. Bias of this estimate does not appear to be a problem for the full range of SNRs. Although the gap between the second and first order variance terms lessens for lower SNRs, at none of the tested SNRs does there seem to be serious need for concern about the variance of the estimate.

3.3.2 Two parameter estimate of c_s and ρ_s

The previous example provides insight into the behavior of the variance and bias for an inversion for a single parameter. Hardly ever is only one parameter of an environment unknown and therefore typically multiple parameters are estimated simultaneously. Figures 3-10 through 3-12 illustrate the effect on the variances and biases of parameter estimates of adding additional parameters to an inversion. Now, both the previous parameter, the sediment sound speed at the top of the sediment layer, c_s, and another parameter, the sediment density, ρ_s, are being estimated.

Figures 3-10a and 3-10b are in the same format as the graphs in Figure 3-7 with an identical line-shading scheme for the first order bias, and the the square root of first and second order variances. Figure 3-10a shows the three statistical moment terms for the c_s estimate and Figure 3-10b shows them for the ρ_s estimate.

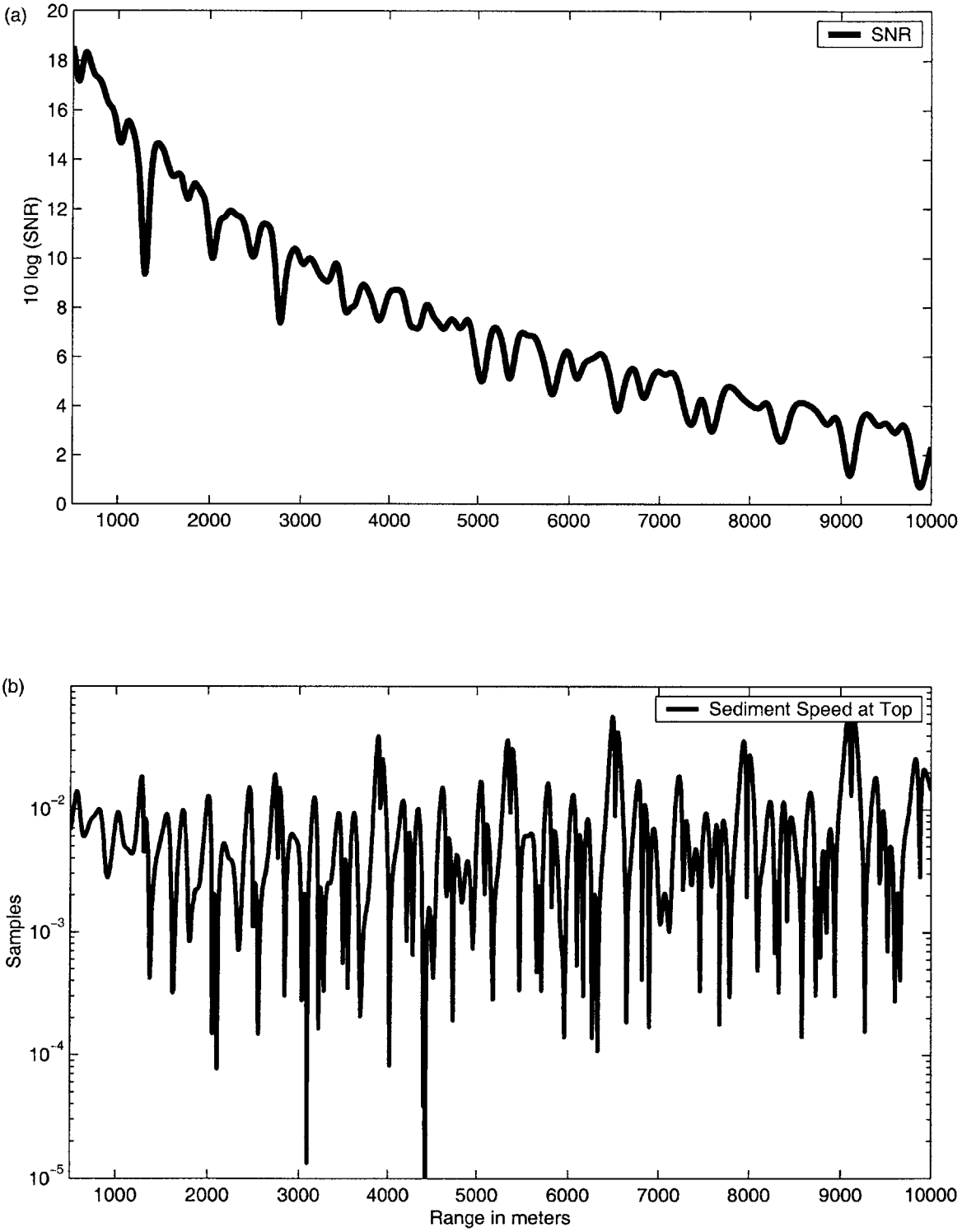

Figure 3-8: SNR versus range and necessary sample sizes for the bias of an estimate of parameter c_s in the Case B waveguide to be asymptotically unbiased.

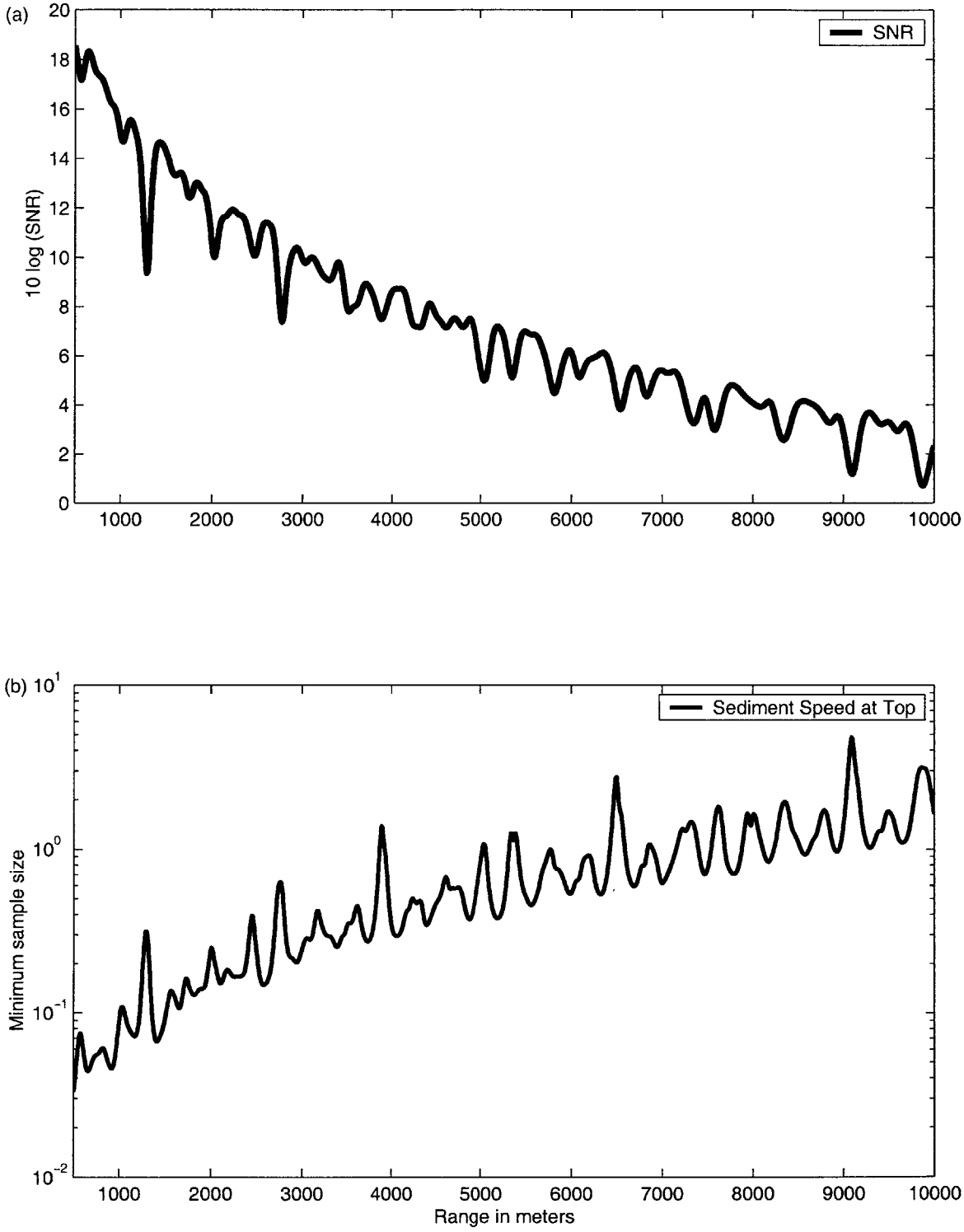

Figure 3-9: SNR versus range and necessary sample sizes for an inversion for parameter c_s in the Case B waveguide to attain the Cramer Rao Lower Bound.

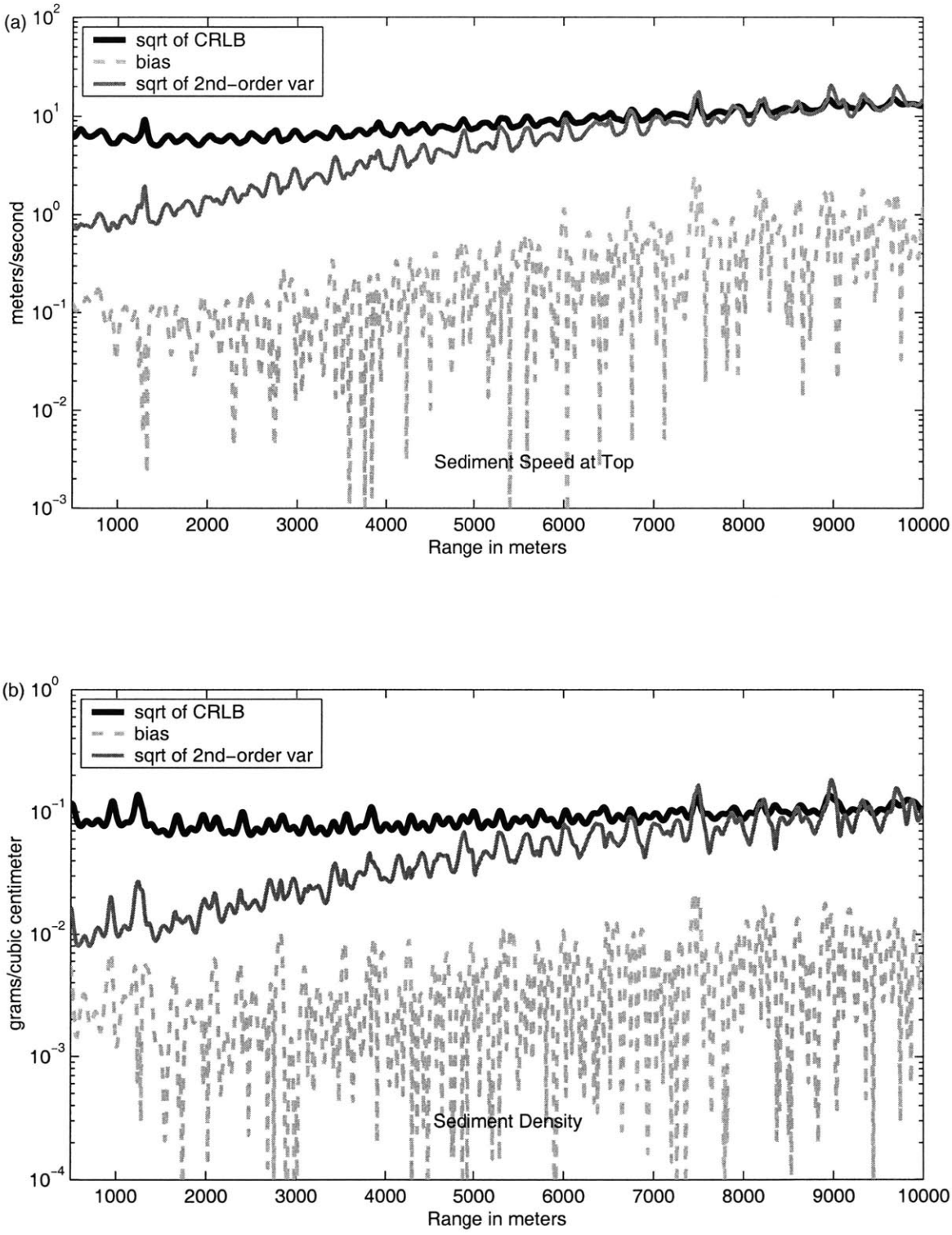

Figure 3-10: Bias and variance terms for an inversion for parameters c_s and ρ_s in the Case B waveguide.(See next figure for SNR vs. range.)

Examination of Figure 3-10a reveals information about how additional unknowns affect the resolution of parameters. It can be directly compared to Figure 3-7 to show how, all other things kept the same, the addition of ρ_s into the vector of inversion parameters has affected the resolvability of the sediment speed at the top of the sediment layer.

Like the first order bias in Figure 3-7, the bias in Figure 3-10a begins between 10^{-2} and 10^{-1} m/s at lower ranges and, as range is increased and the SNR decreased, oscillates around a gradually increasing mean value. However, while in Figure 3-7a the bias peaks just barely below a value of one, in Figure 3-10a the average value of the bias has definitely exceeded 1 m/s by 10 km and peaks at about 2 m/s. This bias in the sound speed is large enough when compared to the true value of the parameter, 1600 m/s, to cause a significant change in the refraction between the water/sediment layer. More samples are required to make the estimate asymptotically unbiased.

The square root of the first order variance remains close to 10 m/s, as it did in the single parameter inversion example. The most obvious and important difference between Figures 3-7a and 3-10a is the behavior of the second order variance. This quantity begins, at a range of 500 m, at a value just below 1 m/s and grows steadily, as range is increased, to a value just over 10 m/s at 10 km range. Essentially, the second order variance curve from Figure 3-7a has moved higher and grown steeper due to the addition of the second unknown. This indicates that if the density is unknown the sediment speed is more difficult to estimate.

Figure 3-10b shows the three statistical moment terms that describe the estimate for sediment density. For the ranges shown, the first order bias oscillates between 10^{-5} and 10^{-2} g/cc, with a gradual upward creep in the steady state value as the SNR is decreased. However, at no range or SNR is this bias comparable to the true value of the parameter, which is 1.75 g/cc.

The square root of the first order variance holds fairly steady, as is the case for the c_s estimate in the previous example, around a value of 10^{-1} g/cc, about $\frac{1}{10}$ of the true value. The square root of the second order variance, exhibits more drastic behavior, beginning at a value of 10^{-2} g/cc at a range of 500 m and growing rapidly

as range is increased to a value of 10^{-1} g/cc, a value *equal* to the first order variance at this range. In summary, this graph shows that the density estimate tends to be unbiased for all ranges and the Cramer-Rao Lower Bound is attained except at all the lowest SNRs.

Figure 3-11 shows the minimum sample size required for the estimates of the two parameters to be considered unbiased. The graphs in this figure are similar in structure and line styles to Figure 3-8 in the single parameter example. Figure 3-11b shows the minimum sample size for the c_s estimate and Figure 3-11c the minimum sample size for the ρ_s estimate.

Figure 3-11b shows that the minimum sample size for the c_s estimate ranges between 10^{-4} and $3 \cdot 10^{-1}$ with a general trend, as SNR is decreased, towards higher values. It is noteworthy that when compared to Figure 3-8b, the comparable graph from the single parameter example, the minimum sample size has generally increased and become steeper due to the addition of density as a second parameter.

In Figure 3-11c, the minimum sample size oscillates between 10^{-4} and 10^{-1}: a single sample is enough to meet our requirement for low estimate bias.

Figure 3-12 shows the sample size necessary to attain the Cramer-Rao Lower Bound for each of the two inversion parameters. Figures 3-12b and 3-12c show the minimum sample size for the estimate of the sediment speed at the top of the sediment layer, c_s, and that of the sediment density, ρ_s, respectively.

The curve in Figure 3-12c shows that a single sample meets our condition for the estimate to attain the CRLB out to a range of 3 km (10 log SNR of about 10 dB), at which point the minimum sample size exceeds 1, eventually growing to 10 samples at 10 km. Comparison of Figure 3-12b with Figure 3-9b, in the spirit of examining the progression from a single parameter inversion to a double parameter inversion, reveals the most interesting information. Basically, while, in Figure 3-9b, the minimum sample size grew from 0.1 to just over 4, the minimum sample size in Figure 3-12b grows from 0.1 at low ranges and large SNRs to nearly 20 samples at high ranges and low SNRs, a difference caused entirely by the addition of the parameter, ρ_s, to the parameter vector. Twenty samples is not a prohibitive number but it is

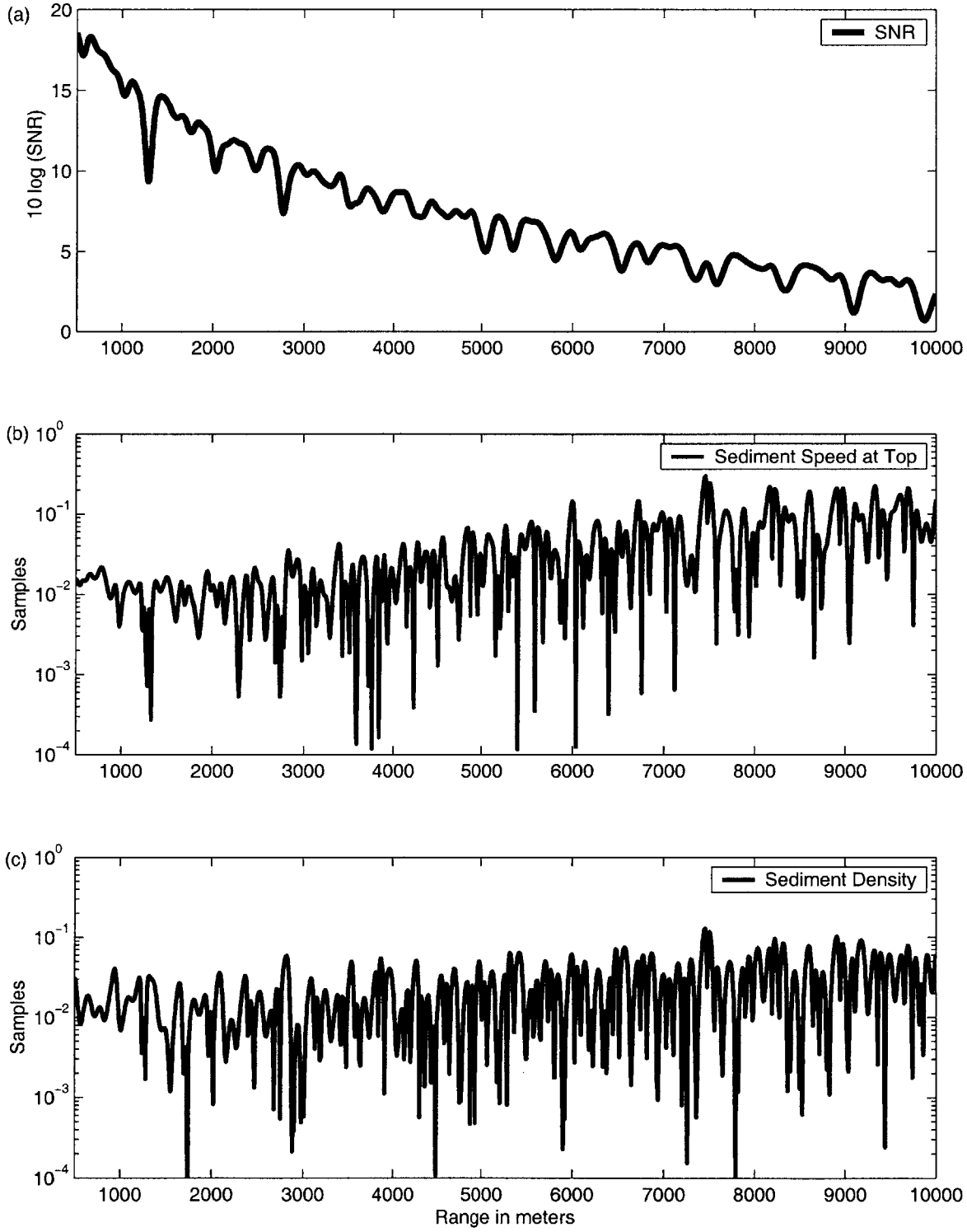

Figure 3-11: SNR versus range and necessary sample sizes for estimates of parameters c_s and ρ_s in the Case B waveguide to be asymptotically unbiased.

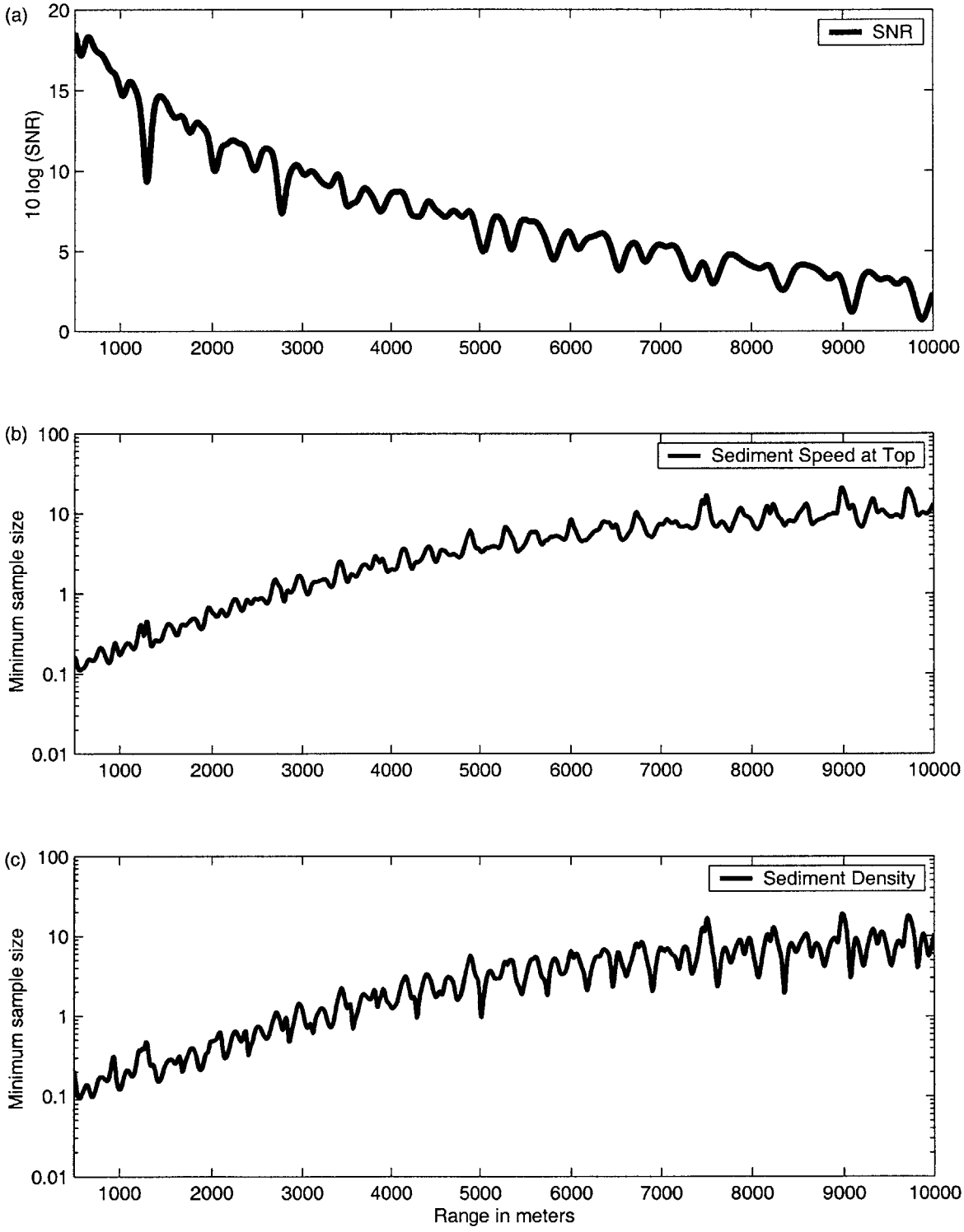

Figure 3-12: SNR versus range and necessary sample sizes for an inversion for parameters c_s and ρ_s in the Case B waveguide to attain the Cramer Rao Lower Bound.

worth recalling that there are only two unknowns in this inversion, while practical applications of geo-acoustic inversions typically have as many as eleven unknowns [5]. Should the trend continue towards a rapid increase in sample size with increased length of the parameter vector to be estimated, minimum sample sizes to guarantee that the Cramer-Rao Lower Bound is attained may, indeed, become prohibitively large.

3.3.3 Difficulty of estimating density and sound speed together in the ocean bottom

Some intuition about why the simultaneous estimation of density and compressional wave speed in the ocean bottom can lead to larger variances and biases can be gained by looking at some limiting examples. Information about the bottom parameters comes from source signal waves reflected off the various interfaces and possibly from waves refracted back up to the receivers after having passed through the sedimentary layers. This makes it informative to explore how the parameters we are trying to estimate affect the reflection coefficient at the interfaces.

Single reflected plane wave A field generated by a single plane wave reflecting from a halfspace as depicted in Figure 3-13 is a function of the Rayleigh reflection coefficient, $\mathcal{R}$, which is itself a function of the halfspace densities, ρ and ρ_1, sound speeds, c and c_1, and the angle of incidence, Θ,

$$\mathcal{R}(\rho_1, c_1, \Theta) = \frac{c_1\rho_1 \cos\Theta - \rho\sqrt{c - c_1 \sin^2\Theta}}{c_1\rho_1 \cos\Theta + \rho\sqrt{c_1 \sin^2\Theta}} \tag{3.1}$$

The likelihood function is also a function of $\mathcal{R}$. For this case, we can calculate the Fisher information matrix for the simultaneous estimation of ρ_1 and c_1:

$$\frac{\partial \ell}{\partial c_1} = \frac{\partial \mathcal{R}}{\partial c_1}\frac{\partial \ell}{\partial \mathcal{R}} \qquad \frac{\partial \ell}{\partial \rho_1} = \frac{\partial \mathcal{R}}{\partial \rho_1}\frac{\partial \ell}{\partial \mathcal{R}}$$

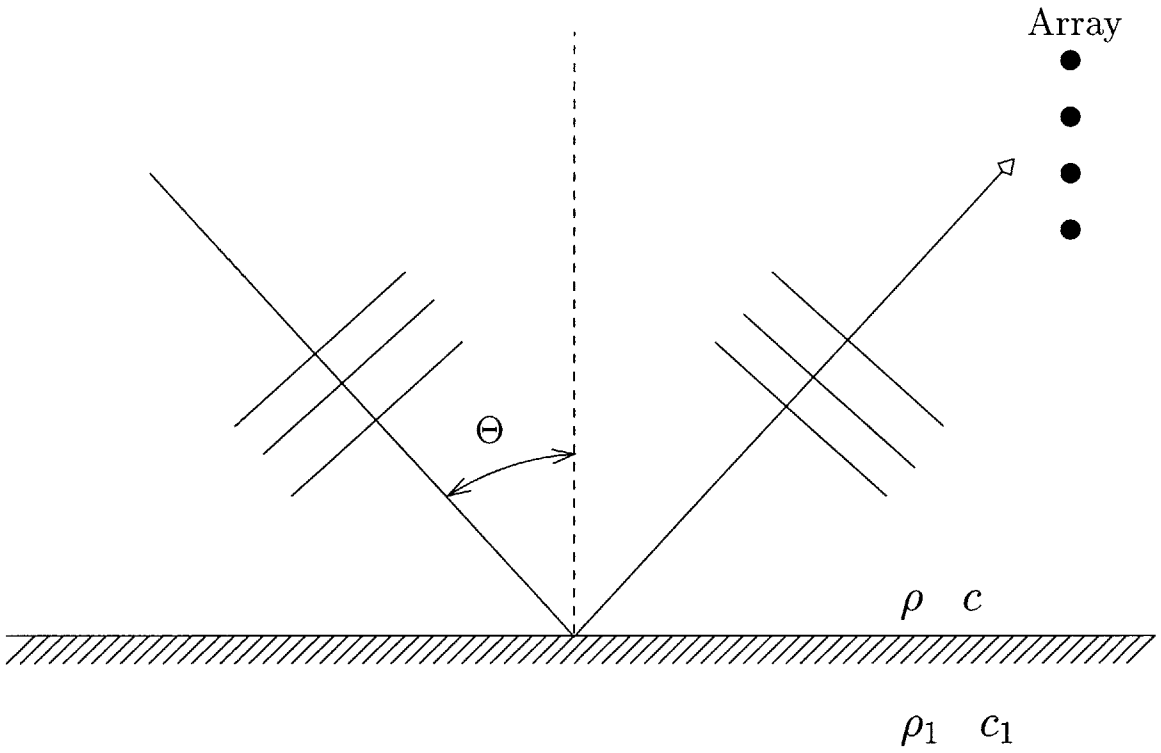

Figure 3-13: Single plane wave reflecting off a acoustic impedance interface.

$$E\left[\frac{\partial^2 \ell}{\partial {c_1}^2}\right] = E\left[\frac{\partial}{\partial c_1}\left(\frac{\partial \mathcal{R}}{\partial c_1}\frac{\partial \ell}{\partial \mathcal{R}}\right)\right] = \left(\frac{\partial \mathcal{R}}{\partial c_1}\right)^2 E\left[\frac{\partial^2 \ell}{\partial \mathcal{R}^2}\right]$$

$$E\left[\frac{\partial^2 \ell}{\partial {\rho_1}^2}\right] = \left(\frac{\partial \mathcal{R}}{\partial \rho_1}\right)^2 E\left[\frac{\partial^2 \ell}{\partial \mathcal{R}^2}\right]$$

$$E\left[\frac{\partial^2 \ell}{\partial \rho_1 \partial c_1}\right] = E\left[\frac{\partial}{\partial \rho_1}\frac{\partial \mathcal{R}}{\partial c_1}\frac{\partial \ell}{\partial \mathcal{R}}\right] = \frac{\partial \mathcal{R}}{\partial \rho_1}\frac{\partial \mathcal{R}}{\partial c_1} E\left[\frac{\partial^2 \ell}{\partial \mathcal{R}^2}\right]$$

$$i = E\left[\frac{\partial^2 \ell}{\partial \mathcal{R}^2}\right] \cdot \begin{pmatrix} \left(\frac{\partial \mathcal{R}}{\partial c_1}\right)^2 & \frac{\partial \mathcal{R}}{\partial \rho_1}\frac{\partial \mathcal{R}}{\partial c_1} \\ \frac{\partial \mathcal{R}}{\partial \rho_1}\frac{\partial \mathcal{R}}{\partial c_1} & \left(\frac{\partial \mathcal{R}}{\partial \rho_1}\right)^2 \end{pmatrix}$$

The determinant of the Fisher information Matrix is therefore given by,

$$\det(i) = E\left[\frac{\partial^2 \ell}{\partial \mathcal{R}^2}\right] \cdot \left(\left(\frac{\partial \mathcal{R}}{\partial c_1}\right)^2 \left(\frac{\partial \mathcal{R}}{\partial \rho_1}\right)^2 - \left(\frac{\partial \mathcal{R}}{\partial c_1}\right)^2 \left(\frac{\partial \mathcal{R}}{\partial \rho_1}\right)^2\right) = \underline{\underline{0}}$$

which means the inverse of i, the CRLB, becomes singular as does the variance. If both parameters are unknown neither parameter can be estimated separately but only the combination given by the acoustic impedance.

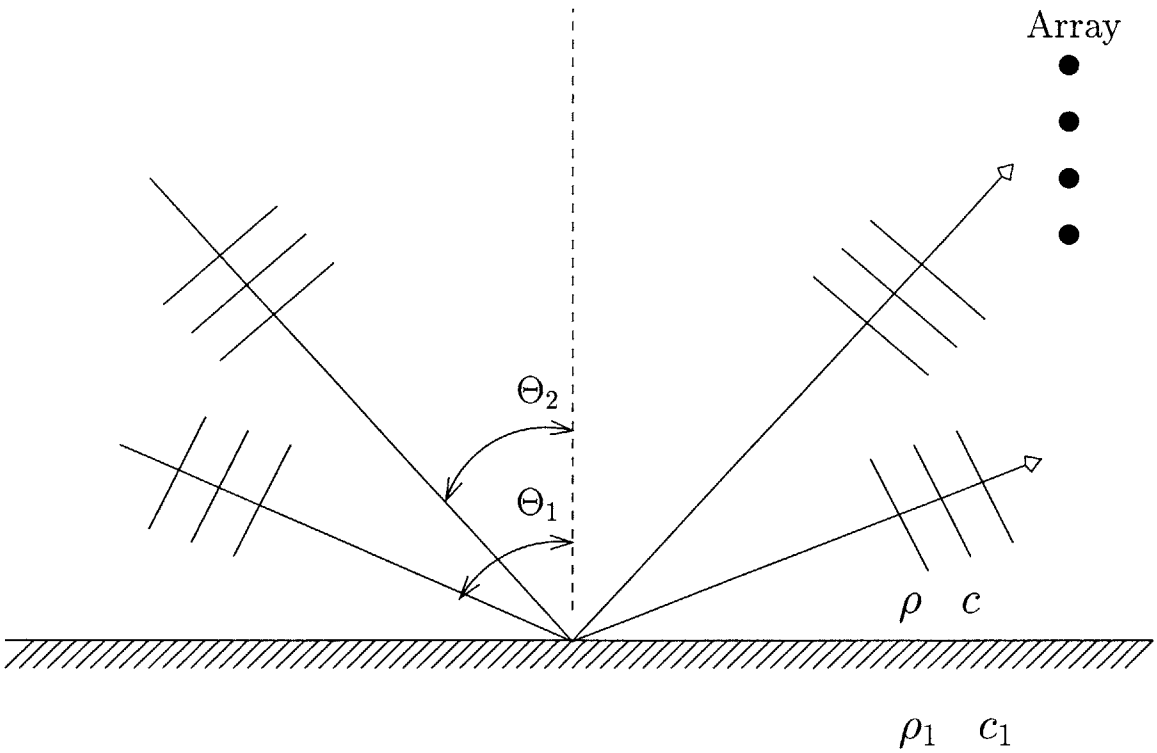

Figure 3-14: Two plane waves reflecting off a acoustic impedance interface.

Two reflected plane waves If two plane waves are incident on the interface between two media, see Figure 3-14, the likelihood function is a function of both reflection coefficients, $\ell(\mathcal{R}_1, \mathcal{R}_2)$.

$$\frac{\partial \ell}{\partial \rho_1} = \frac{\partial \mathcal{R}_1}{\partial \rho_1}\frac{\partial \ell}{\partial \mathcal{R}_1} + \frac{\partial \mathcal{R}_2}{\partial \rho_1}\frac{\partial \ell}{\partial \mathcal{R}_2}$$

$$\begin{aligned} E\left[\frac{\partial^2 \ell}{\partial {\rho_1}^2}\right] &= E\left[\left(\frac{\partial}{\partial \rho_1}\frac{\partial \ell}{\partial \mathcal{R}_1}\right)\left(\frac{\partial \mathcal{R}_1}{\partial \rho_1}\right) + \left(\frac{\partial}{\partial \rho_1}\frac{\partial \ell}{\partial \mathcal{R}_1}\right)\left(\frac{\partial \mathcal{R}_1}{\partial \rho_1}\right)\right] \\ &= \left(\frac{\partial \mathcal{R}_1}{\partial \rho_1}\right)^2 E\left[\frac{\partial^2 \ell}{\partial \mathcal{R}_1^2}\right] + \left(\frac{\partial \mathcal{R}_2}{\partial \rho_1}\right)^2 E\left[\frac{\partial^2 \ell}{\partial \mathcal{R}_2^2}\right] + 2\left(\frac{\partial \mathcal{R}_1}{\partial \rho_1}\right)\left(\frac{\partial \mathcal{R}_2}{\partial \rho_1}\right) E\left[\frac{\partial^2 \ell}{\partial \mathcal{R}_1 \partial \mathcal{R}_2}\right] \end{aligned}$$

$$E\left[\frac{\partial^2 \ell}{\partial c_1^2}\right] = \left(\frac{\partial \mathcal{R}_1}{\partial c_1}\right)^2 E\left[\frac{\partial^2 \ell}{\partial \mathcal{R}_1^2}\right] + \left(\frac{\partial \mathcal{R}_2}{\partial c_1}\right)^2 E\left[\frac{\partial^2 \ell}{\partial \mathcal{R}_2^2}\right] + 2\left(\frac{\partial \mathcal{R}_1}{\partial c_1}\right)\left(\frac{\partial \mathcal{R}_2}{\partial c_1}\right) E\left[\frac{\partial^2 \ell}{\partial \mathcal{R}_1 \partial \mathcal{R}_2}\right]$$

$$E\left[\frac{\partial^2 \ell}{\partial \rho_1 \partial c_1}\right] = E\left[\frac{\partial}{\partial \rho_1}\left(\frac{\partial \mathcal{R}_1}{\partial c_1}\frac{\partial \ell}{\partial \mathcal{R}_1} + \frac{\partial \mathcal{R}_2}{\partial c_1}\frac{\partial \ell}{\partial \mathcal{R}_2}\right)\right]$$

$$= \frac{\partial \mathcal{R}_1}{\partial c_1}\frac{\partial \mathcal{R}_1}{\partial \rho_1}\underbrace{E\left[\frac{\partial^2 \ell}{\partial \mathcal{R}_1^2}\right]}_{A} + \frac{\partial \mathcal{R}_2}{\partial c_1}\frac{\partial \mathcal{R}_2}{\partial \rho_1}\underbrace{E\left[\frac{\partial^2 \ell}{\partial \mathcal{R}_2^2}\right]}_{B} + \left(\underbrace{\frac{\partial \mathcal{R}_1}{\partial c_1}}_{a}\underbrace{\frac{\partial \mathcal{R}_2}{\partial \rho_1}}_{b} + \underbrace{\frac{\partial \mathcal{R}_1}{\partial \rho_1}}_{\gamma}\underbrace{\frac{\partial \mathcal{R}_2}{\partial c_1}}_{d}\right)\underbrace{E\left[\frac{\partial^2 \ell}{\partial \mathcal{R}_1 \partial \mathcal{R}_2}\right]}_{C}$$

$$i = \begin{pmatrix} \gamma^2 A + b^2 B + 2\gamma b C & a\gamma A + bdB + (ab + \gamma d)C \\ a\gamma A + bdB + (ab + \gamma d)C & a^2 A + d^2 B + 2adC \end{pmatrix}$$

A little math gives the determinant of the Fisher Information Matrix,

$$\det(i) = (ab - \gamma d)^2[AB - C^2]$$

where

$$ab - \gamma d = \frac{c \sin(\Theta_1 + \Theta_2)\sin(\Theta_1 - \Theta_2)}{(c - c_1 \sin^2 \Theta_2)^{\frac{1}{2}}(c - c_1 \sin^2 \Theta_1)^{\frac{1}{2}}} \tag{3.2}$$

Inspection of Equation 3.2, or Equation 3.1 from the single plane wave example, reveals that if both waves are perpendicular to the interface the reflection coefficient will depend only on the impedance, the determinant of i will be zero and thus there will be no information about the density and the sound speed. If the two plane waves have the same angle then again the determinant will be zero and there will be no information. This makes sense since this limits the two wave case to the single wave case previously discussed for which no information about density and sound speed can be had. For any other set of grazing angles Θ_1 and Θ_2 the determinant will be non-zero and there will be a non-infinite CRLB i.e. estimation of the two parameters simultaneously may be possible. The Pekeris waveguide studied in Case A behaves like the single reflected plane wave case if at a certain range the absorption has stripped away all but the lowest order mode.

3.3.4 Two parameter estimate of c_s and α_s

Figures 3-15 through 3-17 show similar graphs as are shown for the other examples, but now for an inversion for the sound speed at the top of the sediment layer, c_s, and the sediment attenuation, α_s. Like the previous examples in the Case B waveguides, the second order variance and first order bias grow with increased range and reduced

SNR but both values stay relatively low and therefore one sample meets our criteria on unbiasedness and CRLB attainment. Attenuation appears to be effectively unbiased but has a large first order variance so repeated sampling will be necessary to reduce the variance to a tolerable threshold, i.e. 10% of the true value.

3.3.5 Two parameter estimate of c_s and g_s

Figures 3-18 through 3-20 illustrate a related point. Once again, an example of a two parameter inversion is being performed, however, while the first inversion parameter is still the sediment sound speed at the top of the sediment layer, c_s, the second is no longer the sediment density, ρ_s, but instead the sediment sound speed gradient, g_s. By switching the second parameter and leaving everything else unchanged, it is hoped to illustrate that the resolvability, as exhibited in the bias and variance, of a particular parameter is a function not only of the number of inversion parameters but also of parameter type.

Figure 3-18 shows the values of the three statistical moment terms, the first order bias and the square root of the first and second order variance, for each of the two inversion parameters versus range between the source and receiver array; c_s in Figure 3-18a and g_s in Figure 3-18b.

When Figure 3-18a is placed alongside Figure 3-7a, the same series of comparisons as are made with Figure 3-10a can be made once more to show that, as is true with the addition of parameter, ρ_s, addition of g_s to the parameter vector increases the value of all three statistical moment terms and steepens their gradient with increasing range, especially with the second order variance. More interesting, however, is the comparison between Figure 3-18a and Figure 3-10a. Now the difference in the statistics of the c_s estimate when it is coupled with a g_s estimate instead of a ρ_s estimate, can be seen. The first order bias has increased by roughly an order of magnitude at all ranges, beginning, at 500 m, at 0.1 m/s and ending, at 10 km, at about 10 m/s, oscillating to as low as 10^{-2} m/s. The square root of the first order variance has also shifted up by a factor of roughly three with no obvious increase in the gradient. The square root of the second order variance has shifted even more, so much that it

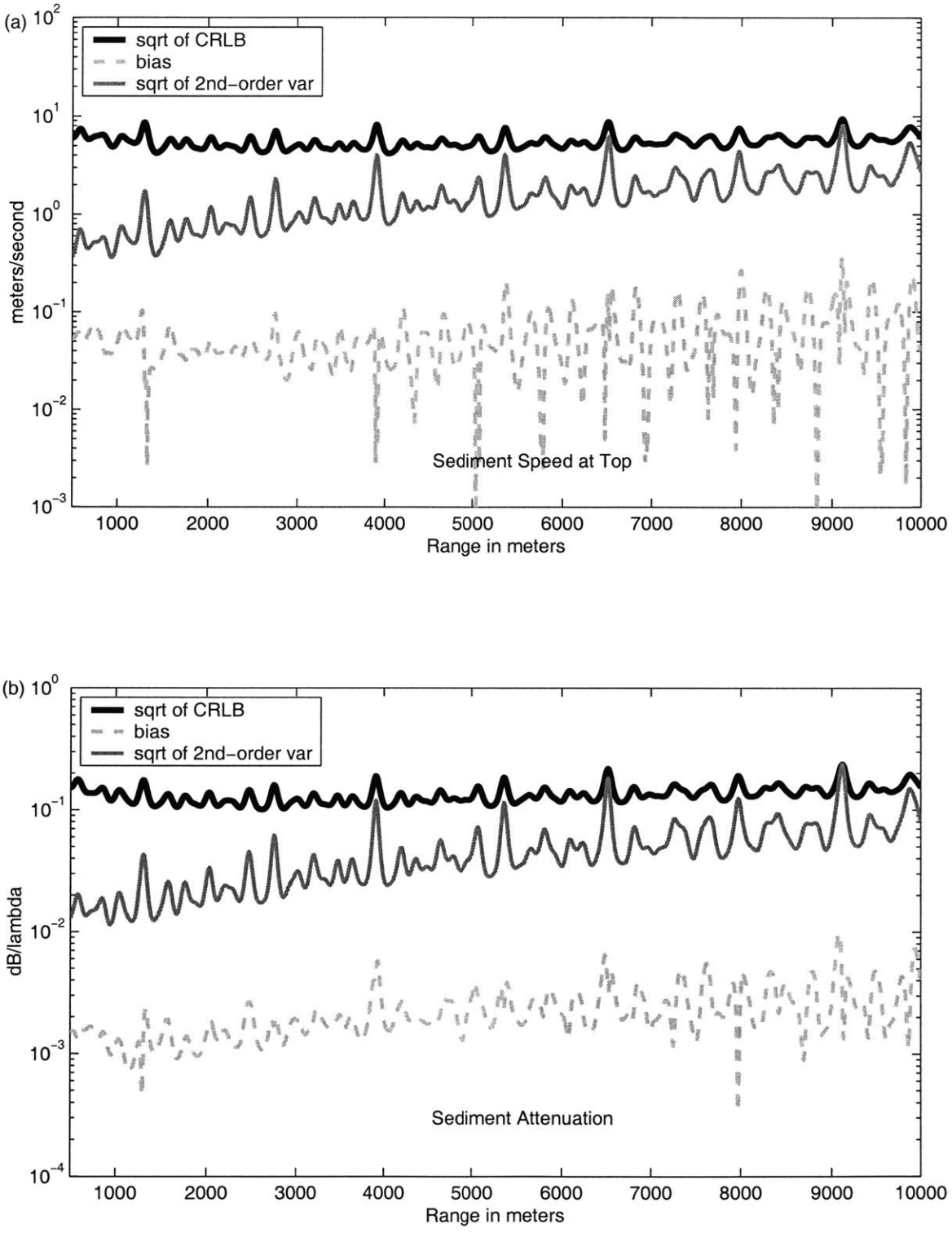

Figure 3-15: Bias and variance terms for an inversion for parameters c_s and α_s in the Case B waveguide.(See next figure for SNR vs. range.)

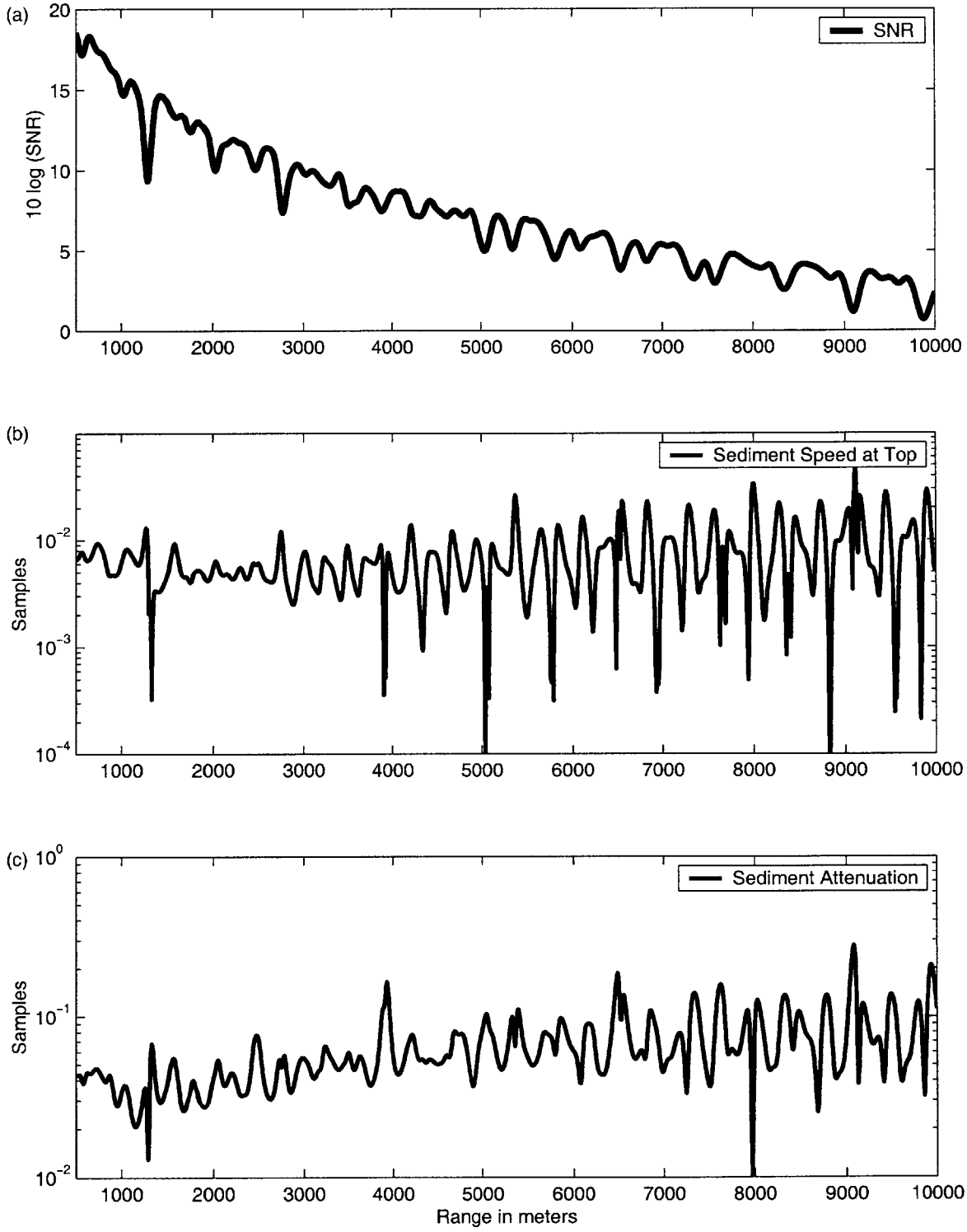

Figure 3-16: SNR versus range and necessary sample sizes for estimates of parameters c_s and α_s in the Case B waveguide to be asymptotically unbiased.

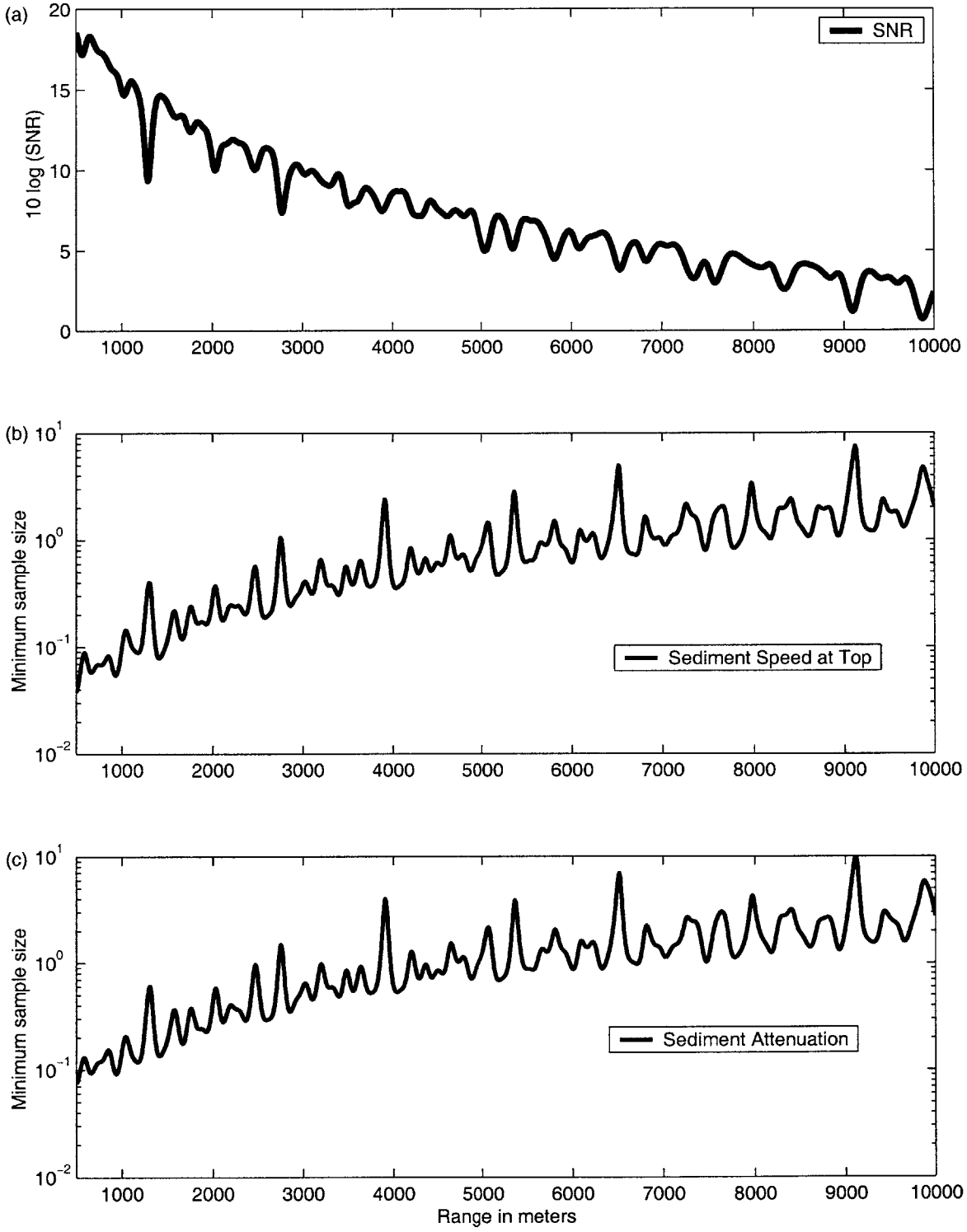

Figure 3-17: SNR versus range and necessary sample sizes for an inversion for parameters c_s and α_s in the Case B waveguide to attain the Cramer Rao Lower Bound.

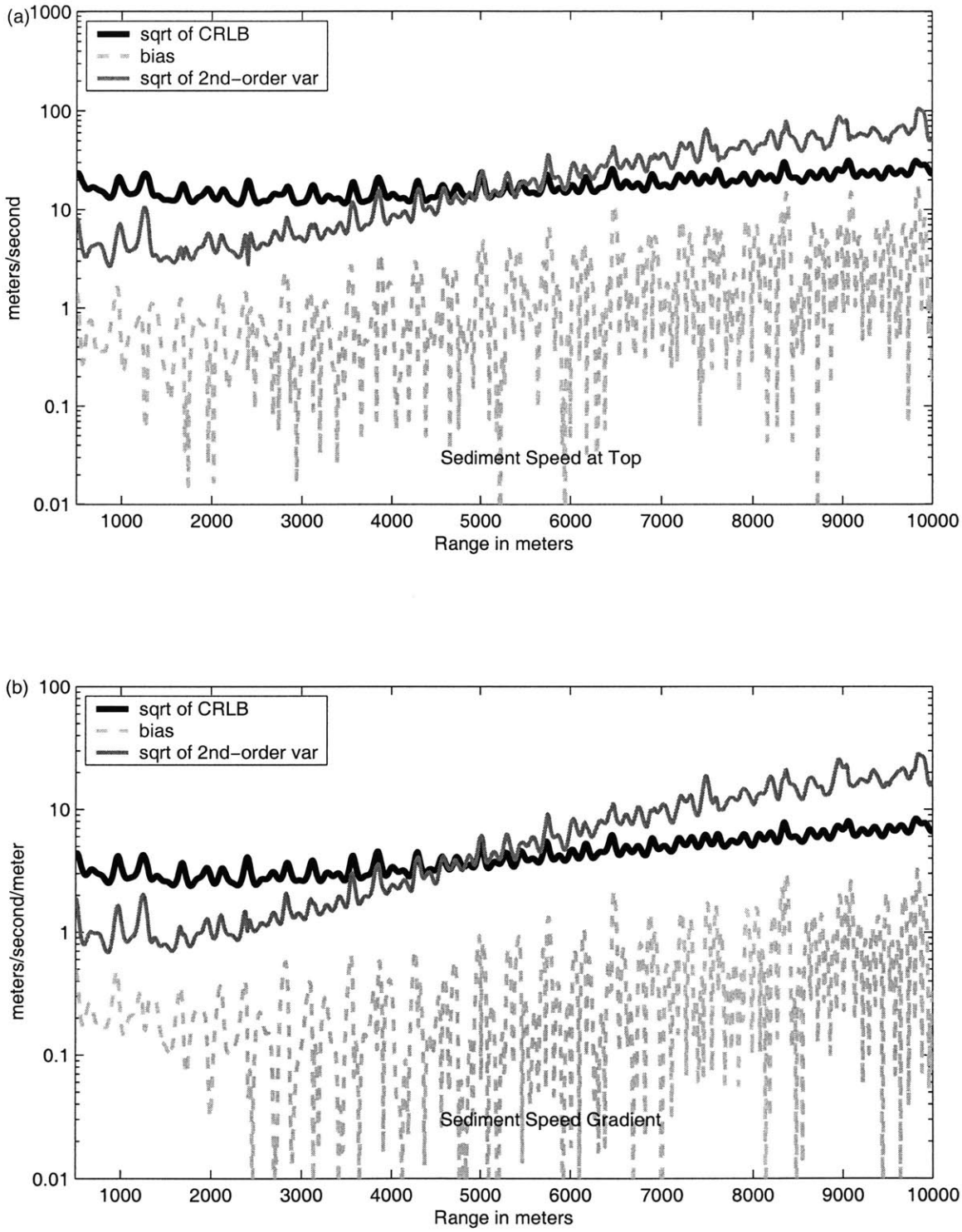

Figure 3-18: Bias and variance terms for an inversion for parameters c_s and g_s in the Case B waveguide.(See next figure for SNR vs. range.)

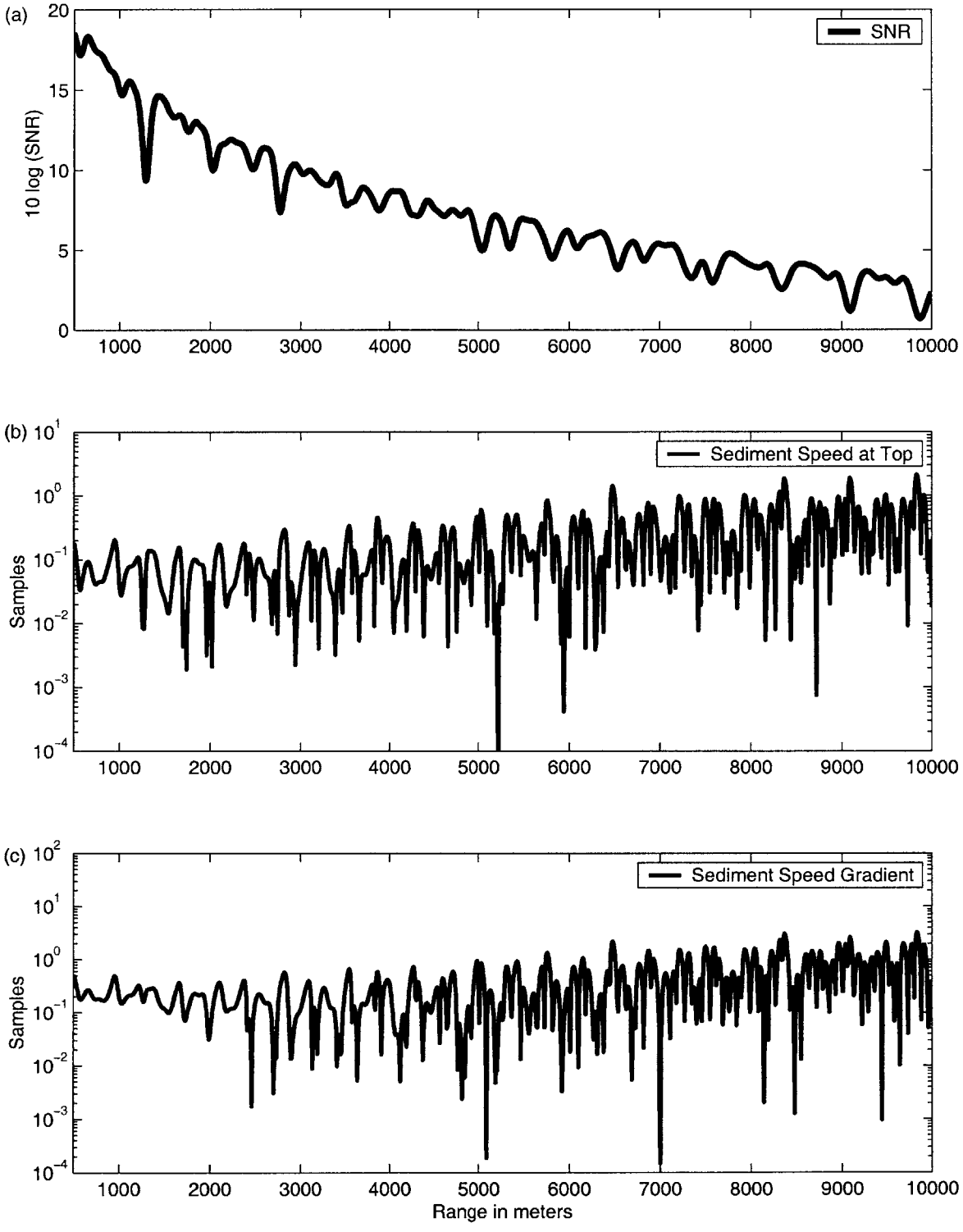

Figure 3-19: SNR versus range and necessary sample sizes for estimates of parameters c_s and g_s in the Case B waveguide to be asymptotically unbiased.

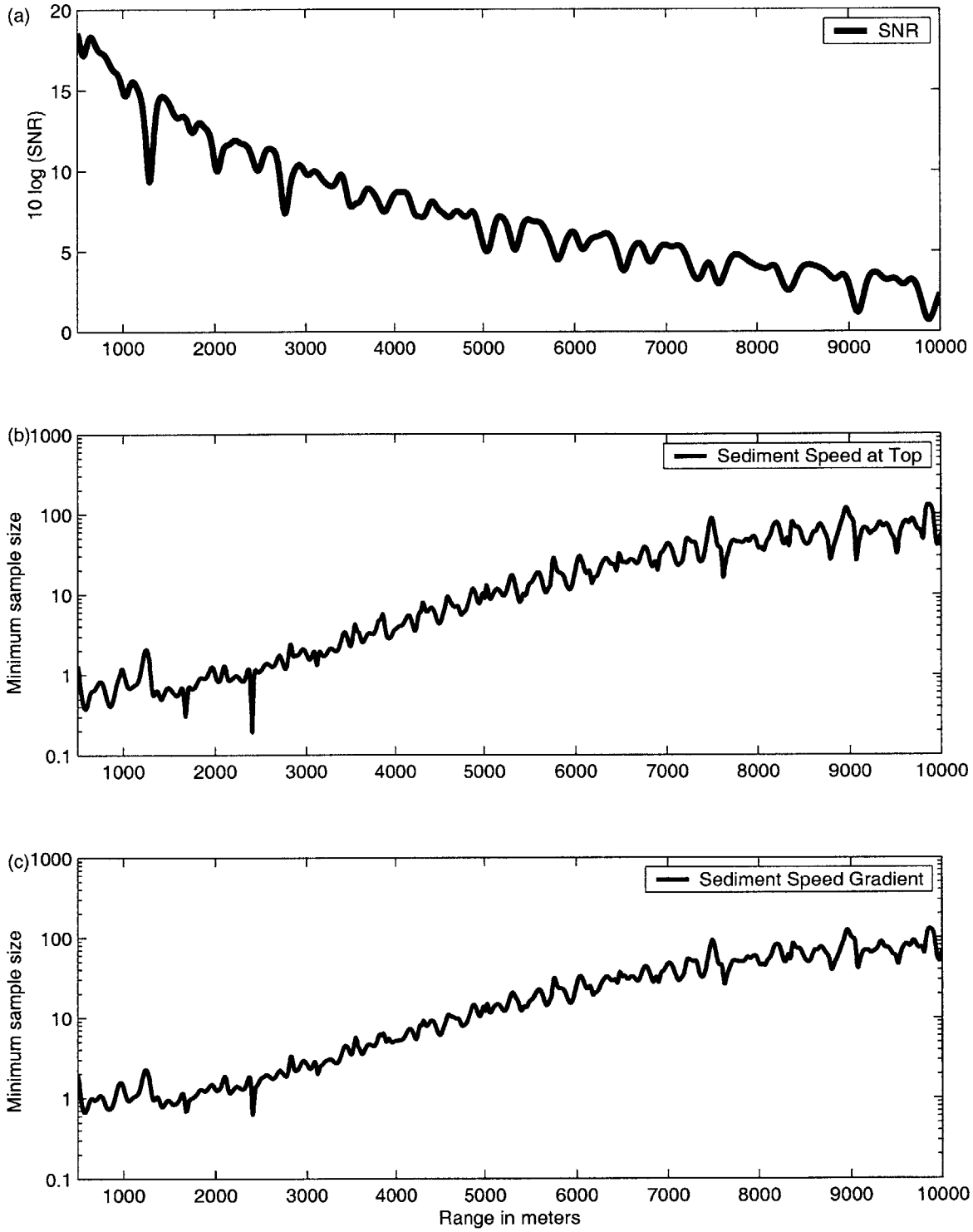

Figure 3-20: SNR versus range and necessary sample sizes for an inversion for parameters c_s and g_s in the Case B waveguide to attain the Cramer Rao Lower Bound.

actually *crosses* the first order variance at a range of 5km, where the the SNR is 5 dB, reaching, at the lowest SNRs near 0dB, a value of 100 m/s. Even at 500 m range, 10 log SNR of 18 d, the square root of the second order variance is close to 10 m/s, about ten times the value for this quantity in Figure 3-10a.

In Figure 3-18b, as is the case for the previous examples, the bias is the most oscillatory of the three quantities, varying between 10^{-3} $\frac{m/s}{m}$ and 3 $\frac{m/s}{m}$, on average increasing as range is increased. The first order variance begins at a range of 500 m with a value of about $4\frac{m/s}{m}$, growing fairly linearly to a value of about $8\frac{m/s}{m}$. Worth noting, is that $8\frac{m/s}{m}$ is the same magnitude as the true value of the parameter, $10\frac{m/s}{m}$, and as this is only the first order term of the variance expansion, it is quite possible that the sum total variance is very much larger. The second order term, grows from a value of $1\frac{m/s}{m}$ at the closest range to a value of $25\frac{m/s}{m}$ at 10 km, exceeding the first order term at about 5 km, where the SNR equals 6 dB. It is already apparent that this will yield the least favorable first order to second order variance ratio yet examined and, in light of the high values of both variance terms with respect to the true value of the parameter, this gradient, g_s, seems particularly hard to resolve.

Figure 3-19 shows the minimum sample size for the two estimates to be considered unbiased. As might be suspected from the foregoing discussion, the minimum sample size has shifted up for the c_s estimate, shown in Figure 3-19b, from its general level for the c_s/ρ_s estimate, shown in Figure 3-11b, so that at lower SNRs, the minimum sample size can be as large as 2 samples.

In Figure 3-19c, the minimum sample size for the g_s estimate is shown. For ranges up to and including 5 km, which corresponds to an SNR of 5dB, the minimum sample size for this estimate is, like all prior examples, less than one. Beyond that point, the minimum sample size frequently oscillated above 1 sample, peaking at a value of 3.

Figure 3-20 shows the minimum sample size for the variance of estimates of the c_s and g_s parameters to attain the Cramer-Rao Lower Bound. As before, Figure 3-20a shows the SNR at all ranges, Figure 3-20b the minimum sample size for the first parameter, in this case c_s, at all ranges, and Figure 3-20c, minimum sample size for the second parameter, g_s, at all ranges. In this figure, the effect of switching g_s for ρ_s

as the second inversion parameter is clearly evident.

Comparison of Figures 3-20b and 3-12c reveals how the c_s estimate fairs when coupled with a g_s estimate instead of a ρ_s one. Essentially, the difference between the ρ_s and g_s minimum sample size profiles is mimicked by the profile for c_s in Figure 3-12 versus the c_s profile in Figure 3-20: at every range and SNR the minimum sample size is ten times in Figure 3-20b what it is in Figure 3-12b. Lack of knowledge about the sediment speed gradient has a much larger effect on the accuracy of an estimate for sediment speed than does lack of knowledge of sediment density.

Comparing Figure 3-20c to Figure 3-12c reveals that the sediment speed gradient is, at least for the environment modeled, a more difficult parameter to determine acoustically. In Figure 3-12c, the minimum sample size for ρ_s is 0.1 at 500 m range and grew fairly steadily as range increased to a value of 20 at 10 km. For Figure 3-20c, this whole picture has essentially been shifted up by a factor of 10, beginning at 500 m at a value of 1 and growing to a value of about 100 at 10 km. For all but the highest SNRs one sample is not enough to resolve g_s, while for the same case with ρ_s virtually the opposite is true.

The resolvability of a particular parameter is affected not only by how many other parameters are unknown, as is discussed in the previous paragraph, but also by which other parameters are unknown. In this example, lack of knowledge about the sediment speed gradient has a much larger effect on the accuracy of an estimate for sediment speed than does lack of knowledge of sediment density. For a given environment and parameterization, it is therefore worthwhile to be wary of which parameters are particularly difficult to resolve as inversions performed with these parameters unknown could significantly affect the performance of estimates of the other unknown parameters.

3.3.6 Three parameter estimate of c_s, ρ_s and g_s

The prior three examples illustrate the effects of unknown parameter choice on the ability of the MLE to produce estimates that are unbiased and attain the Cramer Rao Lower bound. The emphasis has been put on the number of geo-acoustic samples

required to achieve these two goals for each of the examples. Although the number of samples required to attain the Cramer-Rao Lower Bound has reached has high as 100, no minimum sample size yet discussed has been so large that the given estimate might be deemed infeasible. In this next example, a three parameter inversion is discussed and the trend, first noted with the second example, that a greater number of parameters gives rise to reduced resolvability of all parameters is shown to be worthy of concern. The three inversion parameters for this example are c_s, the sediment sound speed at the top of the sediment layer; ρ_s, the sediment density; and g_s, the sediment sound speed gradient.

Figure 3-21 shows the three statistical moment terms for each of the three parameters; c_s in Figure 3-21a, ρ_s in Figure 3-21b, and g_s in Figure 3-21c. At first glance, the significantly poorer performance of the estimates than in both of the two parameter examples is quite apparent. All three estimates have higher values of all three moment terms at all ranges. The curves are steeper and the second order to first order variance ratios are higher at all ranges.

The sediment speed at the top of the sediment layer, c_s, is once again the most interesting parameter to examine as Figures 3-7a, 3-10a, and 3-21a can be compared to paint a picture of how the performance of this parameter estimate has faired as part of inversions for one, two and then three parameters. As discussed before, when going from the single parameter case, the statistics of which are shown in Figure 3-7, to the two double parameter cases, statistics shown in Figures 3-10a and 3-18a, the performance of the statistical quantities worsened. This trend continues in the three parameter case. The bias, which peaks at 0.4 m/s in Figure 3-7, peaks at 3 m/s in Figure 3-10a and now peaks at over 200 m/s for the three parameter case in Figure 3-21a. The square root of the first order variance which is about 7-9 m/s for all ranges for the single parameter case, is just over 10 m/s for all ranges in the two parameter case and about 50-100 m/s for this three parameter example. The square root of the second order variance has, with the addition of parameters to the inversion, increased even more dramatically. Lower than the first order variance, with values between .3-8 m/s, for the single parameter inversion, it ranges between 1-10 m/s for the ρ_s coupled

two parameter case and 3-100 m/s for the g_s coupled two parameter case. When all three parameters are estimated simultaneously, the second order variance begins, at the highest SNRs, at a value of about 10 and grows to a value of more than 1000 at the lowest SNRs: a value equal in magnitude to the parameter.

In Figure 3-21b, the first order bias of the g_s parameter has a low-range value of about 1 $\frac{m/s}{m}$ and grows to 30 $\frac{m/s}{m}$, while for Figure 3-18b these values are .3 $\frac{m/s}{m}$ and 3 $\frac{m/s}{m}$ respectively. The first order variance has risen by about half a decade at every range from its value in Figure 3-18b and the second order variance, which in Figure 3-18b ranged from 1-20 $\frac{m/s}{m}$, now ranges from 1 to 250 $\frac{m/s}{m}$.

In Figure 3-21c, where the statistics for ρ_s are shown, the bias begins, at the closest ranges (largest SNRs), with an average value of a little less than 0.01 g/cc and grows to an average value of just less than 1 g/cc, peaking at about 1 g/cc. The range for the bias in Figure 3-10b is between 10^{-5} g/cc and 10^{-2} g/cc for the same set of SNRs. The square root of the first order variance has risen a bit, fairly uniformly over all ranges, with the addition of the third parameter, with an average value in 3-10b of 10^{-1} g/cc, and in Figure 3-21c of 2×10^{-1} g/cc. However, the square root of the second order variance has risen a decade at the highest SNRs and more than that at the lowest SNRs, peaking at almost 10 g/cc: about 4 times the true value of the parameter.

Figure 3-22 shows the minimum sample sizes for the three parameter estimate. The SNR is shown versus range in Figure 3-22a. Figure 3-22b shows the minimum sample size for the c_s estimate. The bias for this parameter is quite large, especially where 10 log SNR is greater than roughly 8 dB. At the lowest SNRs the minimum sample size is nearly 100. Fewer samples will result in poor estimate resolution.

In Figure 3-22c the bias of estimate of the g_s parameter is shown to be even worse. At no range or SNR is one sample enough for the bias to meet the condition in Equation 1.9. The estimate is very biased. At the highest SNRs, just over one sample is required. At the lowest SNRs tested, close to 70 samples are required. So, while the earlier examples could lead one to believe that bias is not a significant issue for seafloor parameter inversions, this three parameter case indicates it may be one

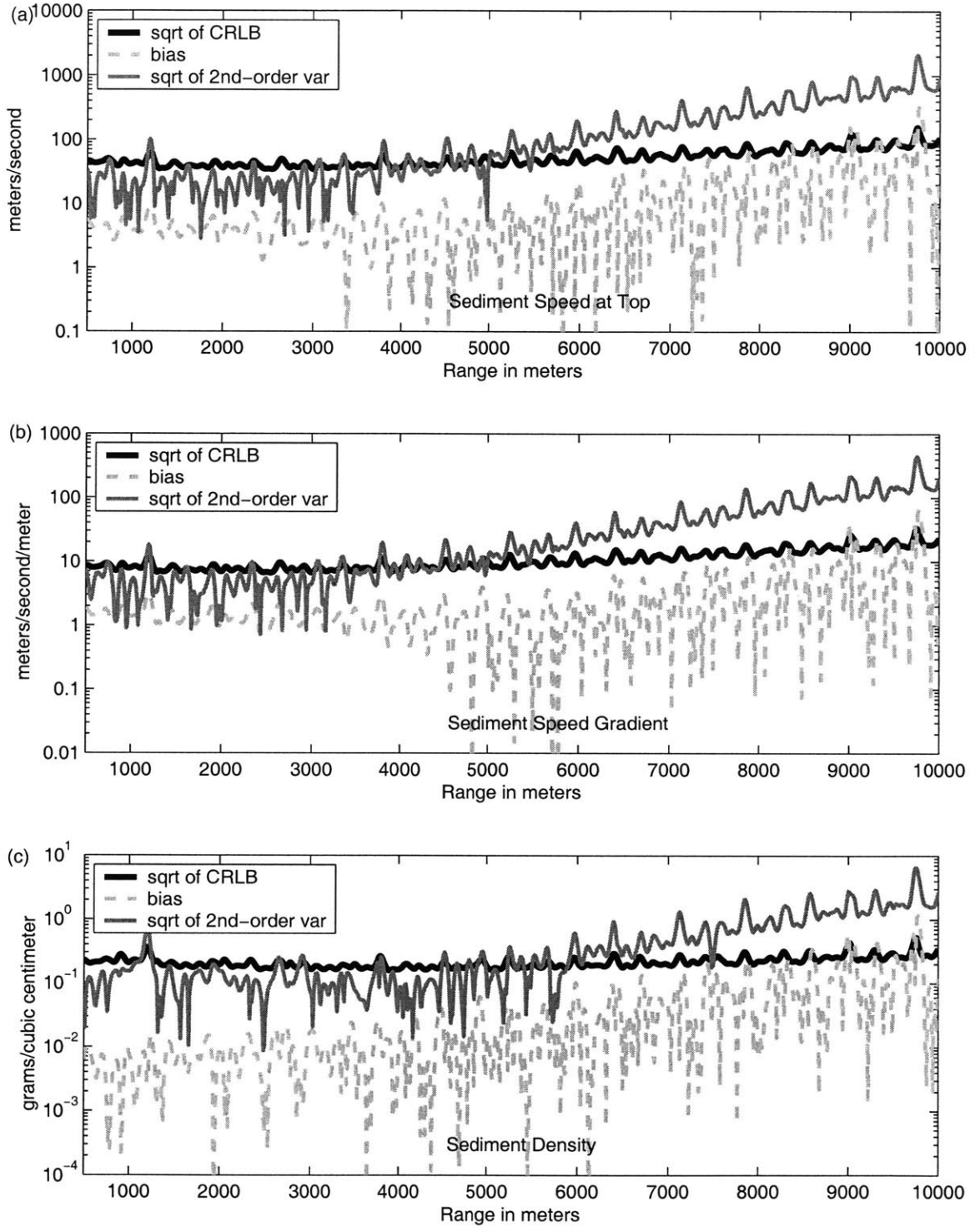

Figure 3-21: Bias and variance terms for an inversion for parameters c_s, g_s and ρ_s in the Case B waveguide.(See next figure for SNR vs. range.)

at higher parameter number, even if usually of less concern than variance. It is also clear that the sediment sound speed gradient is a very difficult parameter to estimate.

Figure 3-23 shows the minimum sample sizes required for the three parameter estimate in the current example to have a variance that attains the Cramer-Rao Lower Bound. Figure 3-23a shows the input SNR versus range. Figures 3-23b- 3-23d show the minimum samples sizes versus range for parameters c_s, g_s, and ρ_s respectively. All three graphs follow a very similar pattern. At the lowest ranges (highest SNRs) about 1-10 samples are required for all of the estimates. This number increases fairly linearly until the lowest SNRs, where the number of samples required for this inversion is more than 1000. A picture of decreased resolvability with parameter number has decidedly emerged. It is true that in the areas of high SNR, resolvability has remained good for all the cases shown. At SNR less than 10 dB, there is marked drop in performance with the addition of each extra parameter. Due to computational limitations with Matlab, only examples with a limited number of parameters have been treated in this paper. In that each parameter has added 1-2 decades to the required samples at the lowest SNRs, and half a decade at SNRs typical of practical scenarios, it is reasonable to be concerned about the statistical errors brought on by inversion of even more unknowns.

3.3.7 Attenuation and Modal Stripping

Attenuation in the sediment is an important parameter in the performance of geoacoustic inversions both as a parameter to be estimated and as one of the primary mechanism for loss of the acoustical energy of the signal and hence information about any other parameters being estimated.

To give a feel for how attenuation affects the present analysis of necessary sample size the three-parameter inversion of c_s, ρ_s and g_s in the Case B waveguide discussed in the previous section is performed for a range of attenuations, α_s, between 0 and 1 dB/λ. The result is plotted in Figure 3-24 with attenuation on the y-axis, range

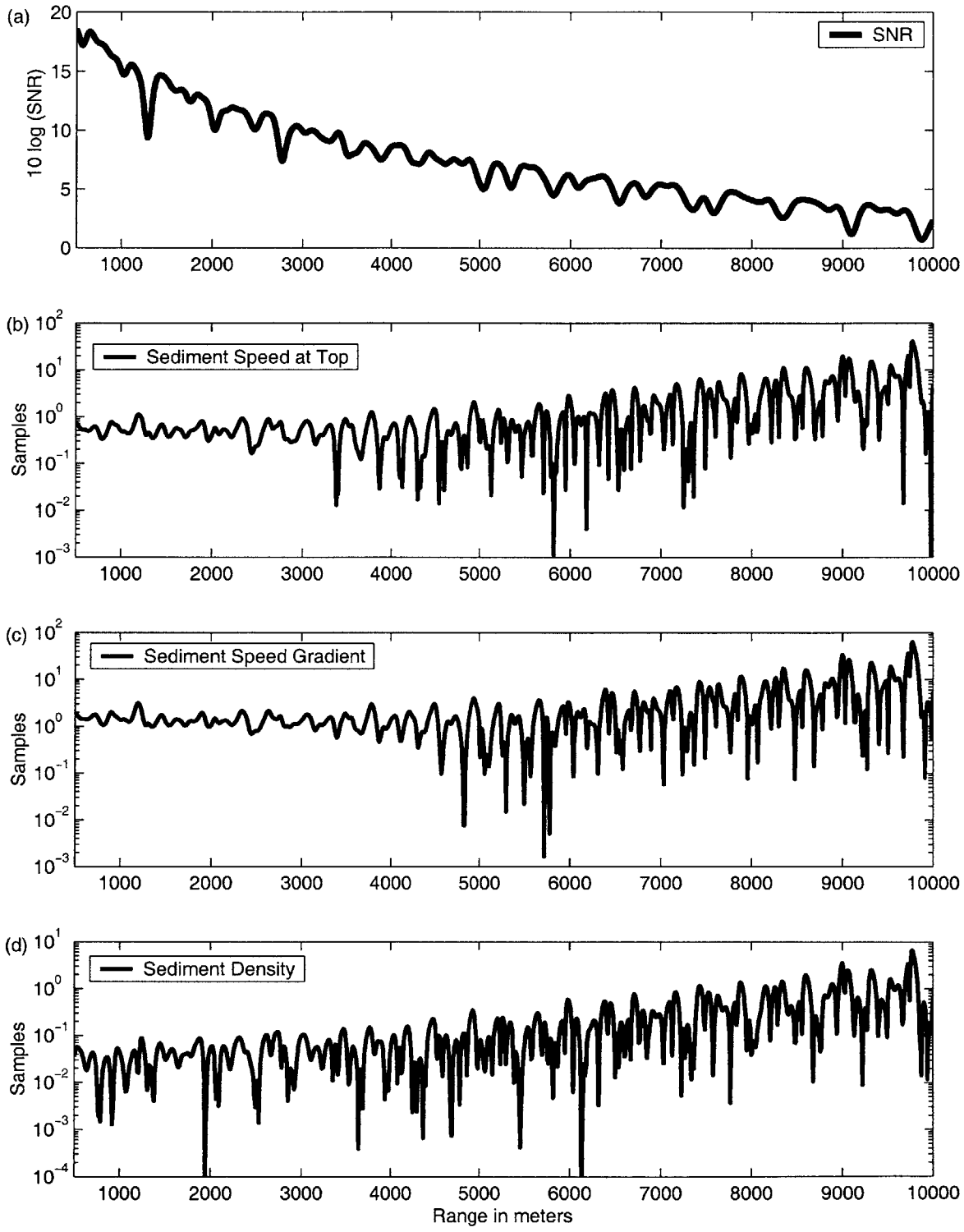

Figure 3-22: SNR versus range and necessary sample sizes for estimates of parameters c_s, g_s, and ρ_s in the Case B waveguide to be asymptotically unbiased.

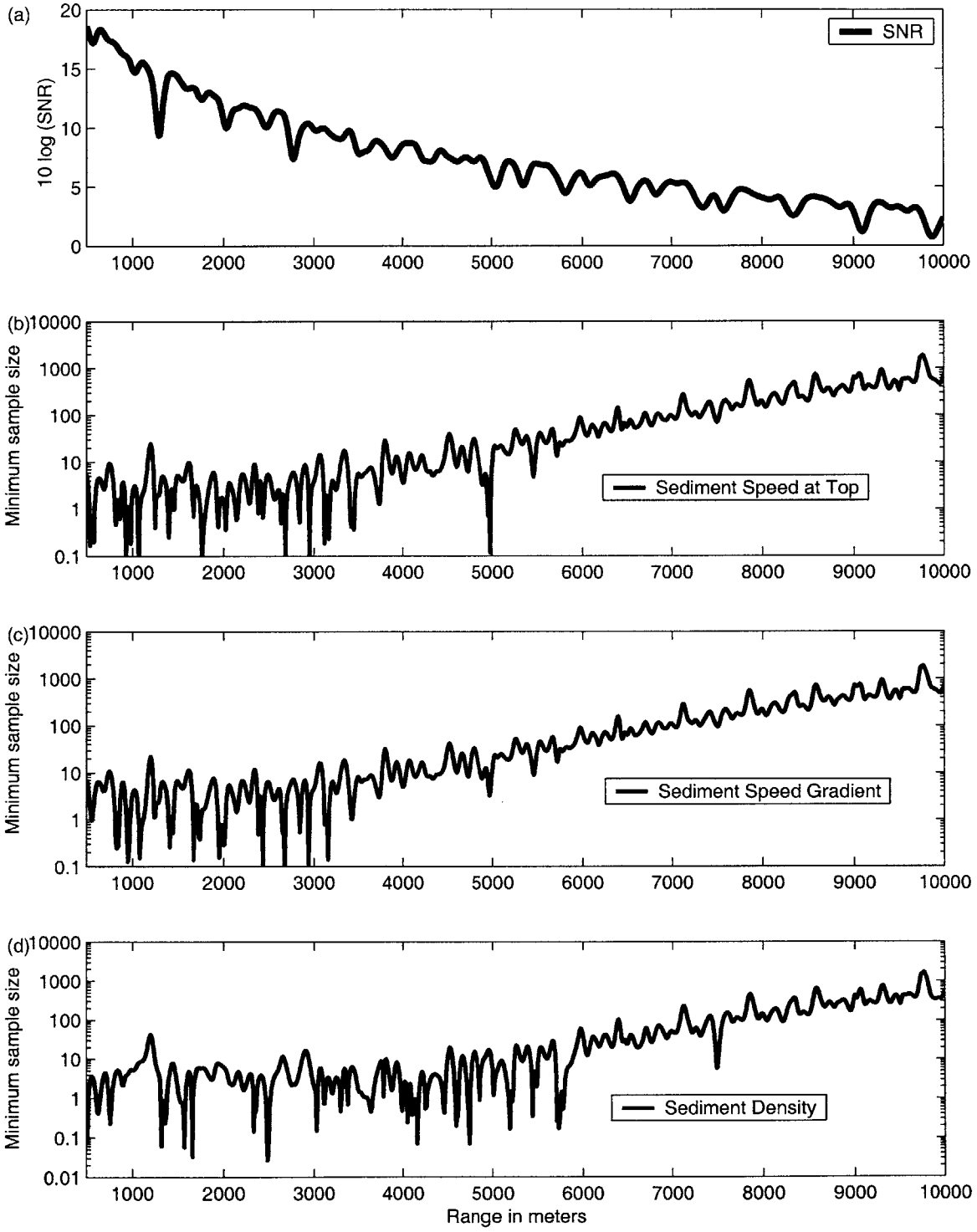

Figure 3-23: SNR versus range and necessary sample sizes for an inversion for parameters c_s, g_s, and ρ_s in the Case B waveguide to attain the Cramer Rao Lower Bound.

on the x-axis and the necessary sample size to attain the CRLB for the c_s estimate [2] represented by tones of gray.

Immediately apparent is the sudden shift in value of the necessary sample size from negligible to quite large at a particular range for each attenuation. For higher attenuations this range is much smaller and therefore is definitely linked to α_s. It is possible that the sudden shift in regime can be thought of as the sudden loss in strength of higher order modes. Possibly at this point, all but the first and zeroth order modes remain, the first becomes negligibly attenuated and we are left with the situation discussed in Section 3.3.3 where there is only one reflecting plane wave and hence little information for estimating ρ and c_s.

3.3.8 Four parameter estimate of c_s, ρ_s, g_s, and h_s

This final example is for a four parameter inversion in the Case B waveguide. The estimation parameters in this example are the top of sediment sound speed, c_s, the sediment sound speed gradient, g_s, the sediment density, ρ_s, plus the sediment thickness, h_s. As is mentioned in Chapter 1, the number of geoacoustic parameters estimated simultaneously in practice is often greater than ten. A four parameter example of the application of our technique for determining the necessary conditions for estimates to be unbiased and to attain minimum variance only begins to explore the effects of larger inversion parameter vectors. However, looking at Figure 3-25, which shows the values of the three statistical moment terms, one can see that already the variances and biases are extremely large. Figure 3-26 shows the necessary sample sizes to attain the CRLB [3]. There is a limit to how quickly experimenters in the field can take samples in order to assure that the samples are uncorrelated. To take the number of samples that the results in these figures indicate are necessary to have unbiased, minimum variance estimates, experimenters would be sampling for far too long to be practical or even for them to reasonably assume that the environment has

[2] The salient, relevant features of this graph are the same for those generated from the other two parameters estimated in this example

[3] The number necessary to attain asymptotic unbiasedness is less at every range

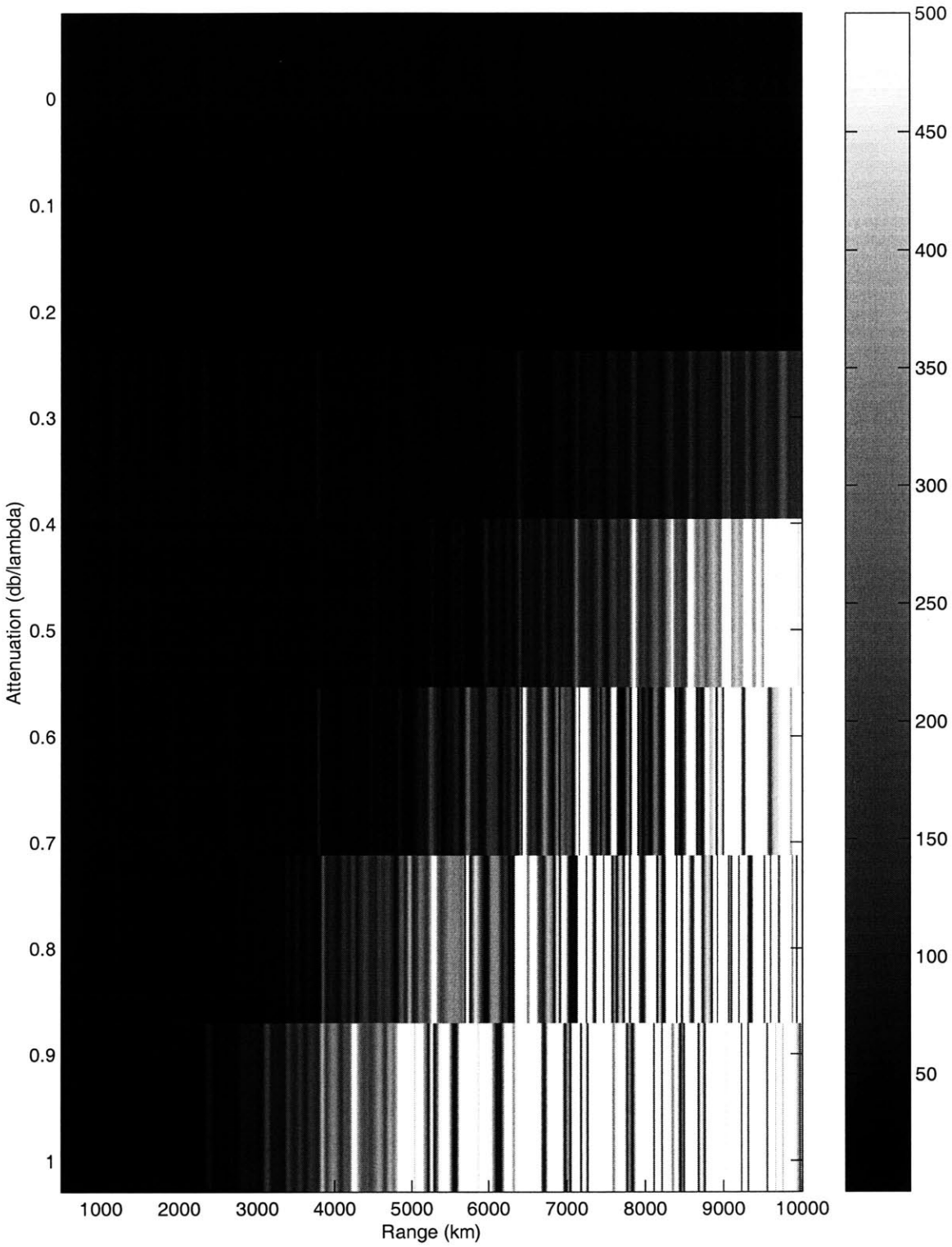

Figure 3-24: Effect of attenuation, α_s, on the necessary sample size to attain the CRLB for the c_s estimate in the Case B waveguide. The x-axis is range of the receiver array from the source. The y-axis is attenuation.

changed little enough for the data to be used all together. In essence, these numbers of samples are prohibitively large in many cases. Increasing the SNR is an option left open to the experimenter but there are also limits on what SNRs can be generated by practical means.

The high minimum sample sizes are probably due to an aggregated effect of all of the previously discussed issues, physical couplings and number of unknowns. It is likely that poor performance of the four parameter example is an amalgamation of the various physical couplings, gradient and thickness, sound speed and density, and, in essence, a result of shear parameter number. It is reasonable to conclude that sediment layer thicknesses are particularly difficult parameters to estimate although it is possible that it is a coupling of the thicknesses with other parameters, likely sediment gradient, that causes the difficulty in its simultaneous estimation with these parameters. This notion is strengthened by the realization that there appears to be no general change in the bias and the variances of the four estimates at lower SNR. For some reason, unlike the previous examples, the statistical moment terms are high for all ranges and SNRs. Perhaps, the aggregate coupling of the four parameters, in the way described for density and sound speed in Section 3.3.3 leaves hardly any information about the seabed parameters and therefore signal strength is not relevant.

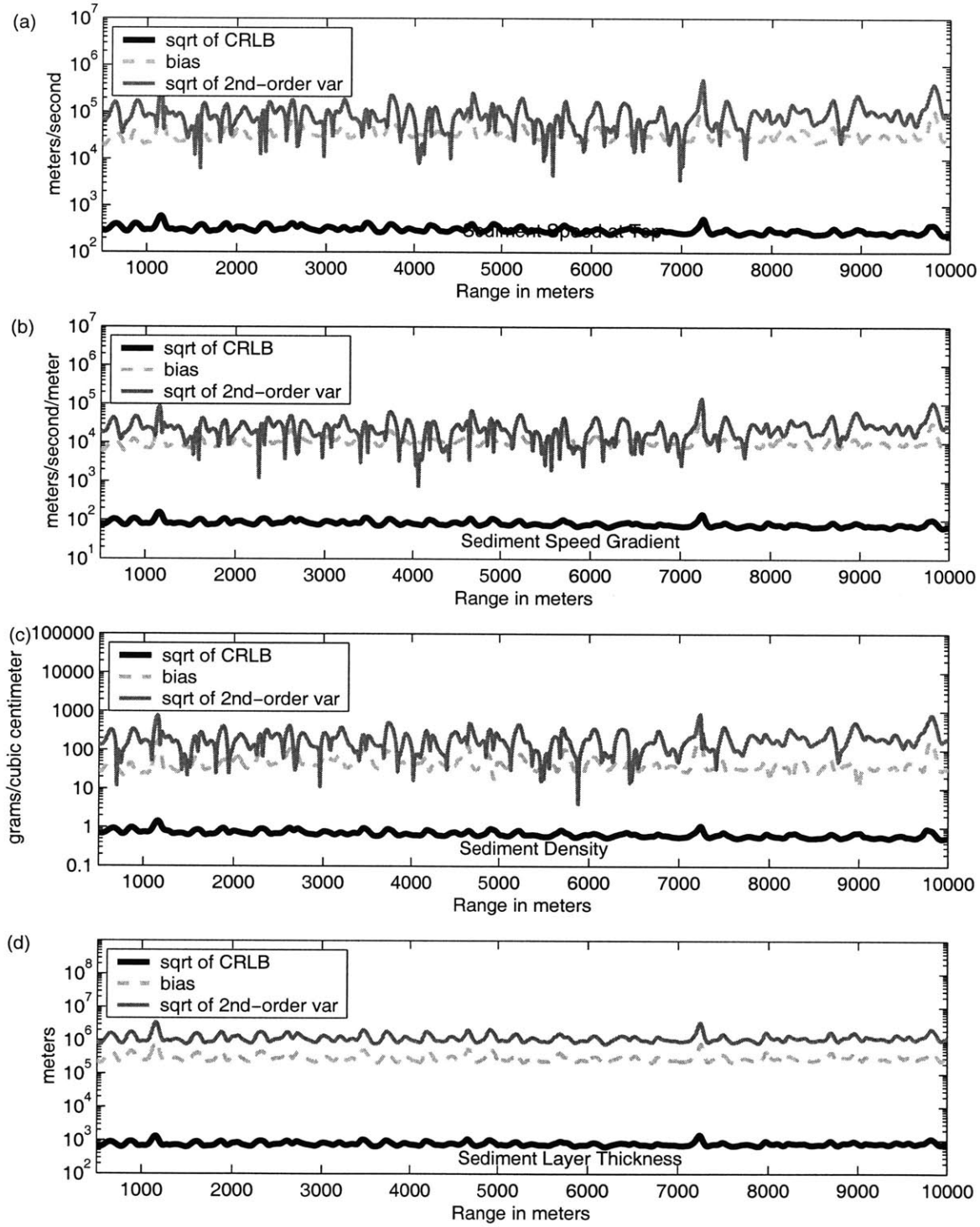

Figure 3-25: Bias and variance terms for an inversion for parameters c_s, g_s, ρ_s, and h_s in the Case B waveguide.(See next figure for SNR vs. range.)

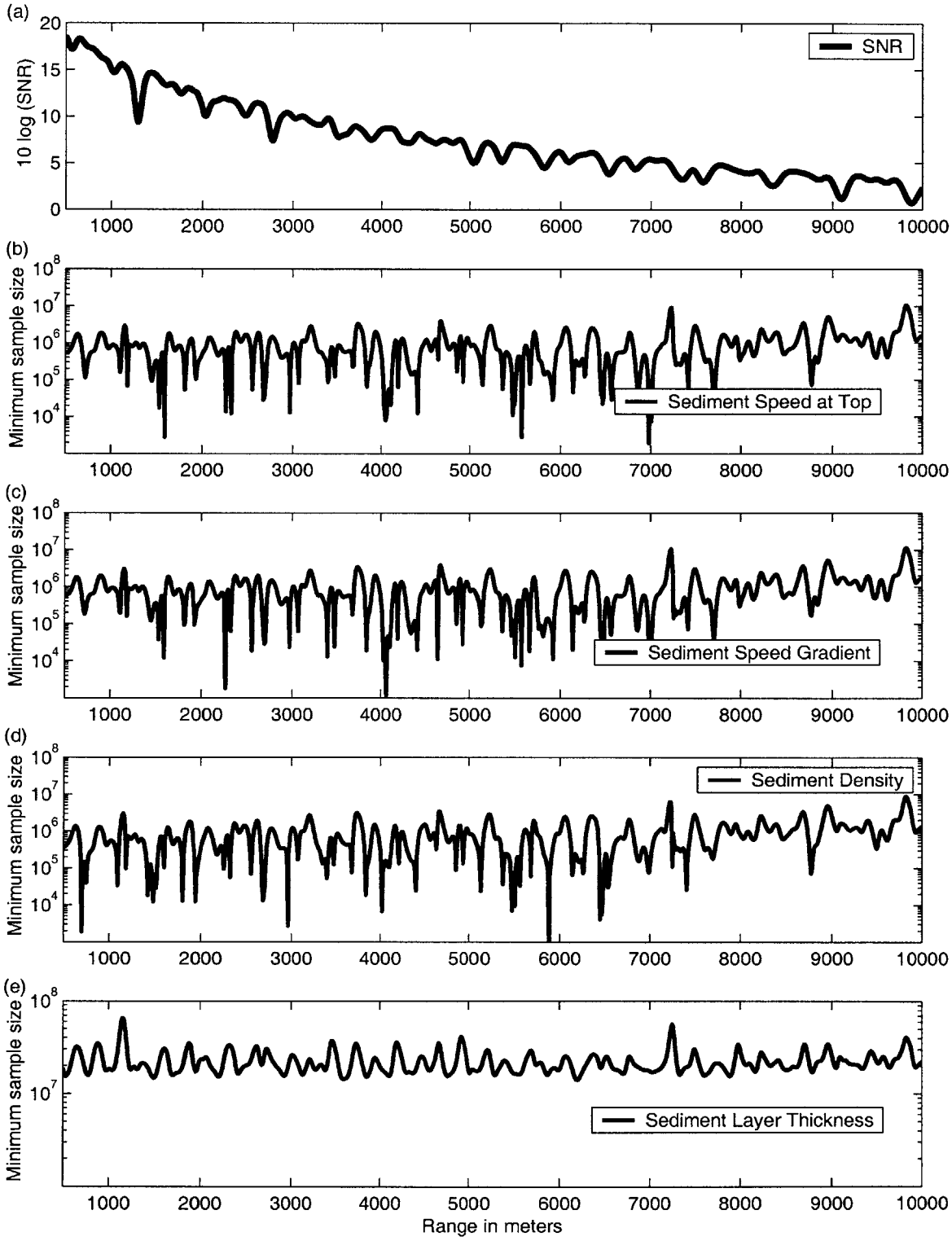

Figure 3-26: SNR versus range and necessary sample sizes for an inversion for parameters c_s, g_s, ρ_s and h_s in the Case B waveguide to attain the Cramer Rao Lower Bound.

Chapter 4

Conclusion and Future Work

In this thesis I use higher order approximations of the bias and variance of the Maximum Likelihood Estimator to show that geoacoustic inversions with vertical array data can very easily be biased and have large variances that do not attain the CRLB. I then use these same tools to develop necessary conditions on sample size to asymptotically render estimates unbiased and attain the Cramer Rao Lower Bound. These tools can be used by researchers to design future experiments to have desired parameter resolutions. In the process, the physical couplings and effects that cause bias and high variance in geo-acoustic inversions are explored.

The results suggest that as signal-to-noise ratio (SNR) at the receiver array descends, the MLE exhibits variances that can exceed the Cramer-Rao Lower Bound by orders of magnitude and has significant biases. The resulting estimates can, therefore, be virtually useless for inferring environmental parameters or for use in environmental models employed by other acoustical schemes. High sample sizes would allow for unbiased, minimum variance estimates, however the required number of samples, can for some scenarios, be so high as to be infeasible.

The examples given indicate that some parameters are more difficult to estimate than others, insofar as the bias and the variance of estimates for these parameters are more likely to be undesirably high for low sample size. Sound speed and sound speed gradients in the sediment layers and sediment layer thicknesses appear to be difficult parameters to resolve. Sediment density also appears to be difficult to estimate,

especially if the sediment sound speed is also unknown. Attenuation does not appear to be difficult to estimate, at least for layers near the interface between the water and the seabed.

Regardless of which parameters are estimated, the more estimated simultaneously the higher the biases and the variances of the estimates of all the parameters will be. Sound speed may have relatively low biases and variances when estimated alone. However, if density is also unknown, the increased general uncertainty will result in worse bias and variance for the sound speed estimate. If then the sediment sound speed gradient is assumed to be unknown, the estimates of the first two parameters will lose resolution. The results of this thesis suggest that this trend will continue ad infinitum as yet more parameters are assumed to be unknown.

In reality, little is usually known *a priori* about the structure of the seabed and the values of the acoustical parameters. Hence the true number of unknowns in these kinds of problems are not even approached by the examples in this thesis. Yet already in these examples, situations are shown where the biases and the variances are very large. There is good reason to be cautious when dealing with the ten to one hundred parameter models often used by field experimenters and researchers running simulations.

Since geo-acoustic parameter inversions are playing an increasingly important role in oceanography, it is hoped that this work will help in the design of future schemes and that their designers will remain aware of the baseline statistical limitations of performing geo-acoustic inversions in the typical ocean environment.

Future work could involve the use of more realistic noise models; the use of a fully-randomized signals; the incorporation of source and receiver array positional uncertainty; the investigation of more diverse waveguide models, perhaps with multiple levels of sediment and different sound-speed profiles in the water-column; and the use of more complicated parameterizations with large parameter vectors that reflect the true number of unknowns encountered in field experiments.

Chapter 5

References

Bibliography

[1] S.D. Rajan, J.F. Lynch, and G.V. Frisk. Perturbative inversion methods for obtaining bottom geoacoustic parameters in shallow water. *J. Acoust. Soc. Am.*, 82:998–1017, 1987.

[2] M.D. Collins, W.A. Kuperman, and H. Schmidt. Nonlinear inversion for ocean-bottom properties. *J. Acoust. Soc. Am.*, 92:2770–2783, 1992.

[3] N.R. Chapman and C.E. Lindsay. Matched field inversion for geoacoustic model parameters in shallow water. *IEEE J. Oceanic Eng.*, 21:347–354, 1996.

[4] E.L. Hamilton. Geoacoustic modelling of the sea floor. *Journal of the Acoustical Society of America*, 68:1313–1340, 1980.

[5] A. Tolstoy, N.R. Chapman, and G.A. Brooke. Workshop '97: Benchmarking for geoacoustic inversion in shallow water. *J. Computat. Acoust.*, 6 (1&2):1–28, 1998.

[6] O. Diachok, A. Caiti, P. Gershoft, and H. Schmidt. *Full field inversion methods in ocean and seismic acoustics.* Kluwer, Dordrecht, 1995.

[7] M.B. Porter. *The KRAKEN normal mode program.* SACLANT ASW Research Centre, La Specia, Italy, s.m.-245 edition, 1991.

[8] F.B. Jensen and M.C. Ferla. *SNAP: The SACLANTCEN normal mode acoustic propagation model.* SACLANT ASW Research Centre, La Specia, Italy, s.m.-121 edition, 1979.

[9] H. Schmidt. *OASES Version 1.6: Application and upgrade notes.* Massachusetts Institute of Technology, Cambridge, MA, 1993.

[10] P. Gerstoft. Inversion of seismo-acoustic data using genetic algorithms and *a posteriori* probability distributions. *J. Acoust. Soc. Am.*, 95:770–782, 1994.

[11] Y. Stephan, X. Demoulin, and O. Sarzeaud. Neural direct approaches for geoacoustic inversion. *J. Computat. Acoust.*, 6 (1&2):151–166, 1998.

[12] S.D. Rajan. Waveform inversion for the geoacoustic parameters of the ocean bottom. *J. Acoust. Soc. Am.*, 91:3228–3241, 1992.

[13] R. Zhang, F. Li, and W. Luo. Effects of source position and frequency on geoacoustic inversion. *J. Computat. Acoust.*, 6 (1&2):245–255, 1998.

[14] P. Ratilal, P. Gerstoft, and J.T. Goh. Subspace approach to inversion by genetic algorithms involving multiple frequencies. *J. Computat. Acoust.*, 6 (1&2):99–115, 1998.

[15] S.D. Rajan. Determination of geoacoustic parameters of the ocean bottom-data requirements. *J. Acoust. Soc. Am.*, 92:2126–2140, 1992.

[16] D. Chazan, M. Zakai, and J. Ziv. Improved lower bounds on signal parameter estimation. *IEEE Trans. Informat. Theory*, IT-21:90–93, 1975.

[17] A.J. Weiss and E. Weinstein. Lower bounds in parameter estimation-summary of results. presented at ICASSP, Tokyo, 1986.

[18] C.R. Rao. *Linear Statistical Inferenec and Its Applications.* Wiley, New York, 1973.

[19] H. Schmidt and A.B. Baggeroer. Physics-imposed resolution and robustness issues in seismo-acoustic parameter inversion. In *Full field inversion methods in ocean and seismo-acoustics.* Kluwer academic publishers, Dordrecht, 1995.

[20] A.B. Baggeroer and H. Schmidt. Parameter estimation theory bounds and the accuracy of full field inversions. In *Full field inversion methods in ocean and seismo-acoustics.* Kluwer academic publishers, Dordrecht, 1995.

[21] D.N. Lawley. A general method for approximating to the distribution of the likelihood ratio criteria. *Biometrika*, 43:295–303, 1956.

[22] S.M. Kay. *Fundamentals of Statistical Signal Processing: Estimation Theory*, volume 1. Prentice-Hall, Englewood Cliffs, NJ, 1993.

[23] M. Zanolin, E. Naftali, and N.C. Makris. Second order bias of a multivariate gaussian maximum likelihood estimate with a chain-rule for higher moments. Submitted to JASA, 2001.

[24] E. Naftali and N.C. Makris. Necessary conditions for a maximum likelihood estimate to become asymptotically unbiased and attain the cramer-rao lower bound. Part I: General approach with an application to time-delay and doppler shift estimation. *Journal of the Acoustical Society of America*, 110(4):1917–1930, 2001.

[25] G.V. Frisk. *Ocean and Seabed Acoustics: A theory of wave propagation.* Prentice-Hall, 1994.

[26] A.S. Willsky, G.W. Wornell, and J.H. Shapiro. Stochastic processes, detection and estimation. Class notes for M.I.T. class 6.432, 2001.

[27] L.L. van Trees. *Detection, Estimation and Modulation Theory*, volume III. Wiley, New York, 1970.

[28] O.E. Barndorff-Nielsen and D.R. Cox. *Inference and Asymptotics.* Chapman & Hall, London, 1994.

[29] N.C. Makris. The statistics of ocean-acoustic ambient noise. presented at Sea Surface Sound, Dordrecht, 1997.

[30] I. Dyer. Fundamentals and applications of underwater sound. Class notes for M.I.T. class 13.851.

[31] F.B Jensen, W. A. Kuperman, M.B. Porter, and H. Schmidt. *Computational Ocean Acoustics.* American Institute of Physics, New York, 1994.

Chapter 6

Appendices

Appendix A

Numerical derivative calculations

Evaluation of Equations 2.5- 2.7 requires knowledge of the first, second and third order derivatives of the log likelihood function with respect to all combinations of the components of $\boldsymbol{\Theta}$. Assuming the experimental data is given by a deterministic part, due to the source, embedded in zero-mean, additive Gaussian noise, can be simplified to expressions that are functions of only a signal-independent covariance matrix and derivatives of the deterministic part of the signal [24].

In our case, the signal vector, $\mathbf{X}$, is the pressure field measurements on the ten element vertical array. For ranges greater than a few ocean depths (for the waveguide models used, $> 300\ m$), the field received by the j-th array element from a discrete acoustic source at range r and depth z at angular frequency ω can be expressed as a sum of normal modes [31]

$$G(z_j, z, r, \omega) = \frac{ie^{-\frac{\pi}{4}}}{\rho(z)\sqrt{8\pi r}} \sum_l \Psi_l(z)\Psi_l(z_j)\frac{e^{ik_l r}}{\sqrt{k_l}} \tag{A.1}$$

where k_l is the horizontal wavenumber of the mode l with modal amplitude $\Psi_l(z)$. Equation A.1 defines the j-th element of the vector pressure field, $\mathbf{G}$. For a signal embedded in zero mean noise, the mean vector, μ, is equal to $\mathbf{G}$. Therefore, it is the derivatives of Equation A.1 with respect to the geo-acoustic inversion parameters that are required.

Although numerical calculation and differentiation of the modes can lead to in-

stabilities, the necessary derivatives for all but the simplest case, Case A, were too difficult to obtain analytically. Therefore normal modes functions and wave numbers were generated using commonly available normal modes codes and these were then plugged into Equation A.1 to compute pressure fields. Pressure fields were calculated for all the perturbations on the environment in the inversion parameters to provide the inputs necessary to use the finite difference equations given at the end of this appendix (Equations A.2 through A.4) to calculate the derivatives required for the asymptotic expressions.

Initially the KRAKEN [7] normal modes package was used to calculate the necessary mode functions and wave numbers. As conventional wisdom held that KRAKEN might yield unacceptable instabilities when used in the calculation of derivatives, the use of another normal modes package, SNAP [8], was also explored. In order to check the accuracy of the close range results from KRAKEN, KRAKENc cite was run for some of the cases. The derivatives resulting from using KRAKEN and SNAP appeared to be virtually identical. As ranges must be suitably large to assume Gaussian noise distribution (more than a few wavelength, for our models $> 300\ m$) and KRAKENc is intended to provide a more accurate modal solution than KRAKEN for short ranges, the differences between the two sets of derivatives calculated using the two programs was only significant at ranges where the noise model was inapplicable. Therefore, KRAKEN was used for all the results present in this paper.

A.1 Determination of optimal step sizes for derivatives

A necessary part of accurately executing finite difference equations for function derivatives is a well-chosen step-size. If the step-size is too small, quantization error will be an issue i.e. the step-size is smaller or on the order of the smallest quantity the computer can resolve and calculated perturbed function values will either not change from the unperturbed function or change in a spurious manner due to sudden jumps

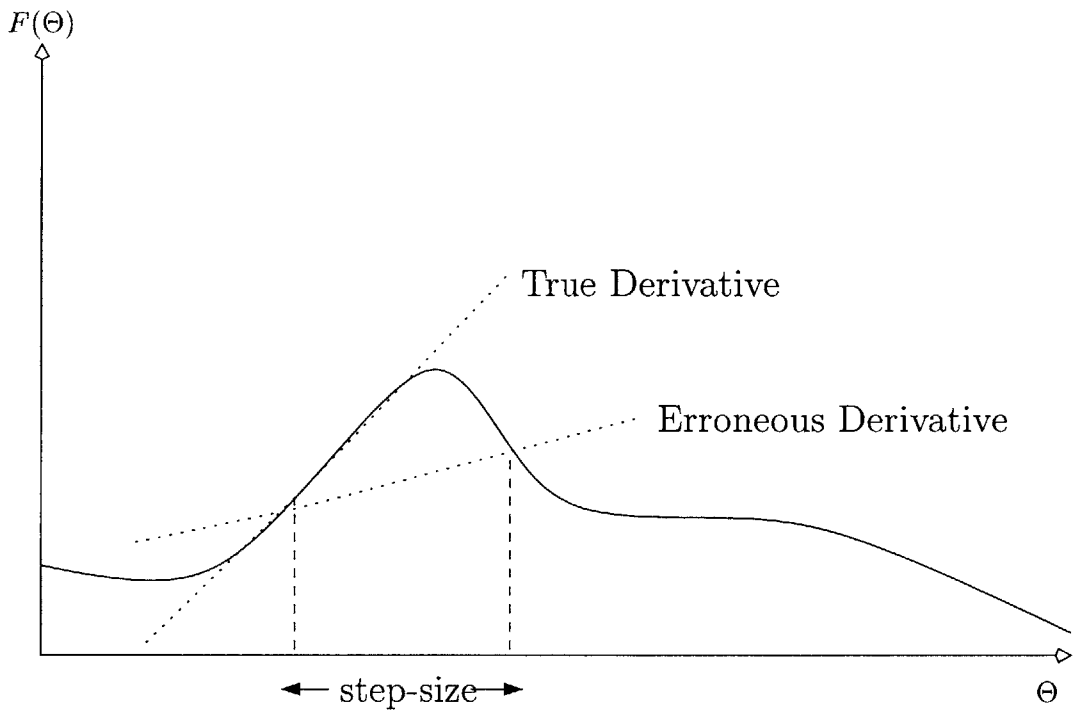

Figure A-1: Demonstration of how too large a step-size can cause errors in derivative calculations.

in the perceived perturbation. Because of binary coding by the computer, it is not always easy to determine this smaller limit. On the other hand when the step-size is too large it is possible to skip features of the function and also get inaccurate derivatives. This is demonstrated in Figure A-1 for a function, $F(\Theta)$ where Θ is a scalar parameter.

Clearly, the optimal step-size is somewhere in between, probably closer to the smaller side. For complicated functions that are non-linearly related to the parameter with respect to which one would like to take derivatives, such as the pressure field in our scenario, it can be difficult to predict the optimal step-sizes. My approach was to calculate the derivatives of the function with respect to each of the parameters of interest for a range of reasonable step-sizes to locate the section of that range that contains step-sizes that all produce similar values for that section i.e. locate the flat section in a plot of derivatives versus step-size. Before performing the calculations for a particular set of parameters in a particular waveguide, I would go through this operation for the first, second and third derivatives with respect to each of the

parameters and use the determined step-sizes for all the other derivative calculations required, assuming that the mixed derivatives would still be sound with these step-sizes.

For this work, I needed to calculate derivatives of the pressure field for a number of ranges between the source and the receiver array. This range could effect optimal step-size for each of these derivatives. however for the sake of ease and to minimize processor demand, I ideally wanted to find a single step-size that would work well enough for all ranges. A weighted, range-summed step-size optimization is also used.

$$\frac{df(\Theta)}{d(\Theta^r)} = \frac{f(\Theta^r + \frac{h}{2}) - f(\Theta^r - \frac{h}{2})}{h} \tag{A.2}$$

$$\frac{d^2f(\Theta)}{d(\Theta^r)^2} = \frac{f(\Theta^r + h) - f(\Theta^r) - f(\Theta^r - h)}{h^2} \tag{A.3}$$

$$\frac{d^3f(\Theta)}{d(\Theta^r)^3} = \frac{f(\Theta^r + \frac{3h}{2}) - 3 \cdot f(\Theta^r + \frac{h}{2}) + 3 \cdot f(\Theta^r - \frac{h}{2}) - f(\Theta^r - \frac{3h}{2})}{h^3} \tag{A.4}$$

where h is the step-size.

Appendix B

Analytic Derivatives for Pekeris Waveguide with Zero Attenuation in Bottom

The pressure field can be modelled as the sum of a set of normal modes:

$$p(r, z_R) = \underbrace{\frac{ie^{-\frac{i\pi}{4}}}{\rho(z_R)\sqrt{8\pi}}}_{C} \sum_{n=1}^{\infty} \underbrace{\Psi_n(z_S)\Psi_n(z_R)}_{A_n} \underbrace{\frac{e^{ik_n r}}{\sqrt{k_n r}}}_{g_n}$$

where $\rho(z_R)$ is the density of the water-column as a function of depth; r is the range of the source from the receiver; k_n are the modal wavenumbers; z_S is the depth of the source; z_R is the depth of the receiver; n is the mode number; and Ψ_n are the mode functions. This equation can be simplified so that each element of the sum consists of two terms, A_n and g_n:

$$p(r, z) = C \sum_{n=1}^{\infty} A_n g_n$$

B.1 Pressure field derivatives

Using the above representation, derivatives of the pressure field with respect to any quantity upon which it depends can be worked out via the chain rule. Shown here

are the first, second and third order derivatives with respect to all the necessary permutations of any two parameters.

$$P_c = C\sum_n A_{n,c}g_n + A_n g'_n k_{n,c}$$

$$P_{cc} = C\sum_n A_{n,cc}g_n + 2A_{n,c}g'_n k_{n,c} + A_n g'_n k_{n,cc} + A_n g''_n (k_{n,c})^2$$

$$\begin{aligned} P_{ccc} &= C\sum_n A_{n,ccc}g_n + 3A_{n,cc}g'_n k_{n,c} + 3A_{n,c}g''_n (k_{n,c})^2 + A_n g'_n k_{n,ccc} \\ &\quad +3A_{n,c}g'_n k_{n,cc} + 3A_n g''_n k_{n,c}k_{n,cc} + A_n g'''_n (k_{n,c})^3 \end{aligned}$$

$$P_{cb} = C\sum_n A_{n,cb}g_n + A_{n,c}g'_n k_{n,b} + A_{n,b}g'_n k_{n,c} + A_n g''_n k_{n,c}k_{n,b} + A_n g'_n k_{n,cb}$$

$$\begin{aligned} P_{cbb} &= C\sum_n A_{n,cbb}g_n + A_{n,bb}g'_n k_{n,c} + 2A_{n,cb}g'_n k_{n,b} + A_{n,c}g''_n (k_{n,b})^2 \\ &\quad +2A_{n,b}g''_n (k_{n,c}k_{n,b}) + A_n g'''_n k_{n,c}(k_{n,b})^2 + A_{n,c}g'_n k_{n,bb} + 2A_{n,b}g'_n k_{n,cb} \\ &\quad +A_n g''_n k_{n,c}k_{n,bb} + 2A_n g''_n k_{n,cb}k_{n,b} + A_n g'_n k_{n,cbb} \end{aligned}$$

$$\begin{aligned} P_{ccb} &= C\sum_n A_{n,ccb}g_n + 2A_{n,cb}g'_n k_{n,c} + A_{n,b}g'_n k_{n,cc} + A_{n,b}g''_n (k_{n,c})^2 \\ &\quad +A_{n,cc}g'_n k_{n,b} + 2A_{n,c}g''_n k_{n,c}k_{n,b} + 2A_{n,c}g'_n k_{n,cb} \\ &\quad +A_n g''_n k_{n,cc}k_{n,b} + A_n g'_n k_{n,ccb} + A_n g'''_n (k_{n,c})^2 k_{n,b} \\ &\quad +2A_n g''_n k_{n,c}k_{n,cb} \end{aligned}$$

Here, g'_n, g''_n, and g'''_n represent the first through third derivatives with respect to k_n.

$$g'_n = \left[-\frac{1}{2k_n} + ir\right] g_n$$

$$g''_n = \frac{1}{2k_n^2} g_n + \left[-\frac{1}{2k_n} + ir\right]^2 g_n$$

$$g_n''' = \left[-\frac{1}{k_n^3} + \frac{3}{2k_n^2}\left(-\frac{1}{2k_n} + iR\right) + \left(-\frac{1}{2k_n} + ir\right)^3 \right] g_n$$

As can the A_n term derivatives

$$A_{n,c} = \Psi_{n,c}(z_S)\Psi_n(z_R) + \Psi_n(z_S)\Psi_{n,c}(z_R)$$

$$A_{n,cc} = \Psi_{n,cc}(z_S)\Psi_n(z_R) + 2\Psi_{n,c}(z_S)\Psi_{n,c}(z_R) + \Psi_n(z_S)\Psi_{n,cc}(z_R)$$

$$A_{n,ccc} = \Psi_{n,ccc}(z_S)\Psi_n(z_R) + 3\Psi_{n,cc}(z_S)\Psi_{n,c}(z_R) + 3\Psi_{n,c}(z_S)\Psi_{n,cc}(z_R) + \Psi_n(z_S)\Psi_{n,ccc}(z_R)$$

$$A_{n,cb} = \Psi_{n,cb}(z_S)\Psi_n(z_R) + \Psi_{n,c}(z_S)\Psi_{n,b}(z_R) + \Psi_{n,b}(z_S)\Psi_{n,c}(z_R) + \Psi_n(z_S)\Psi_{n,cb}(z_R)$$

$$\begin{aligned} A_{n,cbb} &= \Psi_{n,cbb}(z_S)\Psi_n(z_R) + 2\Psi_{n,cb}(z_S)\Psi_{n,b}(z_R) + \Psi_{n,bb}(z_S)\Psi_{n,c}(z_R) \\ &\quad + \Psi_{n,c}(z_S)\Psi_{n,bb}(z_R) + 2\Psi_{n,b}(z_S)\Psi_{n,cb}(z_R) + \Psi_n(z_S)\Psi_{n,cbb}(z_R) \end{aligned}$$

$$\begin{aligned} A_{n,ccb} &= \Psi_{n,ccb}(z_S)\Psi_n(z_R) + 2\Psi_{n,cb}(z_S)\Psi_{n,c}(z_R) + \Psi_{n,b}(z_S)\Psi_{n,cc}(z_R) \\ &\quad + \Psi_{n,cc}(z_S)\Psi_{n,b}(z_R) + 2\Psi_{n,c}(z_S)\Psi_{n,cb}(z_R) + \Psi_n(z_S)\Psi_{n,ccb}(z_R) \end{aligned}$$

All that is left to solve the pressure field derivative equations shown above are the derivatives of the mode function amplitudes, Ψ_n, and of the modal wavenumbers, k_n. Unlike the formulas above not all of these can be derived in general. Instead, they must be derived with respect to the particular acoustical parameters of interest. For a geo-acoustical inversion in the Case A waveguide where the bottom speed and water speed are unknown, the two unknowns are the derivative parameters.

B.2 Wavenumber derivatives

Let $k_c = \frac{\omega}{c_c}$ and $k_b = \frac{\omega}{c_b}$ be the medium wavenumbers for the water column and bottom halfspace, respectively, and ρ_c and ρ_b are the corresponding densities. Let $k_n \equiv k_r$ be the horizontal wavenumber for mode n. Define α_c and α_b as the vertical wavenumbers for the water column and bottom halfspace. Expressions of the

form $x_{\ldots,b}$ represent derivatives with respect to bottom speed c_b, and $x_{\ldots,c}$ represent derivatives with respect to water speed c_c.

Then from the relationships

$\alpha_c^2 + k_r^2 = k_c^2$ and $\alpha_b^2 + k_r^2 = k_b^2$ and the characteristic equation for a Pekeris waveguide of depth D

$$\tan(\alpha_c D) = \frac{-i\rho_b \alpha_c}{\rho_c \alpha_b}$$

one obtains, using $k_{b,c} = k_{c,b} = 0$

$$k_{r,b} = -\frac{k_b k_{b,b} \alpha_c^2}{k_r \Gamma}$$

$$k_{r,c} = \frac{k_c k_{c,c}}{k_r}\left[1 + \frac{\alpha_c^2}{\Gamma}\right]$$

where

$$\Gamma = (k_b^2 - k_c^2 - \alpha_b^3 \Omega)$$

$$\Omega = \frac{i\rho_c}{\rho_b} D \sec^2(\alpha_c D)$$

The vertical wavenumber first-order derivatives are also needed for the next section on modal derivatives:

$$\alpha_{b,b} = \frac{k_b k_{b,b} - k_r k_{r,b}}{\alpha_b}$$

$$\alpha_{c,c} = \frac{k_c k_{c,c} - k_r k_{r,c}}{\alpha_c}$$

$$\alpha_{b,c} = -\frac{k_r k_{r,c}}{\alpha_b}$$

$$\alpha_{c,b} = -\frac{k_r k_{r,b}}{\alpha_c}$$

The second-order derivatives can be found, and after some algebra:

$$k_{r,bb} = k_{r,b}\left[\frac{2k_b k_{b,b}}{\Gamma} - \frac{3}{c_b} - \frac{k_{r,b}}{k_r} - \frac{\Gamma_b}{\Gamma}\right]$$

$$k_{r,cc} = -k_{r,c}\left[\frac{3}{c_c} + \frac{k_{r,c}}{k_r}\right] + \frac{k_c k_{c,c}}{k_r \Gamma}\left[2\alpha_c \alpha_{c,c} - \frac{\alpha_c^2 \Gamma_c}{\Gamma}\right]$$

$$k_{r,cb} = -\frac{k_{r,b}k_{r,c}}{k_r} + \frac{k_c k_{c,c}}{k_r}\left[\frac{2\alpha_{c,b}\alpha_c}{\Gamma} - \frac{\alpha_c^2 \Gamma_b}{\Gamma^2}\right]$$

$$\Gamma_b = 2k_b k_{b,b} - 3\alpha_b^2 \alpha_{b,b}\Omega - \alpha_b^3 \Omega_b$$

$$\Gamma_c = -2k_c k_{c,c} - 3\alpha_b^2 \alpha_{b,c}\Omega - \alpha_b^3 \Omega_c$$

$$\Omega_b = 2D\alpha_{c,b}\tan(\alpha_c D)\Omega$$

$$\Omega_c = 2D\alpha_{c,c}\tan(\alpha_c D)\Omega$$

$$\alpha_{c,bb} = -\frac{k_{r,b}^2 + k_r k_{r,bb} + \alpha_{c,b}^2}{\alpha_c}$$

$$\alpha_{b,cc} = -\frac{k_{r,c}^2 + k_r k_{r,cc} + \alpha_{b,c}^2}{\alpha_b}$$

$$\alpha_{b,bb} = -\frac{k_{b,b}^2 + k_b k_{b,bb} - k_{r,bb}^2 - k_r k_{r,bb} - \alpha_{b,b}^2}{\alpha_b}$$

$$\alpha_{c,cc} = -\frac{k_{c,c}^2 + k_c k_{c,cc} - k_{r,cc}^2 - k_r k_{r,cc} - \alpha_{c,c}^2}{\alpha_c}$$

$$\alpha_{c,bc} = -\frac{\alpha_{c,c}\alpha_{c,b} + k_{r,c}k_{r,b} + k_r k_{r,bc}}{\alpha_c}$$

$$\alpha_{b,bc} = -\frac{\alpha_{b,b}\alpha_{b,c} + k_{r,b}k_{r,c} + k_r k_{r,bc}}{\alpha_b}$$

The third-order wavenumber derivatives are

$$k_{r,bbb} = \frac{k_{r,bb}^2}{k_{r,b}} + k_{r,b}\left[\frac{3}{c_b^2} + \frac{k_{r,b}^2}{k_r^2} - \frac{k_{r,bb}}{k_r} + \frac{2k_{b,b}^2 + 2k_b k_{b,bb} - \Gamma_{bb}}{\Gamma} + \frac{\Gamma_b^2 - 2k_b k_{b,b}\Gamma_b}{\Gamma^2}\right]$$

$$k_{r,ccc} = -k_{r,cc}\left(\frac{3}{c_c} + \frac{k_{r,c}}{k_r}\right) + k_{r,c}\left[\frac{3}{c_c^2} + \left(\frac{k_{r,c}}{k_r}\right)^2 - \frac{k_{r,cc}}{k_r}\right]$$

$$+\left(\alpha_{c,c}\frac{k_{r,c}}{k_r^2} - \frac{\alpha_{c,cc}}{k_r}\right)\left(2\alpha_{c,c} - \alpha_c\frac{\Gamma_c}{\Gamma}\right)$$

$$-\frac{\alpha_{c,c}}{k_r}\left(2\alpha_{c,cc} - \alpha_{c,c}\frac{\Gamma_c}{\Gamma} - \alpha_c\frac{\Gamma_{cc}}{\Gamma} + \alpha_c\frac{\Gamma_c^2}{\Gamma^2}\right)$$

$$k_{r,bbc} = -\frac{k_{r,bb}k_{r,c} + k_{r,b}k_{r,bc}}{k_r} + k_{r,b}^2\frac{k_{r,c}}{k_r^2} + \left(\alpha_{c,c}\frac{k_{r,b}}{k_r^2} - \frac{\alpha_{c,cc}}{k_r}\right)\left(2\alpha_{c,b} - \alpha_c\frac{\Gamma_b}{\Gamma}\right)$$

$$-\frac{\alpha_{c,c}}{k_r}\left(2\alpha_{c,bb} - \alpha_{c,b}\frac{\Gamma_b}{\Gamma} - \alpha_c\frac{\Gamma_{bb}}{\Gamma} + \alpha_c\frac{\Gamma_b^2}{\Gamma^2}\right)$$

$$k_{r,bcc} = -\frac{k_{r,bc}k_{r,c} + k_{r,b}k_{r,cc}}{k_r} + k_{r,c}^2\frac{k_{r,b}}{k_r^2} + \left(\alpha_{c,c}\frac{k_{r,c}}{k_r^2} - \frac{\alpha_{c,cc}}{k_r}\right)\left(2\alpha_{c,b} - \alpha_c\frac{\Gamma_b}{\Gamma}\right)$$

$$-\frac{\alpha_{c,c}}{k_r}\left(2\alpha_{c,bc} - \alpha_{c,c}\frac{\Gamma_b}{\Gamma} - \alpha_c\frac{\Gamma_{bc}}{\Gamma} + \alpha_c\frac{\Gamma_b\Gamma_c}{\Gamma^2}\right)$$

where

$$\Gamma_{cc} = -2k_{c,c}^2 - 2k_c k_{c,cc} - 6\alpha_b \alpha_{b,c}^2 \Omega - 3\alpha_b^2 \alpha_{b,cc} \Omega - 6\alpha_b^2 \alpha_{b,c} \Omega_c - \alpha_b^3 \Omega_{cc}$$

$$\Omega_{cc} = \frac{\alpha_{c,cc}}{\alpha_{c,c}} \Omega_c + \frac{\Omega_c^2}{\Omega} + 2\Omega \left[\alpha_{c,c} D \sec(\alpha_c D) \right]^2$$

$$\Gamma_{bb} = 2k_{b,b}^2 + 2k_b k_{b,bb} - 6\alpha_b \alpha_{b,b}^2 \Omega - 3\alpha_b^2 \alpha_{b,bb} \Omega - 6\alpha_b^2 \alpha_{b,b} \Omega_b - \alpha_b^3 \Omega_{bb}$$

$$\Omega_{bb} = \frac{\alpha_{c,bb}}{\alpha_{c,b}} \Omega_b + \frac{\Omega_b^2}{\Omega} + 2\Omega \left[\alpha_{c,b} D \sec(\alpha_c D) \right]^2$$

$$\Gamma_{bc} = -6\alpha_b \alpha_{b,c} \alpha_{b,b} \Omega - 3\alpha_b^2 \alpha_{b,bc} \Omega - 3\alpha_b^2 \alpha_{b,b} \Omega_c - 3\alpha_b^2 \alpha_{b,c} \Omega_b - \alpha_b^3 \Omega_{bc}$$

$$\Omega_{bc} = \frac{\alpha_{c,bc}}{\alpha_{c,b}} \Omega_c + \frac{\Omega_c \Omega_b}{\Omega} + 2\Omega \alpha_{c,c} \alpha_{c,b} \left[D \sec(\alpha_c D) \right]^2$$

and the first four second-order vertical wavenumber derivatives are

$$\alpha_{c,bbb} = -(3k_{r,bb} k_{r,b} + k_r k_{r,bbb} + 3\alpha_{c,b} \alpha_{c,bb}) / \alpha_c$$

$$\alpha_{b,bbb} = (3k_{b,b} k_{b,bb} + k_b k_{b,bbb} - 3k_{r,bb} k_{r,b} - k_r k_{r,bbb} - 3\alpha_{b,b} \alpha_{b,bb}) / \alpha_b$$

$$\alpha_{c,bbc} = -(k_{r,bb} k_{r,c} + 2k_{r,b} k_{r,bc} + k_r k_{r,cbb} + \alpha_{c,c} \alpha_{c,bb} + 2\alpha_{c,b} \alpha_{c,bc}) / \alpha_c$$

$$\alpha_{b,bbc} = -(k_{r,bb} k_{r,c} + 2k_{r,b} k_{r,bc} + k_r k_{r,cbb} + 2\alpha_{b,b} \alpha_{b,bc} + \alpha_{b,bb} \alpha_{b,c}) / \alpha_b$$

The other four third-order derivatives can be obtained by swapping b and c in the expressions above.

B.3 Amplitude Derivatives

The modal amplitude derivatives for the Pekeris waveguide are shown here:

$$\Psi_n(z) = \underbrace{\sqrt{2}\left[\frac{1}{\rho_b}\left(H - \frac{\sin(2\alpha_c H)}{2\alpha_c}\right) - \frac{i\sin^2\alpha_c H}{\rho_b \alpha_b}\right]^{-\frac{1}{2}}}_{N} \sin(\alpha_c z)$$

where

$$\Psi_n = N\sin(\alpha_c z)$$

$$\Psi_c = N_c\sin(\alpha_c z) + \alpha_{c,c} z N\cos(\alpha_c z)$$

$$\Psi_{cc} = N_{cc}\sin(\alpha_c z) + 2\alpha_{c,c} z N_c\cos(\alpha_c z) - \alpha_{c,c}^2 z^2 N\sin(\alpha_c z) + \alpha_{c,cc} z N\cos(\alpha_c z)$$

$$\begin{aligned}\Psi_{bc} &= N_{bc}\sin(\alpha_c z) + N_c\alpha_{c,b} z\cos(\alpha_c z) + \alpha_{c,c} z N_b\cos(\alpha_c z) \\ &\quad +\alpha_{c,bc} z N\cos(\alpha_c z) - \alpha_{c,c}\alpha_{c,b} z^2 N\sin(\alpha_c z)\end{aligned}$$

$$\begin{aligned}\Psi_{ccc} &= N_{ccc}\sin(\alpha_c z) + 3\alpha_{c,cc} z N_c\cos(\alpha_c z) + 3\alpha_{c,c} z N_{cc}\cos(\alpha_c z) - 3\alpha_{c,c}^2 z^2 N_c\sin(\alpha_c z) \\ &\quad -3\alpha_{c,c}\alpha_{c,cc} z^2 N\sin(\alpha_c z) - \alpha_{c,c}^3 z^3 N\cos(\alpha_c z) + \alpha_{c,ccc} z N\cos(\alpha_c z)\end{aligned}$$

$$\begin{aligned}\Psi_{ccb} &= N_{ccb}\sin(\alpha_c z) + 2\alpha_{c,bc} z N_c\cos(\alpha_c z) + 2\alpha_{c,c} z N_{bc}\cos(\alpha_c z) \\ &\quad -2\alpha_{c,c}\alpha_{c,b} z^2 N_c\sin(\alpha_c z) + N_{cc}\alpha_{c,b} z\cos(\alpha_c z) - 2\alpha_{c,c}\alpha_{c,bc} z^2 N\sin(\alpha_c z) \\ &\quad -\alpha_{c,c}^2 z^2 N_b\sin(\alpha_c z) - \alpha_{c,c}^2\alpha_{c,b} z^3 N\cos(\alpha_c z) + \alpha_{c,ccb} z N\cos(\alpha_c z) \\ &\quad +\alpha_{c,cc} z N_b\cos(\alpha_c z) - \alpha_{c,cc}\alpha_{c,b} z^2 N\sin(\alpha_c z)\end{aligned}$$

$$\Psi_{bbc} = N_{bbc}\sin(\alpha_c z) + 2\alpha_{c,bc} z N_b\cos(\alpha_c z) + 2\alpha_{c,b} z N_{bc}\cos(\alpha_c z) - 2\alpha_{c,b}\alpha_{c,c} z^2 N_b\sin(\alpha_c z)$$

$$+N_{bb}\alpha_{c,c}z\cos(\alpha_c z) - 2\alpha_{c,b}\alpha_{c,bc}z^2 N\sin(\alpha_c z) - \alpha_{c,b}^2 z^2 N_c\sin(\alpha_c z)$$
$$-\alpha_{c,b}^2\alpha_{c,c}z^3 N\cos(\alpha_c z) + \alpha_{c,bbc}zN\cos(\alpha_c z) + \alpha_{c,bb}zN_c\cos(\alpha_c z) - \alpha_{c,bb}\alpha_{c,c}z^2 N\sin(\alpha_c z)$$

$$N_c = -\frac{N^3}{4}[\alpha_{c,c}\Upsilon_1 + \alpha_{b,c}\Upsilon_2]$$

$$N_{cc} = \frac{N_c^2}{N} - \frac{N^3}{4}[\alpha_{c,cc}\Upsilon_1 + \alpha_{b,cc}\Upsilon_2 + \alpha_{c,c}\Upsilon_{1c} + \alpha_{b,c}\Upsilon_{2c}]$$

$$N_{ccc} = \frac{6N_cN_{cc}}{N} - \frac{3N_c^3}{N^2} - \frac{3N^2N_c}{4}[\alpha_{c,cc}\Upsilon_1 + \alpha_{b,cc}\Upsilon_2 + \alpha_{c,c}\Upsilon_{1c} + \alpha_{b,c}\Upsilon_{2c}]$$

The expressions for N_b, N_{bb}, and N_{bbb} are found by substituting b for c in the terms N_c,N_{cc},and in derivatives with respect to c. For example, $\alpha_{c,c}$ will become $\alpha_{c,b}$ and so on.

$$N_{bc} = \frac{3N_cN_b}{N} - \frac{N^3}{4}[\alpha_{c,bc}\Upsilon_1 + \alpha_{b,cb}\Upsilon_2 + \alpha_{c,c}\Upsilon_{1b} + \alpha_{b,c}\Upsilon_{2b}]$$

$$\begin{aligned} N_{bbc} &= \frac{3N_{cb}N_b}{N} + \frac{3N_cN_{bb}}{N} - \frac{3N_cN_b^2}{N^2} - \frac{3N^2N_b}{4}[\alpha_{c,bc}\Upsilon_1 + \alpha_{b,cb}\Upsilon_2 + \alpha_{c,c}\Upsilon_{1b} + \alpha_{b,c}\Upsilon_{2b}] \\ &\quad -\frac{N^3}{4}[\alpha_{c,bbc}\Upsilon_1 + 2\alpha_{c,bc}\Upsilon_{1b} + \alpha_{b,cbb}\Upsilon_2 + 2\alpha_{b,cb}\Upsilon_{2b} + \alpha_{c,c}\Upsilon_{1bb} + \alpha_{b,c}\Upsilon_{2bb}] \end{aligned}$$

$$\begin{aligned} N_{ccb} &= \frac{3N_{cb}N_c}{N} + \frac{3N_bN_{cc}}{N} - \frac{3N_bN_c^2}{N^2} - \frac{3N^2N_c}{4}[\alpha_{c,bc}\Upsilon_1 + \alpha_{b,cb}\Upsilon_2 + \alpha_{c,b}\Upsilon_{1c} + \alpha_{b,b}\Upsilon_{2c}] \\ &\quad -\frac{N^3}{4}[\alpha_{c,bcc}\Upsilon_1 + 2\alpha_{c,cb}\Upsilon_{1c} + \alpha_{b,bcc}\Upsilon_2 + 2\alpha_{b,bc}\Upsilon_{2c} + \alpha_{c,b}\Upsilon_{1cc} + \alpha_{b,c}\Upsilon_{2cc}] \end{aligned}$$

$$\Upsilon_1 = \frac{\sin(2\alpha_c H)}{2\alpha_c^2\rho_b} - \frac{H\cos(2\alpha_c H)}{\rho_b\alpha_c} - \frac{iH\sin(2\alpha_c H)}{\rho_b\alpha_b}$$

$$\Upsilon_2 = \frac{i\sin^2(\alpha_c H)}{\rho_b\alpha_b^2}$$

$$\Upsilon_{1c} = \cos(2\alpha_c H)\left[\frac{3H\alpha_{c,c}}{2\alpha_c^2\rho_b} - \frac{i2H^2\alpha_{c,c}}{\rho_b\alpha_b}\right] + \sin(2\alpha_c H)\left[\frac{2H^2\alpha_{c,c}}{\rho_b\alpha_c} - \frac{\alpha_{c,c}}{\alpha^3\rho_b} + \frac{iH\alpha_{b,c}}{\rho_b\alpha_b^2}\right]$$

$$\Upsilon_{2c} = \frac{iH\alpha_{c,c}\sin(2\alpha_c H)}{\rho_b \alpha_b^2} - \frac{2i\sin^2(\alpha_c H)\alpha_{b,c}}{\rho_b \alpha_b^3}$$

The quantities Υ_{1b} and Υ_{2b} are found by replacing derivatives with respect to c (after the commas) to those with respect to b in the two expressions above.

$$\begin{aligned}
\Upsilon_{1cc} &= -2\alpha_{c,c}H\sin(2\alpha_c H)\left[\frac{3H\alpha_{c,c}}{2\alpha_c^2\rho_b} - \frac{i2H^2\alpha_{c,c}}{\rho_b\alpha_b}\right] \\
&\quad + \cos(2\alpha_c H)\left[\frac{3H\alpha_{c,cc}}{2\alpha_c^2\rho_b} - \frac{3H\alpha_{c,c}^2}{\alpha_c^3\rho_b} - \frac{i2H^2\alpha_{c,cc}}{\rho_b\alpha_b} + \frac{i2H^2\alpha_{c,c}^2}{\rho_b\alpha_b^2}\right] \\
&\quad - 2\alpha_{c,c}H\cos(2\alpha_c H)\left[\frac{2H^2\alpha_{c,c}}{\rho_b\alpha_c} - \frac{\alpha_{c,c}}{\alpha_c^3\rho_b} + \frac{iH\alpha_{b,c}}{\rho_b\alpha_b^2}\right] \\
&\quad + \sin(2\alpha_c H)\left[\alpha_{c,cc}\left(\frac{2H^2}{\rho_b\alpha_c} - \frac{1}{\alpha_c^3\rho_b}\right) + \alpha_{c,c}^2\left(\frac{-2H^2}{\rho_b\alpha_c^2} + \frac{3}{\alpha_c^4\rho_b}\right) + \frac{iH\alpha_{b,cc}}{\rho_b\alpha_b^2} - \frac{2iH\alpha_{b,c}^2}{\rho_b\alpha_b^3}\right]
\end{aligned}$$

$$\begin{aligned}
\Upsilon_{2cc} = &\frac{iH\alpha_{c,cc}\sin(2\alpha_c H)}{\rho_b\alpha_b^2} - \frac{4iH\alpha_{c,c}\alpha_{b,c}\sin(2\alpha_c H)}{\rho_b\alpha_b^3} + \frac{2iH^2\alpha_{c,c}^2\cos(2\alpha_c H)}{\rho_b\alpha_b^2} \\
&+ \frac{6i\alpha_b^2\sin^2(\alpha_c H)}{\rho_b\alpha_b^4} - \frac{2i\alpha_{b,,cc}^2\sin^2(\alpha_c H)}{\rho_b\alpha_b^2}
\end{aligned}$$

The quantities Υ_{1bb} and Υ_{2bb} are found by replacing derivatives with respect to c (after the commas) to those with respect to b in the two expressions above.

Appendix C

Joint moments for asymptotic Gaussian inference: general multivariate Gaussian data

C.1 General multivariate Gaussian data

For the *general multivariate Gaussian* case, both the mean μ and the covariance matrix $\mathbf{C}$ depend on the parameter vector $\mathbf{\Theta}$. The joint moments required to evaluate the first order bias are

$$i_{ab} = \frac{n}{2}\mathrm{tr}(\mathbf{C}^{-1}\mathbf{C}_a\mathbf{C}^{-1}\mathbf{C}_b) + n\mu_a^T\mathbf{C}^{-1}\mu_b, \tag{C.1}$$

$$\begin{aligned}\nu_{abc} = {} & \frac{n}{3}\sum_{a,b,c}\mathrm{tr}(\mathbf{C}^{-1}\mathbf{C}_a\mathbf{C}^{-1}\mathbf{C}_b\mathbf{C}^{-1}\mathbf{C}_c) \\ & -\frac{n}{4}\sum_{a,b,c}\mathrm{tr}(\mathbf{C}^{-1}\mathbf{C}_{ab}\mathbf{C}^{-1}\mathbf{C}_c) - \frac{n}{2}\sum_{a,b,c}\mu_{ab}^T\mathbf{C}^{-1}\mu_c \\ & +\frac{n}{2}\sum_{a,b,c}\mu_a^T\mathbf{C}^{-1}\mathbf{C}_b\mathbf{C}^{-1}\mu_c,\end{aligned} \tag{C.2}$$

$$\nu_{ab,c} = -\frac{n}{2}\sum_{a,b}(tr)(\mathbf{C}^{-1}\mathbf{C}_a\mathbf{C}^{-1}\mathbf{C}_b\mathbf{C}^{-1}\mathbf{C}_c) + n\mu_{ab}^T\mathbf{C}^{-1}\mu_c$$

$$+\frac{n}{2}\mathrm{tr}(\mathbf{C}^{-1}\mathbf{C}_{ab}\mathbf{C}^{-1}\mathbf{C}_c) \qquad (C.3)$$
$$-n\sum_{a,b}\mu_a^T\mathbf{C}^{-1}\mathbf{C}_b\mathbf{C}^{-1}\mu_c,$$

where, for example, $\sum_{a,b,c}$ indicates a sum over all possible permutations of a,b, and c orderings, leading to a total of six terms. Teerms such as $\mathbf{C}_{ab}$ and μ_{ab} represent the derivatives of the covariance matrix $\mathbf{C}$ and the mean vector μ with respect to Θ^a and Θ^b, respectively.

C.2 Multivariate Gaussian data with parameter-independent covariance: deterministic signal in independent additive noise

For this case the covariance matrix is independent of the parameters to be estimated, i.e. $\partial\mathbf{C}/\partial\Theta^i = 0$ for all i. The joint moments required to evaluate the first order bias, as well as the second order error correlation and covariance are

$$i_{ab} = n\mu_a^T\mathbf{C}^{-1}\mu_b \qquad (C.4)$$

$$\nu_{abc}(n^1) = -\frac{n}{2}\sum_{a,b,c}\mu_{ab}^T\mathbf{C}^{-1}\mu_c, \qquad (C.5)$$

$$\nu_{a,b,c}(n^1) = 0, \qquad (C.6)$$

$$\nu_{ab,c}(n^1) = n\mu_{ab}^T\mathbf{C}^{-1}\mu_c, \qquad (C.7)$$

$$\nu_{abcd}(n^1) = -\frac{n}{8}\sum_{a,b,c,d}\mu_{ab}^T\mathbf{C}^{-1}\mu_{cd} - \frac{n}{6}\sum_{a,b,c,d}\mu_{abc}^T\mathbf{C}^{-1}\mu_d, \qquad (C.8)$$

$$\nu_{a,b,c,d}(n^2) = \frac{n^2}{8} \sum_{a,b,c,d} \mu_a^T \mathbf{C}^{-1} \mu_b \mu_c^T \mathbf{C}^{-1} \mu_d, \tag{C.9}$$

$$\nu_{a,b,cd}(n^1) = 0, \tag{C.10}$$

$$\nu_{a,b,c,de}(n^2) = \frac{n^2}{2} \sum_{a,b,c} \mu_a^T \mathbf{C}^{-1} \mu_b \mu_c^T \mathbf{C}^{-1} \mu_{de}, \tag{C.11}$$

$$\begin{aligned} \nu_{a,b,cd,ef}(n^2) = \frac{n^2}{2} & \sum_{(a,b)\times(cd,ef)} \mu_a^T \mathbf{C}^{-1} \mu_{cd} \mu_b^T \mathbf{C}^{-1} \mu_{ef} \\ & + n^2 \mu_{cd}^T \mathbf{C}^{-1} \mu_{ef} \mu_a^T \mathbf{C}^{-1} \mu_b, \end{aligned} \tag{C.12}$$

$$\nu_{a,b,c,def}(n^2) = \frac{n^2}{2} \sum_{a,b,c} \mu_a^T \mathbf{C}^{-1} \mu_b \mu_c^T \mathbf{C}^{-1} \mu_{def}, \tag{C.13}$$

where the notation $\sum_{(a,b)\times(cd,ef)}$ indicates a sum over all possible permutations of a and b orderings combined with permutations of cd and ef orderings, leading to a total of four terms.

C.3 Multivariate Gaussian data with zero-mean: random signal in noise

The following equations are useful only for scenarios where the signal has zero mean and is randomized. None of the exmaples discussed in this thesis use such a signal. However, the code written for the project is designed to allow the calculation of the bias and variance for such signals. Therefore the formulas are included.

For the case of a randomized signal with zero mean in additive noise, the joint moments required to evaluate the first order bias, as well as the second order error

correlation and covariance are

$$i_{ab} = n\frac{n}{2}\mathrm{tr}(\mathbf{C}^{-1}\mathbf{C}_a\mathbf{C}^{-1}\mathbf{C}_b), \tag{C.14}$$

$$\nu_{abc}(n^1) = \frac{n}{3}\sum_{a,b,c}\mathrm{tr}(\mathbf{C}^{-1}\mathbf{C}_a\mathbf{C}^{-1}\mathbf{C}_b\mathbf{C}^{-1}\mathbf{C}_c) - \frac{n}{4}\sum_{a,b,c}\mathrm{tr}(\mathbf{C}^{-1}\mathbf{C}_{ab}\mathbf{C}^{-1}\mathbf{C}_c), \tag{C.15}$$

$$\nu_{a,b,c}(n^1) = \frac{n}{6}\sum_{a,b,c}\mathrm{tr}(\mathbf{C}^{-1}\mathbf{C}_a\mathbf{C}^{-1}\mathbf{C}_b\mathbf{C}^{-1}\mathbf{C}_c), \tag{C.16}$$

$$\nu_{ab,c}(n^1) = -\frac{n}{2}\sum_{a,b,c}\mathrm{tr}(\mathbf{C}^{-1}\mathbf{C}_a\mathbf{C}^{-1}\mathbf{C}_b\mathbf{C}^{-1}\mathbf{C}_c) + \frac{n}{2}\mathrm{tr}(\mathbf{C}^{-1}\mathbf{C}_{ab}\mathbf{C}^{-1}\mathbf{C}_c), \tag{C.17}$$

$$\begin{aligned}\nu_{abcd}(n^1) = & -\frac{3n}{8}\sum_{a,b,c,d}\mathrm{tr}(\mathbf{C}^{-1}\mathbf{C}_a\mathbf{C}^{-1}\mathbf{C}_b\mathbf{C}^{-1}\mathbf{C}_c\mathbf{C}^{-1}\mathbf{C}_d) \\ & +\frac{n}{2}\sum_{a,b,c,d}\mathrm{tr}(\mathbf{C}^{-1}\mathbf{C}_{ab}\mathbf{C}^{-1}\mathbf{C}_c\mathbf{C}^{-1}\mathbf{C}_d) - \frac{n}{16}\sum_{a,b,c,d}\mathrm{tr}(\mathbf{C}^{-1}\mathbf{C}_{ab}\mathbf{C}^{-1}\mathbf{C}_{cd}) \\ & -\frac{n}{12}\sum_{a,b,c,d}\mathrm{tr}(\mathbf{C}^{-1}\mathbf{C}_{abc}\mathbf{C}^{-1}\mathbf{C}_d),\end{aligned} \tag{C.18}$$

$$\nu_{a,b,c,d}(n^2) = \frac{n^2}{32}\sum_{a,b,c,d}\mathrm{tr}(\mathbf{C}^{-1}\mathbf{C}_a\mathbf{C}^{-1}\mathbf{C}_b)\mathrm{tr}(\mathbf{C}^{-1}\mathbf{C}_c\mathbf{C}^{-1}\mathbf{C}_d), \tag{C.19}$$

$$\begin{aligned}\nu_{a,b,cd}(n^1) = & -\frac{n}{2}\sum_{(a,b)\times(c,d)}\mathrm{tr}(\mathbf{C}^{-1}\mathbf{C}_a\mathbf{C}^{-1}\mathbf{C}_b\mathbf{C}^{-1}\mathbf{C}_c\mathbf{C}^{-1}\mathbf{C}_d) \\ & +\frac{n}{2}\sum_{a,b}\mathrm{tr}(\mathbf{C}^{-1}\mathbf{C}_a\mathbf{C}^{-1}\mathbf{C}_b\mathbf{C}^{-1}\mathbf{C}_{cd}),\end{aligned} \tag{C.20}$$

$$\nu_{a,b,c,de}(n^2) = -\frac{n^2}{24}\sum_{(a,b,c)\times(d,e)}\mathrm{tr}(\mathbf{C}^{-1}\mathbf{C}_d\mathbf{C}^{-1}\mathbf{C}_c)\mathrm{tr}(\mathbf{C}^{-1}\mathbf{C}_a\mathbf{C}^{-1}\mathbf{C}_b\mathbf{C}^{-1}\mathbf{C}_c)$$

$$-\frac{n^2}{8}\sum_{(a,b,c)\times(d,e)}\mathrm{tr}(\mathbf{C}^{-1}\mathbf{C}_a\mathbf{C}^{-1}\mathbf{C}_b)\mathrm{tr}(\mathbf{C}^{-1}\mathbf{C}_c\mathbf{C}^{-1}\mathbf{C}_d\mathbf{C}^{-1}\mathbf{C}_e)$$
$$+\frac{n^2}{8}\sum_{(a,b,c)}\mathrm{tr}(\mathbf{C}^{-1}\mathbf{C}_a\mathbf{C}^{-1}\mathbf{C}_b)\mathrm{tr}(\mathbf{C}^{-1}\mathbf{C}_c\mathbf{C}^{-1}\mathbf{C}_{de}), \qquad \text{(C.21)}$$

$$\begin{aligned}
\nu_{a,b,cd,ef}(n^2) = \\
&\frac{n^2}{8}\sum_{(cd,ef)\times(a,b)\times(c,d)\times(e,f)}\mathrm{tr}(\mathbf{C}^{-1}\mathbf{C}_c\mathbf{C}^{-1}\mathbf{C}_d)\left[\mathrm{tr}(\mathbf{C}^{-1}\mathbf{C}_a\mathbf{C}^{-1}\mathbf{C}_b\mathbf{C}^{-1}\mathbf{C}_e\mathbf{C}^{-1}\mathbf{C}_f)\right. \\
&\left.-1/2\ \mathrm{tr}(\mathbf{C}^{-1}\mathbf{C}_a\mathbf{C}^{-1}\mathbf{C}_b\mathbf{C}^{-1}\mathbf{C}_{ef})\right] \\
&+\frac{n^2}{8}\sum_{(cd,ef)\times(a,b)\times(c,d)\times(e,f)}\mathrm{tr}(\mathbf{C}^{-1}\mathbf{C}_a\mathbf{C}^{-1}\mathbf{C}_b)\left[\frac{1}{2}\mathrm{tr}(\mathbf{C}^{-1}\mathbf{C}_c\mathbf{C}^{-1}\mathbf{C}_d\mathbf{C}^{-1}\mathbf{C}_e\mathbf{C}^{-1}\mathbf{C}_f)\right. \\
&\left.-\frac{1}{2}\mathrm{tr}(\mathbf{C}^{-1}\mathbf{C}_c\mathbf{C}^{-1}\mathbf{C}_d\mathbf{C}^{-1}\mathbf{C}_{ef})+\frac{1}{8}\mathrm{tr}(\mathbf{C}^{-1}\mathbf{C}_{cd}\mathbf{C}^{-1}\mathbf{C}_{ef})\right] \\
&+\frac{n^2}{8}\sum_{(cd,ef)\times(a,b)\times(c,d)\times(e,f)}\mathrm{tr}(\mathbf{C}^{-1}\mathbf{C}_a\mathbf{C}^{-1}\mathbf{C}_c\mathbf{C}^{-1}\mathbf{C}_d)\mathrm{tr}(\mathbf{C}^{-1}\mathbf{C}_b\mathbf{C}^{-1}\mathbf{C}_e\mathbf{C}^{-1}\mathbf{C}_f) \\
&+\frac{n^2}{8}\sum_{(cd,ef)(a,b)}\mathrm{tr}(\mathbf{C}^{-1}\mathbf{C}_a\mathbf{C}^{-1}\mathbf{C}_{cd})\mathrm{tr}(\mathbf{C}^{-1}\mathbf{C}_b\mathbf{C}^{-1}\mathbf{C}_{ef}) \\
&-\frac{n^2}{8}\sum_{(cd,ef)\times(a,b)\times(c,d)\times(e,f)}\mathrm{tr}(\mathbf{C}^{-1}\mathbf{C}_a\mathbf{C}^{-1}\mathbf{C}_{cd})\mathrm{tr}(\mathbf{C}^{-1}\mathbf{C}_b\mathbf{C}^{-1}\mathbf{C}_e\mathbf{C}^{-1}\mathbf{C}_f), \qquad \text{(C.22)}
\end{aligned}$$

$$\begin{aligned}
\nu_{a,b,c,def}(n^2) = \\
&\frac{n^2}{18}\sum_{(a,b,c)\times(d,e,f)}\mathrm{tr}(\mathbf{C}^{-1}\mathbf{C}_a\mathbf{C}^{-1}\mathbf{C}_b\mathbf{C}^{-1}\mathbf{C}_c)\mathrm{tr}(\mathbf{C}^{-1}\mathbf{C}_d\mathbf{C}^{-1}\mathbf{C}_e\mathbf{C}^{-1}\mathbf{C}_f) \\
&-\frac{n^2}{24}\sum_{(a,b,c)\times(d,e,f)}\mathrm{tr}(\mathbf{C}^{-1}\mathbf{C}_a\mathbf{C}^{-1}\mathbf{C}_b\mathbf{C}^{-1}\mathbf{C}_c)\mathrm{tr}(\mathbf{C}^{-1}\mathbf{C}_{de}\mathbf{C}^{-1}\mathbf{C}_f) \\
&+\frac{n^2}{8}\sum_{(a,b,c)\times(d,e,f)}\mathrm{tr}(\mathbf{C}^{-1}\mathbf{C}_a\mathbf{C}^{-1}\mathbf{C}_b)\left[\mathrm{tr}(\mathbf{C}^{-1}\mathbf{C}_c\mathbf{C}^{-1}\mathbf{C}_d\mathbf{C}^{-1}\mathbf{C}_e\mathbf{C}^{-1}\mathbf{C}_f)\right. \\
&\left.-\mathrm{tr}(\mathbf{C}^{-1}\mathbf{C}_c\mathbf{C}^{-1}\mathbf{C}_{de}\mathbf{C}^{-1}\mathbf{C}_f)+1/6\mathrm{tr}(\mathbf{C}^{-1}\mathbf{C}_c\mathbf{C}^{-1}\mathbf{C}_{def})\right], \qquad \text{(C.23)}
\end{aligned}$$

where the notation $\sum_{(a,b,c)\times(d,e,f)}$ indicates summation over all possible permutations of d,e,f and a,b,and c, leading to a total of 36 terms.